UNIVERSITY OF CALIFORNIA

Los Angeles

Coupling of Hydride Transfer with Oligomerization and Deoxygenation Reactions on Solid Acid Catalysts

A dissertation submitted in partial satisfaction of the requirements for the degree

Doctor of Philosophy in Chemical Engineering

by

Anas Saleh N. Al Aqeeli

2022

ABSTRACT OF THE DISSERTATION

Coupling of Hydride Transfer with Oligomerization and Deoxygenation Reactions on Solid Acid Catalysts

by

Anas Saleh N. Al Aqeeli

Doctor of Philosophy in Chemical Engineering

University of California, Los Angeles, 2022

Professor Dante A. Simonetti, Chair

The growing demand for aromatic compounds and the desire to produce them in an environmentally sustainable way has encouraged research efforts to tap into renewable sources for their production. Bio-oil, a free-flowing dark brown liquid derived from the depolymerization and fragmentation of cellulose, hemicellulose, and lignin, is considered to be one of the most valuable resources with the potential to replace fossil oils. However, inherent properties of bio-oils such as high-water content, high viscosity, and high process corrosiveness caused by acidic compounds are limiting their industrial applications. These unfavorable properties are mostly caused by the high oxygen content which is the main property that distinguishes bio-oils from fossil oils. As the main constituent of bio-oils, oxygenated hydrocarbons such as organic acids, alcohol, aldehydes, and ketones have been extensively explored for their conversion into valuable products with efforts focusing on developing highly selective and stable catalysts. Zeolites modified with transition metals stand as some of the most selective and highly stable catalysts for the production of

aromatics from oxygenated hydrocarbons thanks to their acid-metal bifunctional nature. In addition, the co-feeding of light alkanes with oxygenates has been regarded as an effective strategy to mitigate prolonged catalyst deactivation due to the active participation of the alkane in the conversion cycle over the bifunctional catalyst. In this dissertation, we aim at exploring the conversion of butanal (as a model compound representing bio-oils) with isobutane co-feed over H-BEA zeolite modified with Zn^{2+} ions. We first assess the conversion of butanal on Zn/H-BEA catalysts with different metal loadings to note the contribution of different Zn^{2+} acid sites in catalyzing various reaction products. Then, we develop a detailed kinetic model, which accounts for catalyst deactivation, for the reaction of butanal over the Zn/H-BEA catalysts to elucidate the effect of Zn^{2+} species on the activation energies of different reactions and the binding energies of reactive surface species. Finally, we investigate the deoxygenation and aromatization of butanal with isobutane co-feed over Zn/H-BEA catalysts to identify the proper loading and proportions of Zn^{2+} sites to boost the deoxygenation rates, increase the selectivity to aromatics, and improve the catalyst stability.

The dissertation of Anas Saleh N. Al Aqeeli is approved.

Panagiotis D. Christofides

Philippe Sautet

Louis-Serge Bouchard

Dante A. Simonetti, Committee Chair

University of California, Los Angeles

2022

To my dad and mom,

my beloved wife, and my sweet daughters …

Table of contents

List of Tables

List of Figures

Acknowledgments

First and foremost, I would like to thank Allah the Almighty, the most Gracious, and the most Merciful for giving me the strength and courage to complete this work.

I would like to express my gratitude and sincere thanks to my advisor Prof. Dante Simonetti for his support and guidance throughout my degree at UCLA. Under his supervision, I learned how to become a well-acquainted, independent, and hard-working researcher. Working in his lab was an exceptional experience and I already realize how it greatly influenced and sharpened my research and technical skills. I truly appreciate all the efforts and time he put to guide me through this journey. I would also like to deeply thank my Ph.D. committee members Prof. Panagiotis D. Christofides, Prof. Philippe Sautet, and Prof. Louis-Serge Bouchard for directing and supporting my research. I very much appreciate their valuable feedback and suggestions which greatly helped in elevating the quality of my research.

To my wife and soulmate Hajar, thank you so much for your love, patience, and encouragement throughout my degree. Together we endured tough moments like Covid lockdowns away from family and enjoyed happy ones like welcoming Deem's first tooth. I'm so proud to have you by my side and I'm forever grateful for all that you have done. My sweet daughter Deem, thank you for your smiles and laughs. Your presence brought so much joy to my heart and I couldn't bear a day without hugging you. My little Farah, welcome to the world sweetie. I'm so glad that you are here to witness the conclusion of this degree journey.

I would like to profoundly thank my dad and mom for their support and motivation. Their words resonate in my mind and have always kept me advancing and moving forward. I would also like to thank my brothers and sisters and recognize them for being my role models in life.

I would like to thank my dear colleague and family friend Mohammed Alhajeri for the time we spent discussing deeply technical subjects or enjoying outdoor outings while our kids play together. In addition, I would like to thank my family friends Abdulaziz Alawadhi, Alwaleed Aldhafeeri, Mohammed Aldakheel, Ali Alshehri, and Obidullah Montasheri. I look forwards to our continued friendship even after we go back to our home countries.

I would like to immensely thank all my colleagues in the Simonetti group including Yen-Wen Tseng, Eric Lin, Abdulaziz Alturki, Luke Minardi, Juan Carlos, and Marios Christofides for all the informative discussions and the delightful moments we had together. I will always cherish the good memories I had with them.

Last but not the least, I would like to thank Saudi Aramco and the Research and Development Center for sponsoring my degree at UCLA. My special thanks to the frontline advisors Suhail Gaydi and Philip Mantaring for their time and support during my time in the US.

Vita

2008 – 2013	B.S. in Chemical Engineering King Fahd University of Petroleum and Minerals Dhahran, Saudi Arabia
2013 – 2015	Research Engineer Research and Development Center, Saudi Aramco Dhahran, Saudi Arabia
2015 – 2016	Process Engineer Rabigh Refining & Petrochemical Company (Petro Rabigh) Rabigh, Saudi Arabia
2016 – 2018	Research Engineer Research and Development Center, Saudi Aramco Dhahran, Saudi Arabia
2018 – 2020	M.S. Chemical Engineering University of California, Los Angeles Los Angeles, United States

Publications

- **Anas Al-Aqeeli** and Dante A. Simonetti, *Enhancing CO_2 desorption from monoethanolamine solutions through in-situ mineralization and generation of solid $CaCO_3$ particles at low regeneration temperatures*, In preparation.

- **Anas Al-Aqeeli** and Dante A. Simonetti, *Reactivity study of butanal with isobutane co-feed on zeolites modified with Zn^{2+}*, In preparation.

- Eric Lin, **Anas Al-Aqeeli**, Adam Hoffman, Simon Bare, and Dante Simonetti, *Nature of active sites in Zn-modified H-BEA zeolites and their role in the conversion of oxygenates*, In preparation.

- **Anas Al-Aqeeli** and Dante A. Simonetti, *Kinetic analysis and modeling of butanal conversion over Zn/H-BEA catalysts*, In preparation.

Chapter 1: Introduction

1.1 Background

1.1.1 Acidity in heterogeneous catalysts

Solid surfaces containing acid-catalytic properties are of major importance in the application of ion exchange and heterogeneous catalysis. The concept of catalytic surface acidities and their relative strengths was first developed by Walling[1] when he defined acidity as the ability of the surface to convert an adsorbed neutral base to its conjugate acid. His acidity determination method was relying primarily on the color change of indicators adsorbed on the surface. According to Brønsted's theory, an acid is defined as a proton donor and the base as a proton acceptor.[2] In acid-base catalysis, the acid transfers the proton and becomes a conjugate base and the base accepts the proton to become a conjugate acid according to the below equation.

$$A - H + B^{-} \leftrightarrow A^{-} + B - H$$

Where $A - H$ represents an acid and A^{-} is its conjugate base and B^{-} represents a base and $B - H$ is its conjugate acid. The negative superscript represents a pair of electrons that are shared with a proton. Similar to Brønsted's theory, Lewis put forth another theory that ascribes the acid as any species with a vacant orbital that can accept a pair of electrons, whereas a base is species that has an unshared pair of electrons.[2]

Heterogenous catalysts are of vital economic importance as they allow us to efficiently convert different raw materials to valuable chemicals and fuels in an environmentally friendly manner. It has been estimated that 90% of the known chemical processes use some sort of catalysis and that highlights the major role these materials take in the field of fuels and chemical

industries.[3] As a broad and industrially applicable class of solid acid catalysts, zeolites are crystalline aluminosilicate structures made from AlO_4 and SiO_4 tetrahedra which are connected by common oxygen atoms at their corners. This configuration results in a three-dimensional framework structure containing channels and cages with dimensions ranging from 0.2 – 1 nm.[4] Zeolites which are merely made from silicon oxides are electrically neutral. When a silicon atom with a formal charge of 4^+ is replaced by an atom with a formal charge of 3^+ (such as aluminum), the lattice bears a negative charge that requires balancing by a proton or a metal cation. When this balancing cation is a proton, it binds with a bridging oxygen and becomes a Brønsted acid site.

1.1.2 Brønsted acidity in zeolites

When a proton is used to balance the negative charge on the zeolite structure (which is induced by the tetrahedrally-bonded aluminum), the resulting hydroxyl group becomes a Brønsted acid site.[2] Brønsted acidity can be generated in various ways such as (1) the direct proton exchange of the metal cations; (2) the ammonium exchange of the same metal cation followed by the thermal decomposition of ammonium cations to protons; (3) the exchange with polyvalent cations capable of generating protons via water hydrolysis and (4) the reduction of the exchanging metal cations by hydrogen to generate surface protons.[2] Equation 1.1 shows one way of generating Brønsted acid sites through the direct ion exchange with mineral acids, such as hydrochloric acid, which is usually the least favored option for Brønsted site generation. This is because exposing the zeolite framework to low pH could result in the dealumination and breakdown of the crystal structure.[4] Equation 1.2 demonstrate the generation of the acid site by the ammonium exchange of the framework cation then heating the zeolite at high temperature to decompose the ammonium and form a proton. Equation 1.3 shows how the multi-valent metal cation ion exchange results in the creation of the acid sites. Equation 1.4 shows how Brønsted acid

sites could be generated by the reduction of noble metals on the catalyst surface by hydrogen gas.[4] The availability of the formed Brønsted sites in any of the previous methods has proven to be highly dependent on the extent of ammonia removal from the zeolite framework by calcination where highly stable ammonium-bonded metal was seen to neutralize the overall acidity of the zeolite.[5] The common factor across all these forgoing methods is that they create the same bridging hydroxyl groups (the proton on the framework oxygen in the silicon-bonded AlO_4 tetrahedron).

$$H^+ + Na^+O^- \xrightarrow{-Na^+} H^+O^- \tag{1.1}$$

$$NH_4{}^+ + Na^+O^- \xrightarrow{-Na^+} NH_4{}^+O^- \xrightarrow{300-400^oC\ (-NH_3)} H^+O^- \tag{1.2}$$

$$[La(H_2O)_n]^{3+} + 3\ Na^+O^- \xrightarrow{-3\ Na^+} [La(H_2O)_n]^{3+}(O^-)_3 \xrightarrow{300^oC\ [-(n-2)\ H_2O]} [La(OH)_2]^+(H^+)_2(O^-)_3 \tag{1.3}$$

$$[Pd(NH_3)_4]^{2+} + 2\ Na^+O^- \xrightarrow{-2\ Na^+} [Pd(NH_3)_4]^{2+}(O^-)_2 \xrightarrow{300^oC\ (-4\ NH_3)} Pd^{2+}(O^-)_2 \xrightarrow{+H_3} Pd^o(H^+)_2(O^-)_2 \tag{1.4}$$

The strength of the Brønsted acid sites depends on a number of structural and chemical factors. For example, mildly steaming a zeolite could result in reduced yet stronger Brønsted acid sites. This phenomenon was seen in zeolites such as H-ZSM-5 where enhancement of the isolated Brønsted acid sites by vicinal extra-framework aluminum species was reported.[6] Earlier studies also confirm the strength of the isolated acid sites (aluminum tetrahedra) compared to ones in close proximity to one another.[7]

1.1.3 Lewis acidity in zeolites

The positively charged ions or oxide clusters within the zeolite act as Lewis acid sites. These acid sites can be generated by the high-temperature dehydration of zeolite structures leading to the dehydroxylation of Brønsted sites as observed upon heating H-Y zeolite at 773 K.[8] Also,

Lewis sites can be generated by mildly steaming the zeolite structure to dislodge aluminum atoms from framework positions. This results in the formation of extra-framework alumina which was found responsible for the polarization of the paraffin molecules in n-hexane cracking on H-ZSM-5 zeolite.[9] Another way to produce Lewis acidity in zeolites is through the ion exchange with polyvalent cations species within their channels and cages. In this case, the metal cation attached to the zeolite framework becomes a Lewis acid site as seen by Zr-Beta zeolites in the cross-aldol condensation of aromatic aldehydes with acetone.[10] Although Lewis acid sites are generally lower in strength than Brønsted acid sites, they are known to provide a synergetic effect of enhancing the overall zeolite acidity when present in close proximity to Brønsted acid sites.[11]

1.1.4 Kinetic modeling for catalyst and process design

It is vital for industrial catalysis research and development to be able to identify optimum catalysts with the reaction conditions necessary to make targeted chemical processes stable and profitable. New efficient approaches to improve the current chemical and petrochemical industries beyond their capacities and limitations are particularly timely considering the growing demand and increasing population. Besides catalyst synthesis, testing and characterization, it is also worthwhile to supplement the experimental studies by quantitively analyzing the chemical reaction kinetics to elucidate the reactivities of different catalysts and extrapolate their performances to various industrially relevant conditions. As a first estimate, the kinetics of a certain chemical reaction can be regressed into a power-low expression where the reaction rates' dependence on temperature and activities are captured into a rate constant and reaction orders, respectively. This method has found extensive use in predicting industrial process performance and in controlling reactors due to its simplicity and applicability[12,13]. In solid catalysis, the concentration of the reactive species on the surface of the catalyst along with important artifacts such as acid site

blocking can be incorporated into a kinetic model by using Langmuir-Hinshelwood-Hougen-Watson (LHHW) rate expressions.[14] For a given reaction, LHHW rate expression is obtained by assuming rate-determining and quasi-equilibrated steps. Although LHHW rate expressions are valid for a wide range of reaction conditions compared to power-law expressions, they assume that the adsorption and reactive sites on the catalyst are identical and the interactions between adsorbed species are negligible. [15] Besides these traditional methods being useful, coupling them with deeper chemical intuition and rigorous surface chemistries is desirable and envisioned to streamline the process of catalyst design.

Microkinetics is a term defined by Domesic et al[16] to denote the reaction kinetic analysis that attempts to incorporate basic surface chemistries involved in the catalytic reaction. Therefore, the model is based on the description of catalytic processes in terms of the information and assumption about active sites and the nature of elementary steps making the reaction scheme. As an advantage, microkinetic modeling doesn't require any assumptions regarding the nature of the rate-determining elementary reactions or the abundant surface species.[17] Microkinetic modeling has been successfully applied to describe and interpret various reaction systems and **Figure 1.1** shows the number of publications and citations for reports on this topic.[18–22]

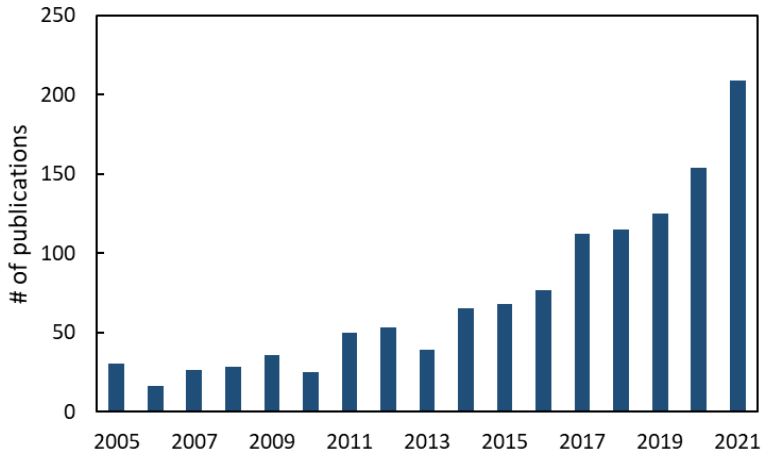

Figure 1.1: Number of publications citing the term "microkinetic modeling" from 2005 to 2021 (Searched through the Web of Science™)

1.1.4.1 Developing a reaction scheme

Identifying the proper reaction conditions to improve the process throughput and developing an optimized catalytic material to serve this purpose are two important goals in industrial research and development. The microkinetic-based analysis provides a framework for analyzing reaction mechanisms to give insights about the rate-limiting steps and dominating surface species in a way that focuses research efforts on designing catalytic material with improved performance. The first step in formulating such a model is to develop a feasible reaction scheme that includes all reaction events occurring on the catalyst surface. Because different reaction schemes could lead to the same apparent rate expression, fitting the experimental data to elucidate the reaction mechanism is not practical.[23] For this reason, the research in chemical kinetics doesn't entirely focus on measuring the reaction rates but also considers collecting other spectroscopic and theoretical information to explain the nature of the intermediates and important steps taking place in the catalytic cycle.[16]

One of the simple ways to investigate the reaction mechanism of a certain solid-catalyzed reactant is to run reaction experiments at varying conversions (by changing space-time and

temperature in flow systems) and observe product selectivities. Following this procedure, a sensible reaction sequence can be formulated by categorizing products as primary or secondary based on how they evolve. For example, Sun et al[24] investigated the reaction pathways for the conversion of methanol to hydrocarbons on H-ZSM-5 zeolite. They varied the total reactant flow and the catalyst weight to achieve different space velocities and alter the conversion. In addition, they assessed the aromatic and olefinic cycles by co-feeding different aromatics and olefins, respectively. Other powerful tools for studying reaction mechanisms include Solid-State Nuclear Magnetic Resonance (NMR)[25], Infrared Spectroscopy (IR)[26], ^{13}C and ^{2}H labeling experiments[27,28], and chemical cluster calculations[29].

1.1.4.2 Model parameterization

The general strategy for most kinetic studies is to analyze the available reaction kinetic data to examine the reaction scheme. This is done by calculating kinetic reaction constants that are bounded within physically sound limits. On the other hand, initial kinetic parameters could also be reasonably estimated by using collision or transition state theories to find preexponential factors which could serve as initial estimates.[16] Despite the underlying difficulty of gaining information about activation energies and heat of reactions, recent developments in quantum chemical calculations made it possible to estimate the energetic properties of molecular species with sufficient accuracy.[22,30,31]

The first step of formulating the microkinetic model is to calculate the equilibrium constants of all elementary reaction steps from the Gibbs free energy relation[16]:

$$K_{eq,i} = \frac{k_{i,for}}{k_{i,rev}} = \exp\left(-\frac{\Delta G^{o}{}_{i}}{k_B T}\right) = \exp\left(\frac{\Delta S^{o}{}_{i}}{k_B}\right)\exp\left(-\frac{\Delta H^{o}{}_{i}}{k_B T}\right) \quad (1.5)$$

Where $K_{eq,i}$ is the equilibrium constant, $k_{i,for}$ is the forward reaction constant, and $k_{i,rev}$ is the reverse reaction constant for the ith elementary step. ${\Delta G^o}_i$, ${\Delta S^o}_i$, and ${\Delta H^o}_i$ are the standard Gibbs free energy, entropy, and enthalpy changes, respectively. k_B is Boltzmann's constant and T is the reaction's temperature. The enthalpy of change for an elementary step could be calculated from the enthalpy of change of the gas-phase species and the change in the binding energy.

$$ {\Delta H^o}_i = {\Delta H^o}_{i,gas} + \Delta BE_i \tag{1.6} $$

The gas phase enthalpies can be obtained from standard references or could be calculated from chemical quantum methods when data are not available.[31] Similarly, the entropy of change for the gas-phase species can be obtained from standard references or from adding the calculated contributions of the translational, rotational, and vibrational entropies. In the case of adsorbed species and activated complexes on the surface, the translational and rotational modes are replaced by a vibrational entropy corresponding to the frustrated surface rotation and translation. In the limiting case when the adsorbed species is considered immobile, the molecule is assumed to retain part of the vibrational and rotational entropies of those of the gas and this is termed the local entropy. Accordingly, the local entropy of such adsorbed species is defined as:

$$ S_{ad} = F_{loc}(S_{rot} + S_{vib}) = F_{loc}S_{loc} \tag{1.7} $$

Where S_{ad} is the entropy of the adsorbed species, S_{loc} is the local entropy of the gas species, and F_{loc} is the fraction of the local entropy retained by the adsorbed species.

The next step is to calculate either the forward or reverse rate constants of every elementary reaction. For the adsorption and desorption steps, the adsorption rate constant is conveniently defined using collision theory. The adsorption rate constant is written as[22]:

$$k_{ads} = \frac{\sigma \exp\left(-\frac{E_{ads}}{RT}\right)}{\sqrt{2\pi m k_B T}} A_{site} \quad (1.8)$$

Where σ is the sticking probability of the adsorbing species, A_{site} is the area occupied per site, and E_{ads} is the adsorption activation energy and it is generally considered negligible.[22] After calculating the rate constants of the adsorption steps, the equilibrium constant of that step is used to calculate the desorption rate constant. For the surface elementary steps, the rate constants are defined in the endothermic or exothermic direction using the relation:

$$k_i = A \exp\left(\frac{-E_i}{RT}\right) \quad (1.9)$$

Where A is the preexponential factor in the selected reaction direction (endothermic or exothermic) and E_i is the activation energy barrier of that step in the same direction. The values for the preexponential factor and the activation energy could either be estimated or calculated by DFT methods.[20,31]

1.1.5 Co-feeding reactants as a way of tailoring reactions

Oxygenated hydrocarbons, whether aldehydes, ketones, or alcohols, are known to undergo chemical transformation over heterogeneous acid catalysts to produce a wide array of chemical products some of which are either undesirable or have a detrimental effect on the catalyst reactivity. One way of controlling the catalytic cycle in a way that tailors the reaction mechanism towards the desired outcome is by co-processing certain compounds alone with the feed. For example, the use of H-BEA zeolite is seen to produce a limited yield of high-octane gasoline (HOC) when converting methanol due to the formation of alkylated aromatics, which are known to deactivate the catalyst and reduce its lifetime and produce high yields of isobutane as a terminal product.[32] This is because such oxygenated hydrocarbon reactions are hydrogen deficient

leading to the excessive formation of unsaturated aromatic species that ends inside the catalyst pores blocking the acid sites. Given this challenge, it seems reasonable to alter the process in a way that limits the formation of the alkylated aromatics to prolong the catalyst life and maximize the utilization of byproducts (such as light alkanes) by converting them into gasoline range products. The modification of H-BEA with Cu was seen to facilitate the incorporation of hydrogen from co-fed H_2 into dimethyl ether homologation pathways resulting in a reduction of unsaturated aromatics in the product.[33] In addition, Cu/BEA was observed to activate the C-H bond in isobutane and produce gaseous H_2 suggesting a potential for re-entry of those species into the dimethyl ether homologation cycle.[34] The co-feeding of aromatics and olefins was also observed to influence the reaction mechanism of methanol conversion over H-ZSM-5 at 723K.[35] For instance, co-feeding p-xylene to methanol at 4 mol% increased both the overall conversion and the selectivities to aromatics and ethene. Similarly, co-feeding 4% of 1-pentene was observed to increase both the conversion and the pentenes products. This signifies the importance of co-processing olefins and aromatics in steering the conversion of methanol toward their respective catalytic cycles. As a way to improve the methanol-to-olefins process, the co-processing of light alkanes such as n-pentane along with methanol on H-ZSM-5 was seen to attenuate the catalyst deactivation by coke formation while reducing the byproduct methane.[36]

In another study, the rate of H-BEA-catalyzed alkylation of phenol with propylene was seen to increase with the co-feeding of water at a 1.4 molar ratio to phenol.[37] This was reasoned by noting the partial conversion of Lewis acid sites within the catalyst to Brønsted sites which are mainly responsible for the conversion enhancement. On the contrary, the presence of water in the feed or when generated as a byproduct of oxygenates dehydration is known to inhibit the C-C bond formation reactions on acid catalysts at relatively low reaction temperatures.[38] These two

findings emphasize that co-feeding different species into a reaction system not only influence the reactivities of different molecules but also could result in changes in the catalyst properties leading to different reaction mechanisms. These studies demonstrate the influence of co-feeding different reactants with oxygenated hydrocarbons and how they could enhance the catalytic process when properly utilized.

1.1.6 Examples of microkinetic models

A microkinetic model for ammonia synthesis over ruthenium catalyst was developed by Dahl et al.[39] Activity experiments were conducted at temperatures in the range of 320 to 440 ^{o}C at varying pressures of H_2 and N_2 mixtures between 1 to 100 bar. Their model consisted of 6 elementary reactions and assumed N_2 dissociation as the rate-controlling step while all other steps are in equilibrium. They formulated an expression to calculate the rate constant of the rate-determining and used measured or estimated energies, vibrational frequencies, and rotational constants to calculate the equilibrium constants for the other reactions. To obtain the reaction rates over the Ru-based catalyst, they used an ideal plug flow reactor model which was numerically treated by dividing it into a large number of reactors each treated as a continuously stirred tank (CSTR) reactor. By adjusting the adsorption energies of HN and HN_2 species and the number of active sites, the model was able to accurately predict the synthesis rates of ammonia at varying reaction conditions.

Kandoi et al[40] used both DFT and microkinetic modeling to compare the oxidation of H_2 by CO on (111) facets of Au, Cu, and Pt. Periodic, self-consistent total energy calculations based on gradient-corrected DFT (using DACAPO with Au(111), Cu(111), and Pt(111) surfaces presented as three-layer slabs with vacuum layers separating them) were performed to elucidate the reaction mechanism and the thermochemistry and activation energy barriers of each step. Using a set of 10

elementary steps to model the reaction, they concluded that variations in product selectivities among the tested metals were due to differences in the rate constants of CO and H oxidation reactions as well as their respective surface coverages.

Stegelmann et al[41] developed a microkinetic model for ethylene oxidation on Ag. By using available literature knowledge regarding surface chemistry, they proposed 17 elementary steps for the reaction mechanism and considered two different sites participating in the reaction namely, double Ag-Ag surface atoms and a surface oxide site formed by the dissociative adsorption of oxygen on Ag. Because the latter site was a result of the dissociation of O_2 on the catalyst surface, metallic Ag was considered the only kind of site. They used a set of steady-state site balance equations (for adsorbed species) and mass balance equations (for gas-phase species) modeled as a steady-state plug flow reactor. The rate constants of the adsorption and desorption steps were determined by collision theory from measured values of sticking coefficients and assuming zero adsorption activation barrier. Estimation of rate constants and Arrhenius parameters were made by fitting some of the literature results on similar reaction systems. Their developed simulation was able to reproduce laboratory-generated results with supported and unsupported Ag catalysts by only fitting the site densities to establish turnover frequencies corresponding to Ag(111) single crystal.

In another study, Kandoi et al[22] developed a microkinetic model for the methanol decomposition reaction on Pt meta. Based on periodic, self-consistent DFT calculations done on Pt(111) to study the competitive and minimum energy paths of the reaction[29], they were able to identify dominant reaction pathways, rate-determining steps, surface coverages by species, and the effect of pressure under practical reaction conditions. The model was developed by considering 13 elementary reactions and accounting for CO binding energy dependence on the catalyst surface

coverage. The model constituted three differential equations for the gaseous flow rates versus reactor length, nine steady-state fractional coverage equations for the adsorbed species, and one site balance equation. They used the fractional local entropy, the binding energies, the sticking coefficients, and the adsorption energies as fitting parameters for their experimental data using Athena Visual Workbench engineering software.[42]

Gokhale et al[31] conducted a detailed DFT-based microkinetic modeling of low-temperature water gas shift (WGS) reaction on copper. Estimates for the Zero-Point-Energy (ZPE) corrections, the binding energies, activation energies, and frequency factors for adsorbed intermediates were obtained from their DFT calculations. Entropies and heats of formation for gaseous species were obtained from standard references. They constructed the microkinetic model by considering 16 reactions and accounting for the CO binding energy dependence on the catalyst surface coverage. By fitting the model parameters, their model was able to reproduce two sets of experimental data (for both CSTR and PFR reactors) covering a wide range of temperatures, pressures, and feed compositions.

Aparicio et al[43] studied ammonia synthesis over iron catalyst and compared available kinetic models based on surface science data. They concluded that the available models can be used to extrapolate the surface science data to industrial conditions with great accuracy by increasing the activation energies and the pre-exponential of the N_2 dissociative adsorption step by 67 kJ mol^{-1} and by a factor of 1.6×10^5, respectively.

Aside from modeling reactions on metal surfaces, Alexopoulos et al[44] developed a detailed microkinetic model of ethanol dehydration on H-ZSM-5 zeolite using Brønsted acidity as reactive sites. They considered 21 elementary reactions derived from their periodic DFT calculations and used an isothermal plug flow reactor for the simulation.

1.1.7 Butanal reaction on acid catalysts

Over the years, there has been a growing interest in the utilization of bio-oils (sometimes referred to as pyrolysis oils) as either renewable fuels or for the production of a variety of chemicals ranging from food flavoring to biodegradable agricultural fertilizers.[45] Bio-oils are free-flowing dark brown liquids made of multicomponent mixtures derived from the depolymerization and fragmentation of cellulose, hemicellulose, and lignin.[45] However, inherent properties of bio-oils such as their poor volatility, coking ability, and high viscosity are behind their limited industrial applications. The challenges arising from the processing and conversion of bio-oils on acid catalysts are due to oxygenated hydrocarbons such as aldehydes and oxyphenols which are known to undergo thermal degradation by forming carbonaceous deposits on the catalyst surface resulting in its deactivation.[46] Because oxygenated hydrocarbons constitute the majority of bio-oils with contents reaching 60 wt, research efforts are focused on studying the reactivities of these different oxygenates on acid catalysts to shed light on their reaction mechanism and improve their catalytic conversion to valuable products.[35,38,47–52]

Aldehydes are one of the oxygenated hydrocarbons of interest which are known to react on both Brønsted and Lewis acid catalysts. Numerous research efforts have been devoted to studying the mechanism of aldehydes conversion on acid or base catalysts with the aid of various analytical and calculation techniques. One of the commonly encountered reactions is the aldol-type condensation where alkanal and alkanone molecules are coupled such that the carbon chain length is increased while the water molecule is ejected.[51] Acid-catalyzed C-C bond formation of this sort starts with keto-enol tautomerization of the alkanal to form a conjugate enol. The aldehyde or ketone molecule adsorbs on the Brønsted acid site through their oxygen to form a hydrogen-bonded complex as observed by both quantum chemical calculations, IR, and NMR results for the

H/D exchange on H-ZSM-5 zeolite.[26,53,54] This adsorption causes protonation of the carbonyl group and the proton transfer weakens the C=O bond evident by the lower vibrational shifts observed in the IR experiments. As the proton transfers from the Brønsted acid site to the carbonyl oxygen of the aldehyde, the neighboring framework oxygen of the catalyst attacks its alpha hydrogen forming an enol. The formed enol then attacks a nearby protonated aldehyde forming a new C-C bond which upon dehydration evolves a larger condensation product.[55] Aside from the aldol condensation, other reactions such as hydrogenation and dehydrogenation also occur to yield other olefins, dienes, and aromatic products.

1.2 Motivation

The utilization of renewable resources such as bio-oils to produce valuable fuel and petrochemical products makes an advantageous alternative to ever-depleting fossil fuel reserves. Bio-oils are free-flowing dark liquids that are primarily made of oxygenated hydrocarbons such as organic acids, alcohols, aldehydes, and ketones. The presence of the oxygen heteroatom in these compounds causes them to polymerize thereby increasing their boiling point range which results in processing difficulties. In addition, when processed over solid catalysts, these oxygenated hydrocarbons result in sever catalyst deactivation. Acidic molecular sieves such as zeolites stand as one of the highly selective and stable catalysts for the deoxygenation and conversion of oxygenated hydrocarbons into valuable products. However, the conversion of oxygenates on zeolites suffers from the prolonged deactivation caused by the deposition of heavy condensed products and the blocking of the active acid sites. Because the conversion of oxygenates is a hydrogen-deficient reaction, supplying external molecular hydrogen is envisioned to facilitate the removal of the heteroatom oxygen through dehydration. This could either be accomplished by co-feeding hydrogen or a hydrogen-donating species (such as alkanes) with the oxygenated

hydrocarbon. Besides providing molecular hydrogen, hydrogen-donating species such as alkanes could also favorably contribute to the catalytic cycle and steer the reactions to more desirable products. The modification of zeolites with transition metals such as Zn, Ga, and Cu is an effective method for dehydrogenating co-fed alkanes while still maintaining adequate dehydration ability for oxygenates. Zn/H-BEA is one notable example of a highly active and selective catalyst for the dehydrogenation and aromatization of light alkanes due to the combination of the strong acidity of the large-pore BEA zeolite and the hydride-transfer ability of Zn metal. Such a catalytic system could potentially be utilized to facilitate the deoxygenation or some of the less explored aldehydes such as butanal in the presence of co-fed alkane such as isobutane while simultaneously driving the reactions into more favorable products. Validating this potential approach requires a deeper understanding of the individual catalytic conversions of the aldehyde and alkane, the catalytic properties of different Zn species on Zn/H-BEA, and the combined reactivities of both reactants and their translation into any observed enhancement.

1.3 Dissertation objectives and structure

The objective of this research is to attempt to deoxygenate butanal (as a model compound representing bio-oils) by co-feeding isobutane as a hydrogen donor on Zn/H-BEA catalysts. The research aims at developing a microkinetic-based model to first explain the conversion of butanal on Zn/H-BEA catalysts with different metal loadings. This entails proper catalyst characterization to quantify and distinguish between Brønsted and Zn Lewis acid and to establish product-site relationships. The research also entails assessing the individual reactivities of butanal and isobutane on different Zn/H-BEA catalysts to clarify their distinctive contributions to the collaborative conversion in the case of their co-feed. More specifically, this research aims at addressing the following topics:

1. Assessing the reactivity of butanal on H-BEA and Zn/H-BEA zeolites at 200 ^{o}C and relating deactivation behaviors and formations of primary products to the different acid sites within each catalyst.
2. Developing a detailed kinetic model that accounts for the catalyst deactivation for the conversion of butanal on Zn/H-BEA catalysts to elucidate the influence of Zn on the binding energies and surface coverages of different reactive species as well as activation energies of all rection steps.
3. Understanding the reactivities of Zn/H-BEA catalysts for the conversion of butanal with isobutane co-feed at 300 ^{o}C and explaining their observed conversion synergies based on prior catalytic and kinetic knowledge.

To achieve this objective, the research is broken down into sections presented as successive chapters. Chapter 2 introduces the reaction setup and experimental methods used to conduct this research. Chapter 3 explores the reactivities of different oxygenated hydrocarbons on acidic zeolites by comparing their reaction mechanisms and experimentally testing their conversions on the H-BEA zeolite. Chapter 4 investigates the reactivity of Zn/H-BEA zeolites prepared to contain different metal species that include $Zn(OH)^{+}$, $[Zn\text{-}O\text{-}Zn]^{2+}$, $[Zn\text{-}O\text{-}Al]^{2+}$, and ZnO in converting butanal. The metal loadings of the resulting Zn/H-BEA catalysts were determined by inductively coupled plasma – optical emission spectrometry. Temperature programed desorption (TPD) of isopropylamine was used to quantify and distinguish between Brønsted and different Zn Lewis acid sites. Brønsted acid site densities were measured by *in situ* titration with 2,3-di-tert-butyl-pyridine during acid-catalyzed isopropanol conversion. Using the catalysts with different Zn loadings, the conversion of butanal was investigated to note the influence of the metal local structures on rates and selectivities to various products at 200 ^{o}C.

Chapter 5 walks the reader through the development of a detailed kinetic model for the conversion of butanal over Zn/H-BEA catalysts with different metal loadings. The kinetic model was developed based on the derived reaction sequence from the product selectivity trends over H-BEA catalysts and using kinetic and thermodynamic parameters that were estimated by fitting the experimental turnover rates over each catalyst. The ion exchange with Na^+ was used as a technique to control the concentration of Brønsted acid sites on H-BEA. The concertations of Brønsted and Lewis acid sites were measured by acid site iteration experiments with pyridine as a probe molecule. The modeling results show how changes in metal loading, acid sites, and metal type make measurable alterations in the binding energies of reactive species, the activation energies to primary reactions, and the surface coverages of adsorbed reactants.

Chapter 6 reports the conversion of butanal with isobutane co-feeding on Zn/H-BEA at 200 and 300 ^oC. The catalysts were loaded with Zn using ion exchange to produce samples with varying Zn/Al ratios. Temperature programed desorption (TPD) of isopropylamine was used to quantify the proportions of Brønsted and different Zn Lewis acid sites on the catalysts. The objective of this work was to capitalize on the results from the kinetic model of butanal to identify the proper loading and proportions of Zn sites on H-BEA zeolite which result in enhancing the deoxygenation reaction of butanal with isobutane co-feed, increasing the selectivity to aromatics, and improving the catalyst stability. This was accomplished by assessing the reactivities of butanal and isobutane individually to construct simplified reaction sequences which were used to explain their collaborative chemistries in the co-feeding experiments.

Chapter 2: Experimental methods and setups

2.1 Reactor and catalyst systems

2.1.1 Experimental setup

All kinetic and reaction studies were conducted using a stainless-steel tubular reactor with a 6.4 mm outer diameter placed inside a ceramic shell furnace (Series 3210 Applied Tests Systems). The temperature of the reactor was controlled by a K-type Omega thermocouple which was attached to the external surface of the reactor tube. The temperature was controlled by an EZ-ZONE PM Express PID temperature controller (Watlow, USA). Three gas flow controllers of the type GE50A (MKS Instruments, USA) were used to control the flow of all gases going into the reactor. The liquid feeds were introduced by 1-5 ml gas-tight syringes (SGE, USA) through a NE-1000 syringe pump (New Era Pump Systems, USA). All the gas lines were heated at 180 ^{o}C with electrical resistance thermal tapes by manually adjusting the heating voltage and checking the temperatures with read-out thermocouples placed along the lines. The outlet gas streams were analyzed using online gas chromatography (7518A Agilent Technologies, USA) connected to mass spectroscopy (5977A Agilent Technologies, USA). The GC was equipped with a Flame Ionization Detector (FID) and used an HP-5ms UI column (30 m, 0.25 mm, 0.25 μm). **Figure 2.1** shows the reactor setup used in all studies.

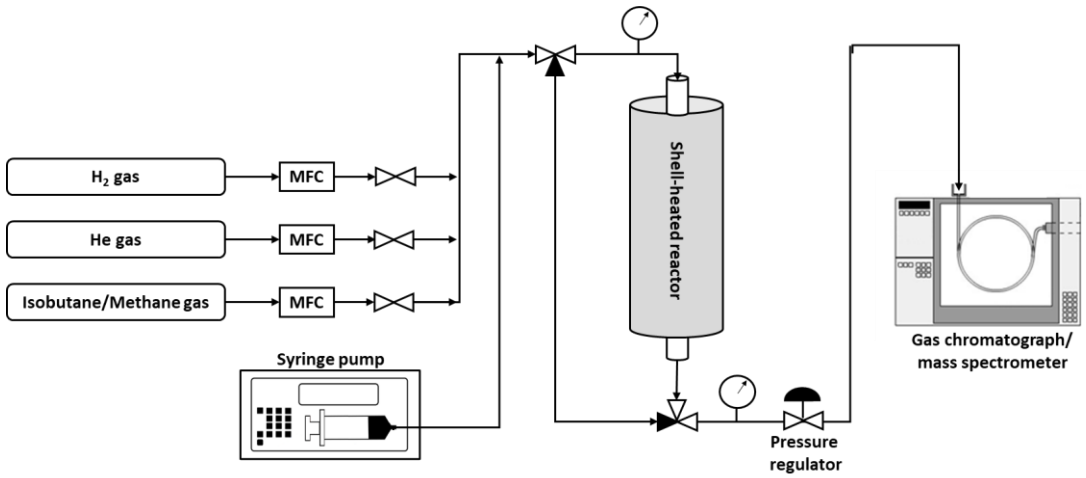

Figure 2.1: The experimental setup used for the reaction and kinetic studies in this research.

2.1.2 Catalyst selection and preparation

All solid catalysts used for the reaction studies were crushed and sieved to 60 - 80 mesh size (0.177 – 0.250 mm). The particle size range was chosen to ensure adequate bed porosity to avoid pressure buildup across the reactor while minimizing mass transfer fragments. As the primary type of catalyst for the study, zeolite NH_4-BEA with a Si/Al ratio of 12.5 (Zeolyst International, USA) was heated to 500 ^oC at a 1 $^oC\ min^{-1}$ rate for 4 hours in flowing dry air to convert it into the acidic form H-BEA upon ammonia desorption. Zeolite BEA (12-membered ring openings and 0.66×0.67 nm channel sizes) in its acidic form H-BEA was selected as the main catalyst for this research due to its high activity in dimethyl ether (DME) homologation and conversion to higher hydrocarbons such as 2,2,3-trimethylbutane.[56] In addition, H-BEA zeolites are known for their hydride transfer ability during the conversion of DME to C_7 hydrocarbons indicative of their high selectivity to triptyl isomers and as revealed by C^{13} labeling experiments.[28,57] H-BEA hydride transfer property was also evident from the co-homologation of light alkanes with DME resulting in a decreased formation of unsaturated

aromatics.[58] In order to vary the acid site concentration within the catalyst (Bronsted and Lewis acid sites), batches of H-BEA were ion-exchanged with different concentrations (0.01 – 0.5 M) of NaCl aqueous solutions to obtain different loadings of Na^+. In a typical ion exchange experiment, a certain amount of H-BEA was mixed with NaCl solution at 80 ^oC for 2 hours and this procedure was repeated three times.[59] The solids were separated from the solution by centrifugation (at 3000 rpm for 5 minutes) then washed with deionized and separated using the same method. The resulting solids were dried in flowing air at 90 ^oC overnight to obtain the sodium-exchanged zeolite Na-BEA. The use of Na^+ in exchanged zeolites has proven to be an effective way of poisoning the Bronsted acid sites without inducing major structural changes to the zeolite.[51] To synthesize the hydride transfer catalyst, H-BEA was mixed with an aqueous solution of zinc acetate or nitrate (0.01 – 0.06 M) and stirred at 80 ^oC for 2 - 14 hours. Then, the solids were separated using the same centrifugation procedure mentioned earlier and washed with deionized water up to three times. The solid sample was dried at 90 ^oC overnight before calcining at 500 ^oC in dry air.

2.1.3 Reaction experiments

A predetermined amount of catalyst (10 -100 mg) was loaded into the tubular reactor by placing it between two plugs of quartz wool. The thermocouple of the furnace controller was attached to the outer surface of the reactor where the catalyst bed was held using a thermally resistant tape. The reactor temperature was increased at a rate of 10 $^oC\ min^{-1}$ while purging the catalyst bed with 99.99% He gas (Airgas, USA) at 20 ml min^{-1} until reaching the desired temperature. After stabilizing the reactor temperature, the flow of He gas was directed to the bypass position while adjusting the gas flow to the desired feeding rate of 30 – 120 ml min^{-1}. At the same time, the liquid feed was introduced by the syringe pump at a flow of 1 – 10 µl min^{-1} to

a gas-mixing zone (heated to 10 ^{o}C above the boiling point of the feed) where the liquid was evaporated and swept with the He gas. The feed mixture was allowed to stabilize the feed composition before switching the flow to the reactor to start the reaction and gas analysis.

2.1.4 Zeolite acidity measurement

2.1.4.1 Acid titration with pyridine and 2,3-di-tert-butyl-pyridine

Acid site titration was chosen as the technique of choice to determine the total acidity of the zeolite and the relative Brønsted and Lewis site densities as the most predominant acid sites in such solid catalysts. The advantage of using acid site titration techniques is the ability to probe the acidity of the catalyst at normal operating conditions as opposed to other chemisorption techniques which could operate at conditions very far from relevant.[60] Pyridine as a strong base molecule was used to titrate the acidity of the zeolite and the number of acid sites was determined assuming a 1:1 adsorption stoichiometry. 2,6-di-tert-butyl-pyridine was used to selectively titrate and identify Brønsted acid sites using the same stoichiometric relation. 2,6-di-tert-butyl-pyridine has been shown to titrate Brønsted acid sites by observing the direct correlation between the absorption IR spectroscopy band in zeolite BEA and the cracking activity.[61] This is because the hindrance around the nitrogen atom in this molecule makes the coordination to Lewis acid sites difficult.[62] As opposed to acid site titration, IR spectroscopy techniques require knowledge of reliable extension factors to accurately quantify relative Brønsted and Lewis acid sites which are often difficult to obtain.[4]

A mixture of either pyridine (99.8%, Sigma Aldrich) or 2,6-di-tert-butyl-pyridine (>97%, Sigma Aldrich) in isopropanol (95.5%, Sigma Aldrich) resulting in a molar ratio of 1:250 was used to titrate the total (Brønsted and Lewis acid sites) and Brønsted acid sites, respectively. In a typical titration experiment and using the same setup for the reaction studies, the titrant mixture was fed

into a gas-mixing vaporization zone heated at 130 ^{o}C and mixed with flowing He (UHP >99.999%, Praxair) resulting in a stream containing 11.4 kPa isopropanol and 45.6 Pa titrant. The turnover rates of isopropanol dehydration over the tested catalysts were measured while simultaneously calculating the cumulative pyridine or 2,6-di-tert-butyl-pyridine adsorption rate. The titrant uptake was calculated from the difference between the concentration of the titrant in the feed and the gas outlet. The titration experiment was considered complete when the concentration of isopropanol in the effluent gas became steady for one hour.

2.1.4.2 Temperature-programed-desorption (TPD) of isopropylamine

The reactive desorption of isopropylamine has been used to quantify the amounts of Brønsted and different Zn Lewis acid sites. Isopropylamine adsorbs on Brønsted acid sites and forms isopropyl ammonium ion which decomposes upon heating via Hoffmann elimination reaction to yield propylene and ammonia.[63] Isopropylamine TPD has been widely used as a technique to quantify Brønsted sites on metal-loaded zeolites including BEA and ZSM-5. [64–66] In addition to quantifying Brønsted acid sites, this technique has also been used to quantify and distinguish between different Lewis acid sites generated by the incorporation of Zn into the zeolites. [67,68] In every TPD experiment, 20 mg of catalyst was saturated with a stream of isopropylamine gas (2.75 kPa in He) at 40 ^{o}C for 1 hour. The catalyst was then purged with 20 ml min^{-1} of He gas (UHP >99.999%, Praxair) for 1 hour to strip off weakly adsorbed isopropylamine. After that, the reactor temperature was raised from 40 ^{o}C (at 5 ^{o}C min^{-1} rate) to 680 ^{o}C while monitoring the reactor effluent gases with a GC-MS. The total amounts of desorbed propylene were quantified from the MS signals at 41 m/z.

2.2 Reaction system checkup

2.2.1 Gas chromatograph (GC)

A set of experiments were performed to verify the performance of the GC to ensure a linear response (concentration) given by the FID detector upon analyte concentration change. To check the FID response, different concentrations of methanol and butanol were analyzed by the GC and the area responses were measured and compared. It is known that the response of the FID is linearly proportional to the total number of carbons in the analyzed hydrocarbon feed irrespective of its structure or functional groups.[69] This unique property allows calculating the concentrations of the unknown products in a complex mixture by relating their FID weight responses to the response of a single compound with a known concentration. **Figure 2.2** shows the FID area response as a function of inlet carbon concentrations using different concentrations of methanol and butanol. As can be observed from **Figure 2.2**a, the FID response given in arbitrary unit (a.u.) seems to deviate from linearity as the concentration is increased. By adjusting the dilution of the sample analyzed by the GC (by the feed split ratio) and running additional experiments, it was concluded that acceptable response linearity is achieved at below 4.0×10^{8} FID response unit. **Figure 2.2**b shows the response to different carbon concentrations withing this suggested response region.

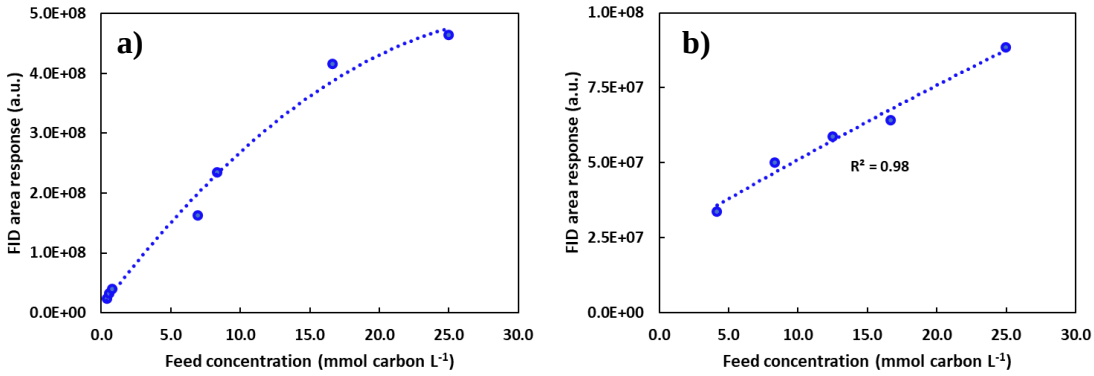

Figure 2.2: Response area of the FID at different carbon concentrations from different methanol and butanol mixtures in He

2.2.2 Diffusion-free kinetics check

One of the commonly practiced tests to check the influence of diffusional limitations on the rate of a gas-phase reaction on a solid catalyst is by observing the conversion when the flow to the reactor is changed at constant space velocity. If the conversion stays invariant, this would indicate the absence of diffusional mass transfer resistance.[55] **Figure 2.3** shows butanal conversion change on H-BEA at 200 ^{o}C when the total flow is changed at the same space velocity. As can be observed from **Figure 2.3**, the conversion and selectivity trends are almost invariant when the total flow was doubled. This proves a diffusion-free condition for the experimental setup and the conditions used.

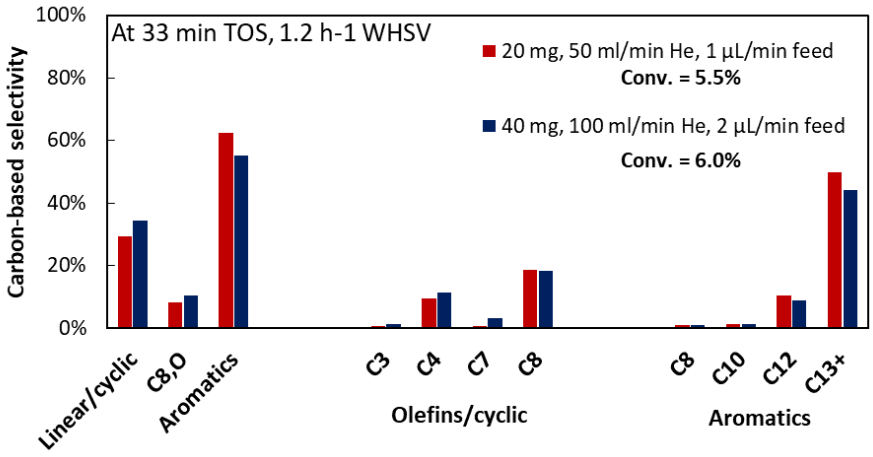

Figure 2.3: The influence of doubling the flow rates of butyraldehyde over H-BEA at 200 ^{o}C and constant WHSV (13.7 h^{-1}) on the selectivity and conversion.

Another more rigorous test is the Koros-Nowak[55] criterion which states that in the kinetic regime, the rate of the catalytic reaction is proportional to the number of active sites per catalyst volume or weight. This means that plotting the reaction rate versus the number of active sites within a catalyst would result in a straight-line relationship.[70] To test this criterion, a set of Na^{+} exchanged H-BEA zeolites were prepared to vary the acid site concentrations. These zeolites were tested for the conversion of butanal at 200 ^{o}C. By plotting the overall reaction rates versus the concentration of the acid sites (Brønsted and Lewis) a linear relationship was obtained as depicted in **Figure 2.4**. These tests indicates that our catalytic system and conditions are free from transport fragments and that measured reaction rates are purely intrinsic.

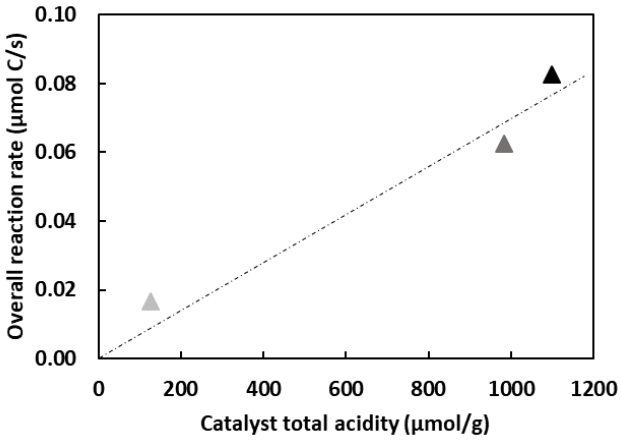

Figure 2.4: Total acidity of Na/H-BEA zeolites versus the turnover rates of butanal at 200 ^{o}C and 13.7 h^{-1} WHSV

Chapter 3: Comparing the reactivities of different oxygenates on H-BEA zeolite

3.1 Introduction

The increasing global demand for energy and for products that feed into industrial revolutions has fueled interest in developing processes that maximize the utilization of renewable sources like natural gas and biomass to meet these demands. Biomass feeds can be obtained from cheap plant-based sources such as lignocellulose which can be derived from various feedstocks that include forest wastes (e.g. wood and logging residues), agricultural wastes (e.g. corn stover and crop residues), energy crops (e.g. corn, sugar cane, and grass), and aquatic plants (e.g. hyacinth).[71] The thermal decomposition of lignocellulose in the absence of oxygen is one of the rapidly developing methods to produce fuel oils from biomass. Commonly known as fast pyrolysis, this method is responsible for the production of high yields of bio-oils which are dark and free-flowing liquids that contain a wide range of organic-oxygenated hydrocarbons and has the potential for replacing petroleum fuels.[72] However, the intrinsic properties of these bio-oils as compared with fossil fuel sources create a bottleneck for their processing and utilization in industrial applications. The high viscosity, wide boiling range, corrosiveness, and high miscibility with water are some of the challenges of bio-oils and most of which are tied to their high oxygen contents which could range from 35 to 40 wt%.[45] Methanol is another bio-based feedstock that has high utilization potential and could be obtained by the conversion of syngas (obtained by steam reforming of natural gas or thigh the gasification of biomass) into methanol through the reverse of the water-gas-shift (WGS) reaction.[73] The heavier alcohol ethanol, which is mostly produced through the fermentation of agricultural products such as sugar corps and starch, is also another

important feedstock that finds extensive application in transportation fuels.[74] While the majority of C_2+ alcohols like n-propanol, i-propanol, and n-butanol are primarily produced from nonrenewable petrochemical feedstocks, there is a reasonable potential for their production from biological sources.[75]

The availability of oxygenates from renewable sources and the ever-growing demand for specialty products which are normally of fossil-based origins promoted the discoveries of new catalytic systems that target the conversion of these oxygenates into more value-added products. Brønsted acid zeolites have found extensive applications in the conversion of methanol[76–78], C_2+ alcohols[79–83], and aldehydes and ketones[10,55,84–86] to various hydrocarbons. The distinction in reactivities among each of these oxygenates given by their structures and chemical affinities towards different Brønsted and Lewis acid sites is what dictates their conversion products. Therefore, a deeper understanding of the surface reaction steps of various oxygenated hydrocarbons like alcohols, aldehydes, and ketones is paramount for proper feed selection and catalyst design. In this chapter, we aim to explore the mechanistic details of the conversion of alcohol on the zeolites and compare them with the conversion of aldehydes (or ketones). The goal is to establish a fundamental structure-reactivity relationship to explain the catalysis of these oxygenates and their evolution into heavier and oxygen-free products.

3.2 Mechanism of oxygenates conversion on zeolites

3.2.1 Methanol conversion

Since the discovery of the methanol-to-hydrocarbon (MTH) process over acid catalysts by Mobil Research Laboratories in 1976[87], there have been interests in understanding the origin of the first C-C bond formation mechanism and how subsequent methylation results in the expansive

reaction products. The general consensus about the mechanism of methanol conversion is that there is an induction period where the first olefin forms from a hydrocarbon pool on the catalyst surface, then progressive methylation of the olefins would lead to larger products.[88] Experimental and theoretical evidence on Brønsted acid catalysts have backed up the mechanism of the methylation of the formed olefin (or aromatic) suggesting either 1) the formation of a surface methoxide following the dehydration of methanol or dimethyl ether (DME) which desorbs upon its reaction with an olefin or 2) the co-adsorption of the methanol with the olefin on a single acid site and their subsequent reaction.[24,88] Scheme 3.1 shows the mechanism of methoxide formation and the subsequent reaction with methanol to form dimethyl ether (DME).[89] Scheme 3.2 demonstrates the mechanism of olefin methylation with methoxide surface species which represents the pathway for carbon chain growth in methanol conversion on Brønsted acid sites.

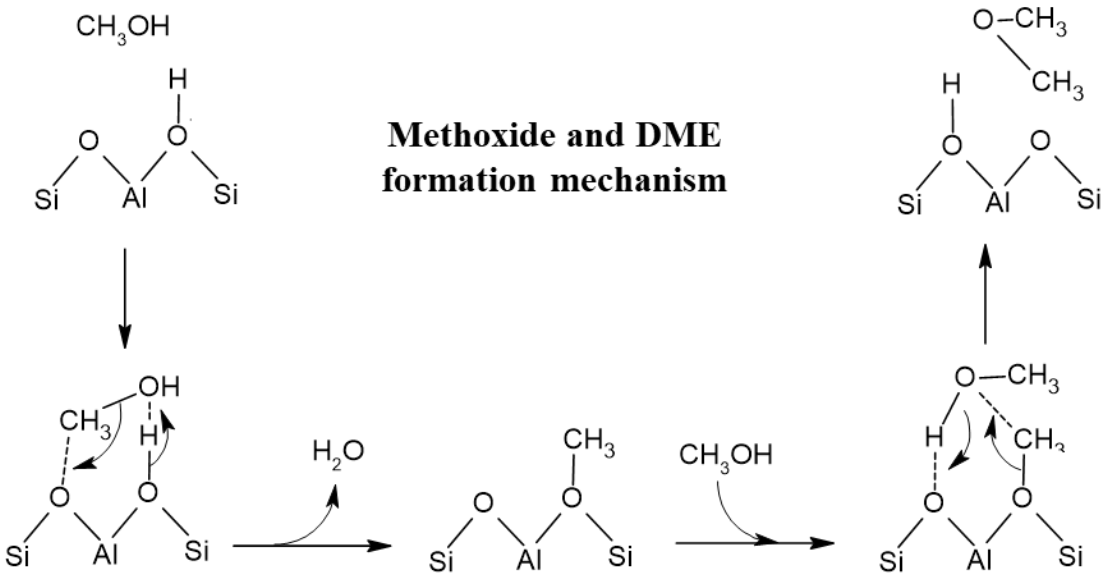

Scheme 3.1: Mechanism of methoxide and DME formation on Brønsted acid sites.

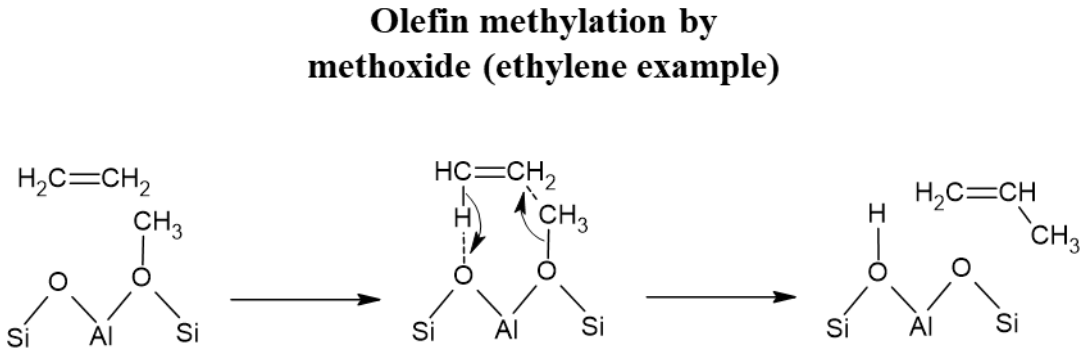

Scheme 3.2: The mechanism of olefin methylation (ethylene example) with methoxide species resulting from methanol conversion on Brønsted acid sites

Besides Brønsted acid sites, DME also forms on Lewis acid sites but requires the adsorption of two methanol molecules which then form DME upon dehydration. [90] Even though the primary product DME contains an oxygen heteroatom, its subsequent reactions combined with the methylation events with methoxide species all favor the dehydration and oxygen removal resulting in mainly olefinic and aromatic products that are mostly oxygen-free. [87]

3.2.2 C_2+ alcohols conversion

Unlike methanol, the mechanism of C_2+ conversion on Brønsted acid sites starts with the non-dissociative adsorption of the OH on the catalyst proton (cation) with the lattice oxygen (anion) interacting with the α-hydrogen of the alcohol.[62,91] Depending on the reaction conditions on Brønsted acid catalysts, C_2+ alcohols could also undergo dehydrogenation into the corresponding aldehydes or combine with another alcohol to yield ethers upon dehydration.[79,83,92] Scheme 3.3 shows the mechanism of ethanol dehydration on Brønsted acid sites.

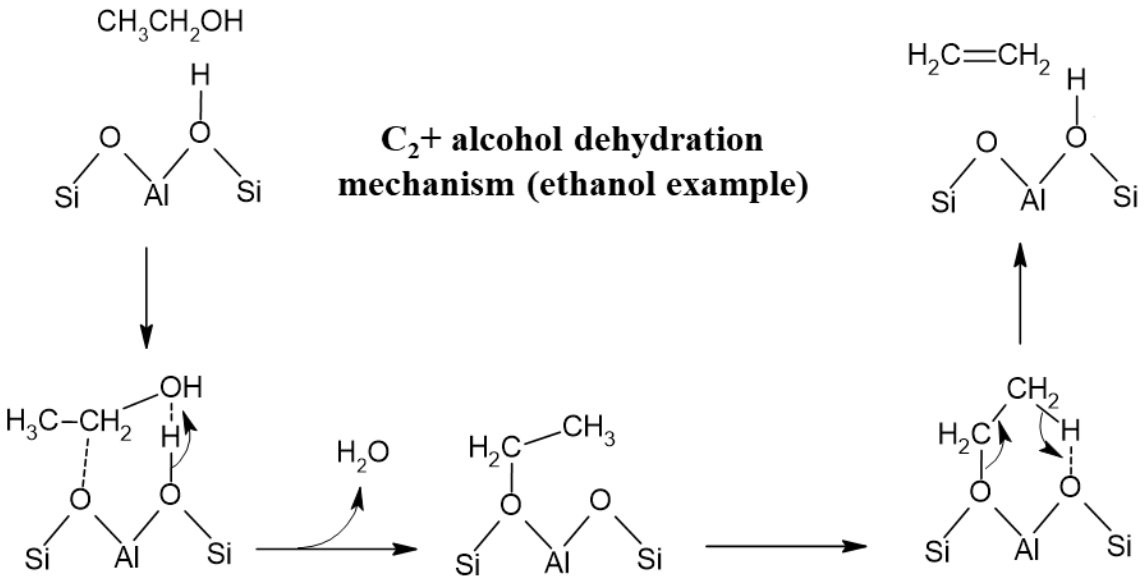

Scheme 3.3: The mechanism of C_2+ alcohol dehydration (ethanol example) to the corresponding olefin on Brønsted acid sites.

Because the dehydration of C_2+ alcohols primarily yields their corresponding olefins, the propagation of the C_2+ alcohols into heavier products relies on the oligomerization reactions between these olefins.[93] This has led to research efforts attempting to directly convert alcohols to higher olefins and aromatics over zeolite catalysts.[80,81,94] Scheme 3.4 shows the mechanism of ethylene oligomerization to butenes.

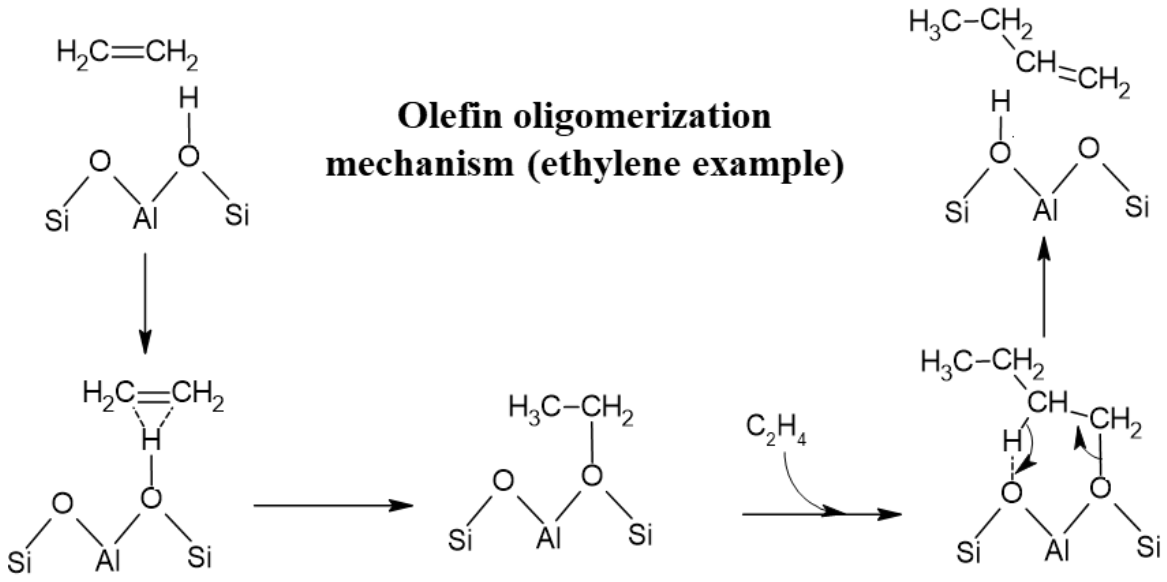

Scheme 3.4: The mechanism of olefin (ethylene example) oligomerization on Bronsted acid sites as the main chain growth pathway for C_2+ alcohol conversion.

3.2.3 Aldehydes and ketones conversion

The first step that aldehydes and ketones encounter during their transformation on Brønsted acid sites is keto-enol tautomerization.[53] In this step, the aldehyde or ketone interacts with the acid and base pairs of the zeolite resulting in a proton transferring to its carbonyl oxygen. At the same time, the aldehyde or the ketone adsorbs on the Brønsted acid site through the carbonyl oxygen atom causing its protonation.[26] The formed enol from the tautomerization step then attacks this protonated aldehyde creating an intermolecular C-C bond which results in generating a larger unsaturated aldehyde after dehydration.[95] Supported by both experimental and theoretical evidence[96], the mechanism of this aldol-condensation reaction is depicted in Scheme 3.5.

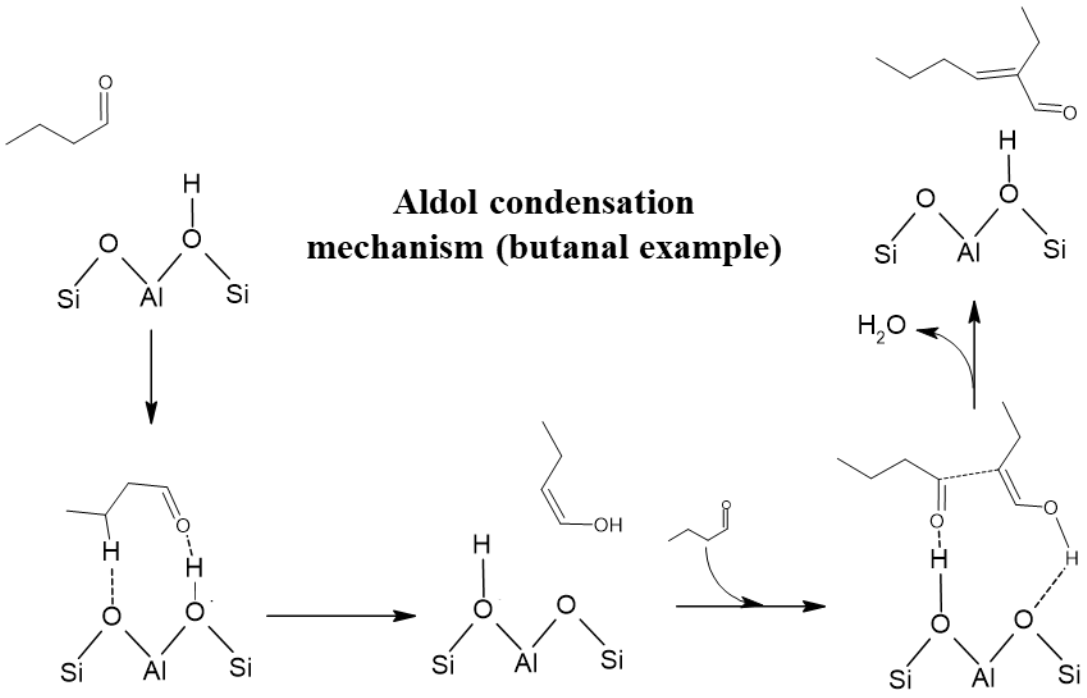

Scheme 3.5: The mechanism of the aldol condensation reaction of aldehydes (butanal example) on Brønsted acid sites.

The unique chemistry of aldehydes and ketones compared with that of alcohols is the reason why the conversion of the former results in a wide range of oxygenated hydrocarbons, especially at low temperatures.[51,87] This also results in aldehydes and ketones becoming much more reactive in producing aromatic compounds through the aldol condensation mechanism compared with the oligomerization of olefins containing the same number of carbon atoms.[48] Because the main mechanism of carbon chain growth of C_2+ alcohols is through olefin oligomerization, this makes aldehydes and ketones much more reactive than their counterpart alcohols.

3.3 Experimental comparison of the conversion of butanol and butanal on H-BEA zeolite

Because bio-oils contain a wide range of oxygenated hydrocarbons which include organic acids, alcohols, aldehydes, and ketones, understanding the reactivities of each class of these molecules is paramount for proper product-specific catalyst designs. As an active catalyst, zeolite BEA has been used to study the conversion of butanol and butanal to compare the reactivities of alcohols and aldehydes with the same number of carbon atoms. **Figure 3.1** shows the selectivity of different products when converting butanol and butanal on H-BEA zeolite at 250 ^{o}C. As can be observed from **Figure 3.1**a, the conversion of butanol was nearly invariant at 100% over the 66 minutes of time-on-stream (TOS) with butenes as the primary dehydration product. Despite the complete butanol conversion, product selectivities were observed to slightly change with TOS and this result is in line with similar literature results suggesting potential deactivation behavior caused by heavy product deposits.[79] On the other hand, butanal overall conversion (**Figure 3.1**b) was seen to decrease from 18 to 13% over a 44 TOS period. This indicates that the butanal reaction produced heavy condensed products that might have resulted in catalyst deactivation by blocking the active sites. This type of deactivation was expected to happen as a result of aldol condensation reactions over acid catalysts.[46] Another observation was that all products resulting from butanol conversion were oxygen-free whereas the majority of the products from butanal contained at least one heteroatom oxygen.

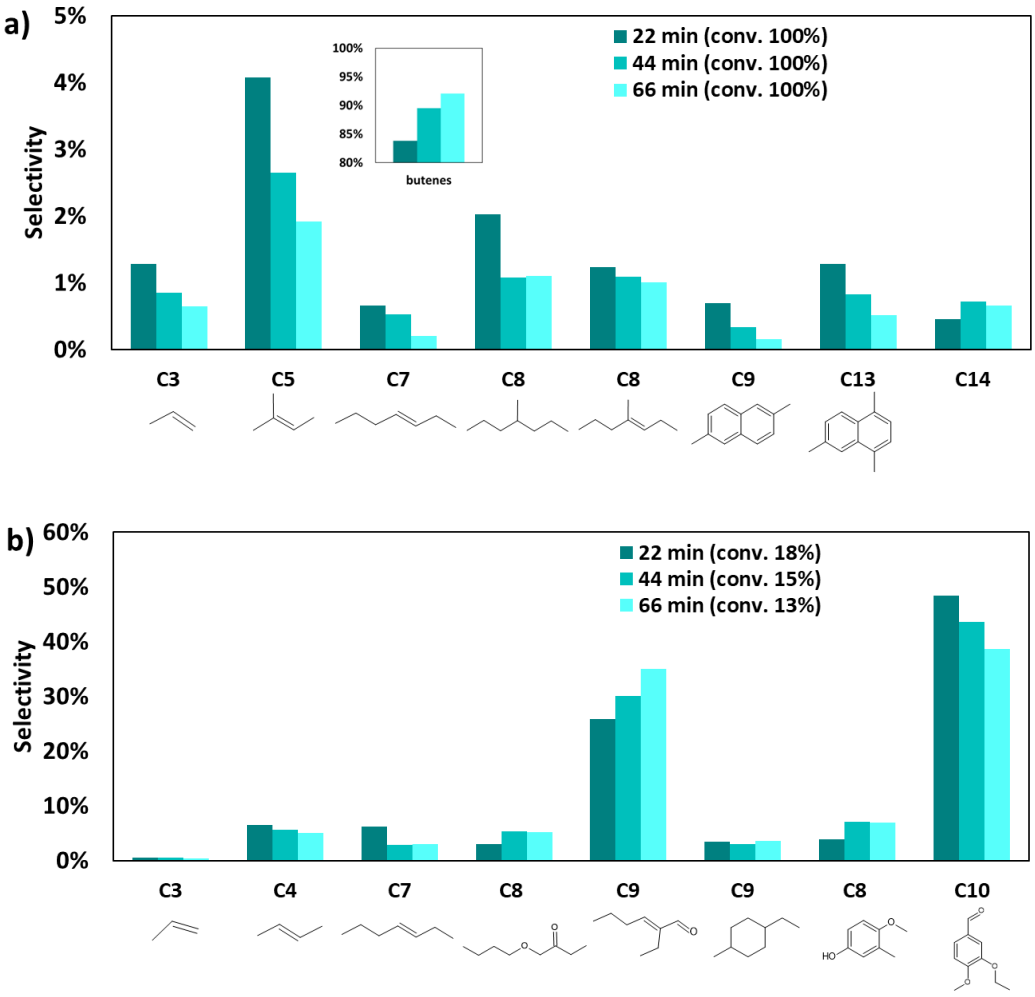

Figure 3.1: Comparing the conversion of a) butanol and b) butanal on H-BEA. Reactants were fed at 5.11 kPa in He gas over 100 mg of catalyst (WHSV=9.8 h^{-1}) at 250 ^{o}C.

Chapter 4: The influence of Zn/H-BEA acid sites on the conversion of butanal

4.1 Introduction

Zeolites modified with transition metals such as Zn have been shown to be active catalysts for the conversion of light alkanes to aromatics.[97–100] Zn sites also facilitate alkane dehydrogenation over zeolites to increase hydrodesulfurization rates during thiophene desulfurization reactions.[101,102] Some studies demonstrate that desulfurization-derived species interact with hydrogen-donating and enable the desorption of aromatic intermediates preventing catalyst coking and deactivation. Zeolites modified with Zn are known to participate in both alkane dehydrogenation and C-C bond cleavage resulting from the collaborative activity of strong Brønsted acid and Zn Lewis acid sites. Depending on the preparation method, Zn species could exist as $Zn(OH)^+$ ions exchanged to one aluminum site[67,103], Zn^{2+} exchanged to two aluminum sites $[Zn\text{-}O\text{-}Al]^{2+}$ [67,103,104], two aluminum-exchanged Zn^{2+} bridged by oxygen $[Zn\text{-}O\text{-}Zn]^{2+}$ [67,103,105,106], extra-pore large ZnO clusters or isolated Zn^{2+} ions at the cation-exchange site[107–110]. There are a number of commonly used methods to prepare Zn-exchanged zeolites including incipient wetness impregnation (IWI), ion exchange, and chemical vapor deposition techniques (CVD). Incipient wetness impregnation techniques result in homogeneous species of Zn sites with higher Zn content.[97,111] Chemical vapor deposition techniques form isolated Zn^{2+} cations from the interaction of Brønsted acid sites with the vapor of metallic zinc [100,109,112,113]. On the other hand, ion exchange techniques with solutions from various Zn precursors result mainly in $Zn(OH)^+$ ions, binuclear $[Zn\text{-}O\text{-}Zn]^{2+}$ clusters, and Zn^{2+} exchanged to two aluminum sites. Unlike the ZnO clusters and isolated Zn^{2+} cations which have been

extensively applied to alkane activation and aromatization [100,110,111,114], examining the Zn^{2+} exchanged to neighboring aluminum and the binuclear $[Zn\text{-}O\text{-}Zn]^{2+}$ sites is crucial to understanding the nature of Zn sites for better catalyst design. Penzien et al.[67] have demonstrated the ability to prepare BEA zeolites with well-defined Zn^{2+} species using ion exchange for metal loading. The systematic preparation of Zn/H-BEA by ion exchange would, therefore, allow probing of their catalytic activity for the conversion of hydrocarbons.

Aldehydes are known to undergo different reactions over acid, base, or acid-base bifunctional catalysts resulting in the formation of new C-C bonds and the removal of oxygen heteroatom.[52,115,116] The conversion of butanal was used to compare the reactivities of the Zn/H-BEA catalysts and note the contributions of different catalytic sites to the various reaction routes. Butanal conversion on acidic and basic catalytic sites is known to proceed through distinct parallel and sequential routes which can be broken into 3 primary pathways, each containing characteristic species prior to ring-closing reactions to form arenes. The dehydration-hydrogenation pathway is characterized by selectivity towards butenes and butadienes. 2-ethyl-2-hexenal is the primary product of the aldol condensation pathway. Finally, Tishchenko esterification yields butyl butanoate which subsequently forms heptanone upon losing CO and hydrogen.[47,117] Because Zn species could retain different coordination, and therefore different activities, within Zn exchanged zeolite framework depending on the metal loading and the temperature treatment [103], it is desirable to relate these different sites to the aforementioned three catalytic routes of butanal conversion.

In this study, we explore the reactivity of butanal on Zn/H-BEA samples prepared to contain $Zn(OH)^{+}$, $[Zn\text{-}O\text{-}Zn]^{2+}$, and Zn^{2+} cations. The chemical composition of the resulting Zn/H-BEA samples was determined by inductively coupled plasma–optical emission spectrometry (ICP-

OES). Brønsted acid site density was measured by *in situ* titration during acid-catalyzed isopropanol dehydration using 2,6-di-tert-butyl-pyridine as a probe molecule. We also investigated the conversion of butanal over a range of Zn loadings on Zn/H-BEA to probe how the local structure of Zn sites influences the rates and selectivity of the various pathways of butanal reaction.

4.2 Experimental methods

4.2.1 Catalyst synthesis

Zeolite NH_4-BEA Si/Al 12.5 (Zeolyst International) was heated to 500^{o}C (at 1 ^{o}C s^{-1}) for 4 h in flowing dry air to synthesize the acidic form of zeolite BEA (H-BEA). To prepare Zn/H-BEA samples, H-BEA was mixed in aqueous solutions of zinc acetate (0.02-0.06 M) and stirred at 80 ^{o}C for 14 to 69 h. The solids were then separated from the solutions by centrifugation at 3000 rpm for 5 min and then washed with excess deionized water. The samples were then dried at 40 ^{o}C for 20 h and temperature treated in flowing dry air. For Zn/H-BEA samples with Zn/Al ratios less than 0.15, the temperature treatment was RT to 120 ^{o}C, 0.5 ^{o}C/min; 120 ^{o}C, 3h; 120 - 500 ^{o}C, 1 ^{o}C/min; 500 ^{o}C, 2 h. For samples with Zn/Al greater than 0.15, the temperature treatment was RT to 500 ^{o}C, 5 ^{o}C/min; 500 ^{o}C, 5 h. This synthesis method has been shown to create well-defined Zn^{2+} Lewis acid sites in BEA zeolites.[67,103] All catalysts were pressed and sieved to 60-80 US mesh (177 – 250 μm agglomerate diameter) to minimize the effects of mass transfer artifacts on reaction kinetics data.

4.2.2 Catalyst characterization

To determine the chemical composition of the Zn/H-BEA samples, the catalysts were mixed in 1 M HNO_3 and sonicated at 50 ^{o}C for 4 hours to ensure full digestion of the solids. The

concentrations of the elements were measured through ICP-OES (Avio 200, Perkin Elmer). The measured concentrations were used to calculate concentrations of Zn, Si, and Al for the zeolites.

The number of active Brønsted acid sites was quantified during isopropanol dehydration catalysis by *in situ* titration with 2,6-di-tert-butyl-pyridine (≥97%, Sigma Aldrich). 2,6-di-tert-butyl-pyridine is a base molecule that has been shown to effectively titrate Brønsted acid sites on solid catalysts.[118] Quantification of the acid site concentrations was carried out in the same reactor system as the reaction kinetic studies. Steady-state measurements of isopropanol dehydration during titration were performed in the reactor heated at 200 ^{o}C (at 1.0 ^{o}C s^{-1}). A mixture of the titrant in isopropanol (molar ratio of 250:1 isopropanol to titrant) was fed into the vaporization zone heated at 130 ^{o}C with flowing He (UHP >99.999%, Praxair) forming a stream containing 1.55 kPa isopropanol and 6.25 Pa titrant. Cumulative 2,6-di-tert-butyl-pyridine uptake was calculated from the difference in titrant concentration in feed and effluent vapor stream as measured by online gas chromatography. The titration was considered complete after an hour of steady-state isopropanol concentration in the effluent stream.

Temperature-programmed-desorption (TPD) of isopropylamine (> 99.5% Sigma Aldrich) was conducted in the same reactor system. In a typical TPD experiment, 20 mg of catalyst was heated to 40 ^{o}C and saturated with a stream of isopropylamine gas (2.75 kPa in He) for 1 hour. The catalyst was then purged with He gas (50 ml min^{-1}) for 1 hour to strip off weakly adsorbed isopropylamine. After that, the reactor temperature was raised from 40 ^{o}C (at 5 ^{o}C min^{-1}) to 640 ^{o}C while the reactor effluent gases were analyzed using the GC-MS. The total amount of desorbed propylene was quantified from the MS signals at 41 m/z.

4.2.3 Catalytic reaction studies

Reaction kinetic studies over the Zn-incorporated zeolites were conducted in a stainless-steel tubular reactor with a 6.4 mm (0.25 in) outer diameter. A bed of fresh powder catalyst (50-100 mg) was loaded in the center of the reactor and placed between two plugs of quartz wool. The reactor was heated in a furnace consisting of a ceramic shell heater (Applied Test Systems) in a stainless-steel shell. Liquid feed was introduced to the gaseous reactant stream by pumping through a 5 mL gas-tight syringe into a vaporization zone heated to 10 ^{o}C above the normal boiling point of the reactant. A reactor bypass line was used to allow stabilizing the feed composition and flow before introduction to the reactor. Catalyst samples were heated to the reaction temperature of 200 ^{o}C (at 10 ^{o}C min^{-1}) in helium before starting the reaction. In some experiments, the catalyst was first activated by heating to 450 ^{o}C (at 10 ^{o}C min^{-1}) for 1 hour before cooling to the reactor temperature. Reactor effluent lines were heated to 180 ^{o}C to ensure all species remained in the vapor phase. Reactant and product stream compositions were measured using online gas chromatography (GC 7890B, Agilent Technologies) equipped with a flame ionization detector (FID) and an HP-5ms column and connected to a mass spectrometer (MS 5977A, Agilent Technologies).

4.3 Results and discussion

4.3.1 Acid site titration

The Brønsted acid site concentration in BEA samples was determined by *in situ* titration with 2,6-di-tert-butyl-pyridine during isopropanol dehydration. Site density on Zn/H-BEA samples showed a decrease in the available acid sites as shown in **Table 4-1**. As can be inferred from **Table 4-1**, the Brønsted acid site concentration gradually deceased with Zn loading with

values of 357 μmol g^{-1} for H-BEA, 297 μmol g^{-1} for 0.08Zn-BEA (0.08 Zn/Al), 132 μmol g^{-1} for 0.19Zn-BEA (0.19 Zn/Al), and 149 μmol g^{-1} for 0.35Zn-BEA (0.35 Zn/Al). In addition, the acid site count on Zn/H-BEA zeolites after the thermal treatment showed a 57 μmol g^{-1} decrease for 0.08Zn-BEA, a 24 μmol g^{-1} decrease for 0.19Zn-BEA, and a 49 μmol g^{-1} decrease for 0.35Zn-BEA compared with their untreated versions. Changes in the number of Brønsted acid sites suggest that Zn^{2+} cation readily replaces Brønsted acid sites during the thermal treatment process. Penzien et al.[67] reported that Zn^{2+} ion exchange in lower Zn/Al loadings preferentially exchanges on neighboring tetrahedral framework aluminum pairs. Previous studies have also shown that ion-exchanged BEA samples with Zn/Al in the 0 – 0.15 range favorably form $Zn(OH)^{+}$ sites which upon thermal treatment dehydrates into Zn^{2+} cation binding to two tetrahedrally coordinated aluminum sites.[67,119] At Zn/Al above 0.15, however, ion exchange begins to preferentially form pairs of Zn^{2+} cations with bridging oxygen.

Table 4-1: Brønsted acid site density of tested catalysts measured by 2,6-di-tert-butyl-pyridine titration.

Catalyst	Zn/Al	Brønsted acid sites (μmol g^{-1})
H-BEA	0.00	357
0.08Zn-BEA	0.08	297
0.08Zn-BEA-pt	0.08	240
0.19Zn-BEA	0.19	132
0.19Zn-BEA-pt	0.19	107
0.35Zn-BEA	0.35	149
0.35Zn-BEA-pt	0.35	100

4.3.2 Isoproylamine temperature programmed desorption (TPD)

Reactive desorption of alkylamines, such as isopropylamine, has been used to quantify the amount of Brønsted acid sites in tested zeolites.[120] Isopropylamine protonates upon adsorption

at Brønsted acid sites forming isopropyl ammonium ion which reacts in a narrow desorption temperature range via Hoffmann elimination reaction to yield propylene and ammonia.[120] Besides Brønsted acid sites, the decomposition of isopropylamine has also been reported for metal-loaded zeolites, such as BEA, due to the strong interaction of such a molecule with the metallic Lewis sites.[67,85] Therefore, the decomposition of isopropylamine to propylene at different temperatures would suggest the formation of Zn sites with varying interaction energies and bonding coordination. By quantifying the amounts of desorbed propylene at their specific temperatures, one could quantify the respective Zn site species.

In our experiments, propylene desorption from all the catalysts could be divided into three TPD peaks with their maxima centered around 350, 397, and 479 ^{o}C as can be seen in **Figure 4.1**. H-BEA and H-BEA-pt catalysts resulted in similar propylene desorption intensities (**Figure 4.1**a,b, and **Figure 4.2**) centered around 350 ^{o}C, a temperature around which isopropylamine decomposes on the Brønsted acid site.[67] This suggests that the activation of the metal-free catalyst doesn't make notable changes to the concentration of the Brønsted acid sites. However, propylene was also seen to desorb at higher temperatures of around 397 and 479 ^{o}C, respectively. These peak intensities increase post the activation of H-BEA-pt which suggests the formation of other acid sites that are weaker than Bronsted acid sites. The intensity of the 350 ^{o}C peak was seen to gradually decrease with the metal loading which is consistent with the fact that Brønsted acid sites are converted into Zn Lewis sites upon ion exchange. Except for 0.08Zn-BEA, all Zn-loaded zeolites showed a reduction in the 350 ^{o}C peak after activation which could be attributed to the dehydration of $Zn(OH)^{+}$ with an acidic proton (Brønsted acid site) resulting in an overall reduction of the site count.[103]

Penzien et al. [67] attributed the desorption of propylene from Zn-exchanged H-BEA zeolites at 394 and 476 ^{o}C to two Zn^{2+} sites bridged by oxygen and to Zn^{2+} sites connecting two Al tetrahedra, respectively. In our analysis, the TPD peaks centered at 397 ^{o}C (**Figure 4.1**c, e, and g) were observed to proportionally increase with all Zn-loaded catalysts to almost the same intensity regardless of the Zn/Al ratio (**Figure 4.2**). This could be a result of propylene desorption from $[Zn - O - Zn]^{2+}$ sites as well as the interaction with undehydrated $Zn(OH)^{+}$. Lower desorption peaks at 479 ^{o}C, which tends to slightly decrease with Zn loading, were observed for the same three catalyst samples as seen in **Figure 4.1**c, e, and g. The activation of Zn-loaded catalysts (**Figure 4.1**b, d, and f) resulted in a reduction of the 397 ^{o}C peak intensities of Zn-BEA catalysts to a level where they show an increasing trend with Zn loading as seen in **Figure 4.2**. This is expected considering the gradual increase of $[Zn - O - Zn]^{2+}$ sites with higher Zn loading. The exception was 0.35Zn-BEA-pt which showed a reduction of the 397 ^{o}C peak intensity compared to the untreated version. This could be due to the conversion of $[Zn - O - Zn]^{2+}$ sites to TPD-invisible ZnO sites at such a higher loading.[67] The desorption peak centered at 479 ^{o}C, which is associated with Zn^{2+} sites bridging two aluminum tetrahedra[67] was observed to gradually decrease with Zn-loading with this reduction becoming more apparent after catalyst thermal treatment. As such, 0.08Zn-BEA-pt showed the highest peak intensity which is in line with the fact that Zn^{2+} species become more isolated at lower loadings. In addition, the concomitant reduction of the 479 ^{o}C peak with the increase of the 397 ^{o}C peak is indicative of the conversion of the isolated Zn^{2+} species to a more packed exchange site $[Zn–O–Zn]^{2+}$.[67]

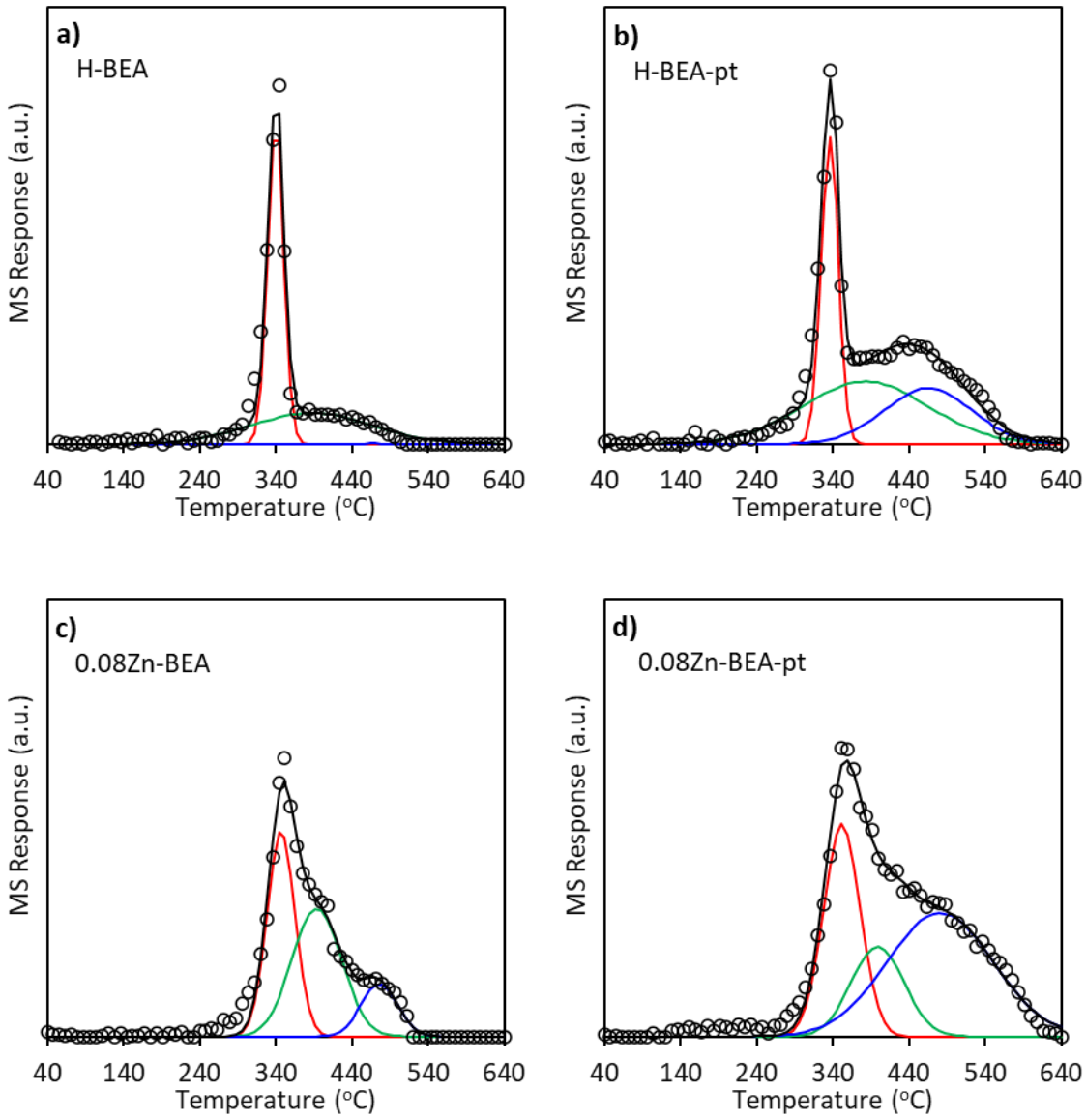
a)
H-BEA
b)
H-BEA-pt
c)
0.08Zn-BEA
d)
0.08Zn-BEA-pt
MS Response (a.u.)
Temperature (°C)
40
140
240
340
440
540
640

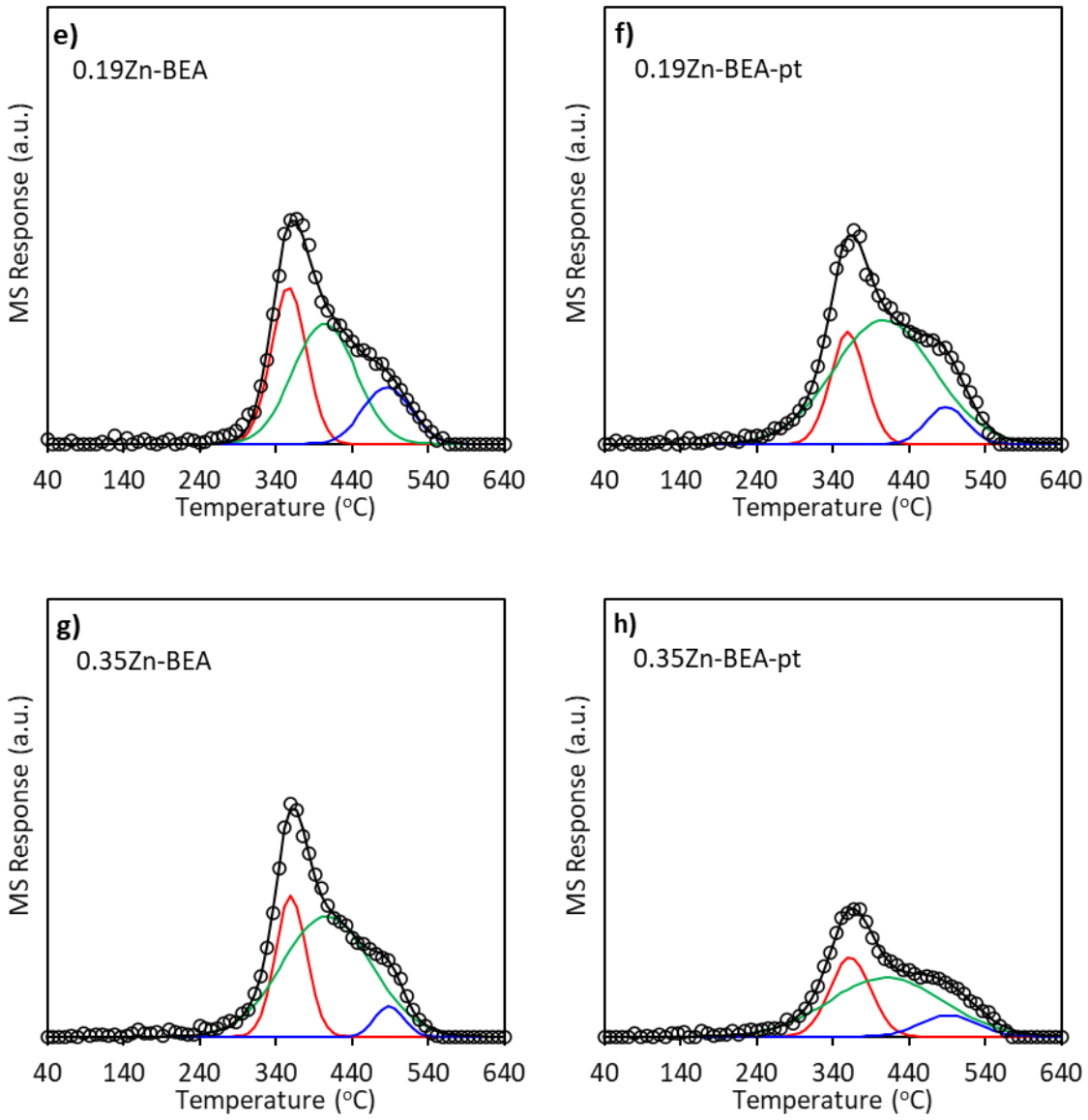

Figure 4.1: Isopropylamine TPD using MS for gas analysis. Circles; experimental data, red lines; the first deconvoluted peak (336 – 363 °C), green lines; second deconvoluted peak (383 – 410 °C), blue lines; third deconvoluted peak (465 – 492 °C), black lines; fitted data. 20 mg of catalysts samples were saturated with isopropylamine (2.75 kPa in He) at 40 °C for 1 hour, purged with 50 ml min^{-1} He for 1 hour, then heated from 40 °C to 640 °C at 4 °C min^{-1} heating rate.

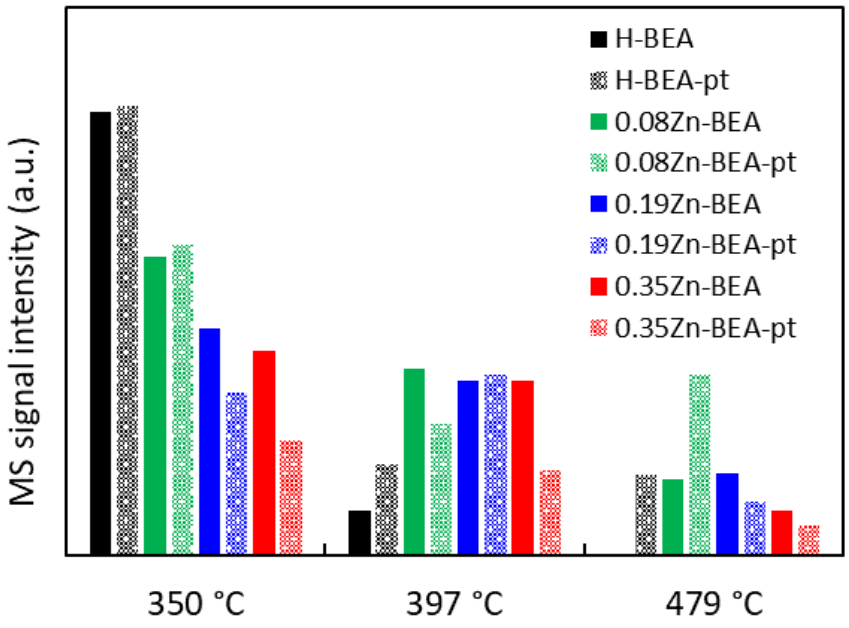

Figure 4.2: MS signal intensities (41 m/z) of desorbed propylene following isopropylamine TPD.

4.3.3 Butanal reaction kinetics

The reactivity of butanal was performed at 200 ^{o}C over the Zn/H-BEA catalysts with their loadings targeting specific Zn site coordination. **Figure 4.3** shows the product selectivities of butanal conversion over the tested Zn/H-BEA catalysts compared with H-BEA. As can be inferred from **Figure 4.3**a, the selectivity to butenes was 8.2% for H-BEA, 7.2% for 0.08Zn-BEA, 5.7% for 0.19Zn-BEA, and 5.5% for 0.35Zn-BEA. As a primary product, butene selectivity was seen to decrease with Zn loading which is consistent with the fact that Zn^{2+} ion exchange decreases the number of Brønsted acid sites, as confirmed from the titration results, and that such product is catalyzed by the dehydration of the aldehyde on Brønsted acid sites [51]. Zn/H-BEA catalysts pretreated at 450 ^{o}C prior to the reaction showed a slight decrease in butenes selectivity relative to those untreated (**Figure 4.3**a and b). This observation is also in line with the decrease in Brønsted

acid sites concentration upon pretreatment (**Table 4-1** and **Figure 4.2**) and that butenes turnover rates increase linearly with their concentration as seen in **Figure 4.4**a.

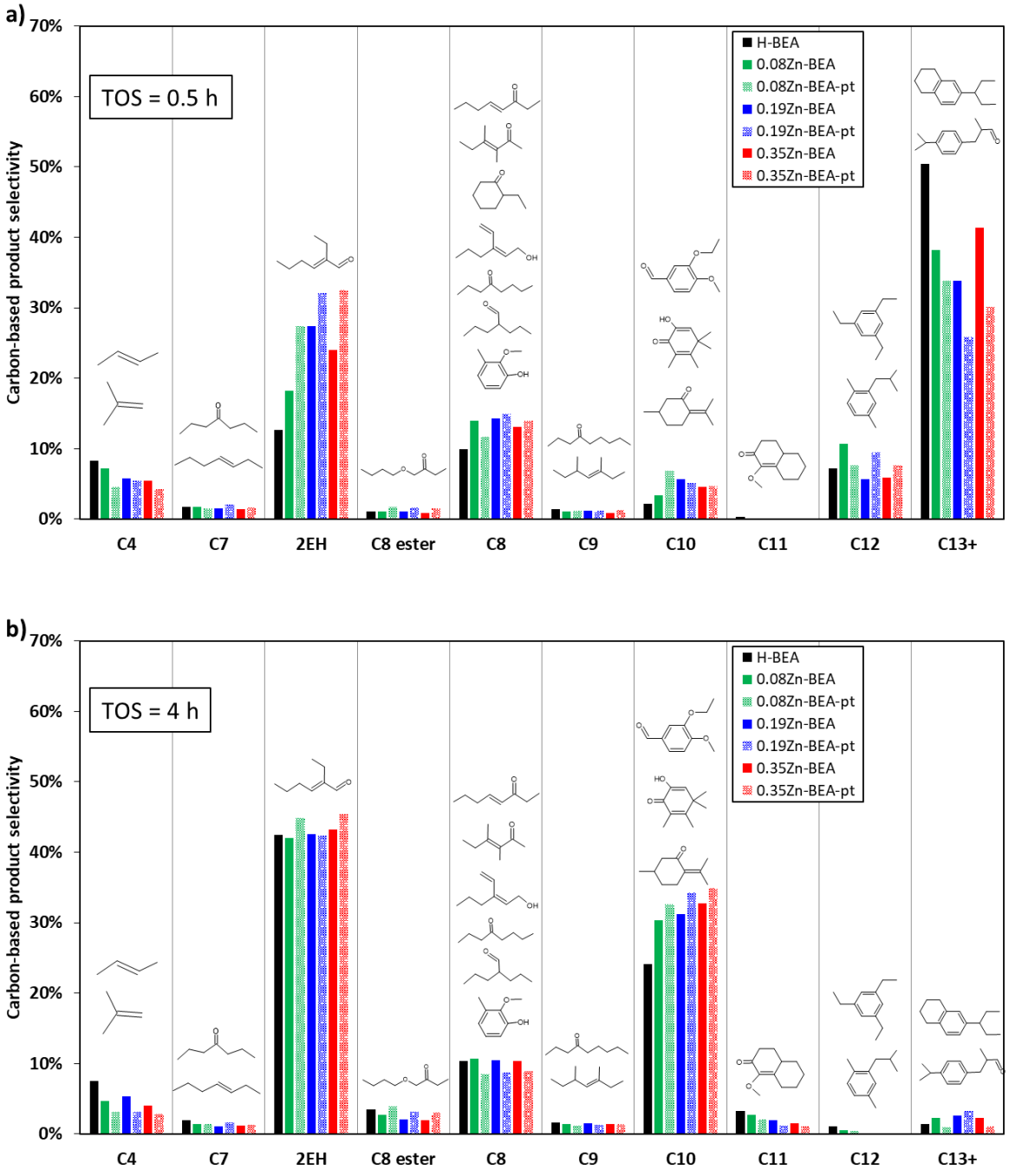

Figure 4.3: The carbon-based product selectivities for the products resulting from the conversion of 0.54 kPa butanal over 100 mg of catalyst at (a) 0.5 h time-on-stream (TOS) and (b) 4 h TOS

and 200 °C K. Sample names ending with "-pt" represent thermally-pretreated catalysts at 450 °C before reaction.

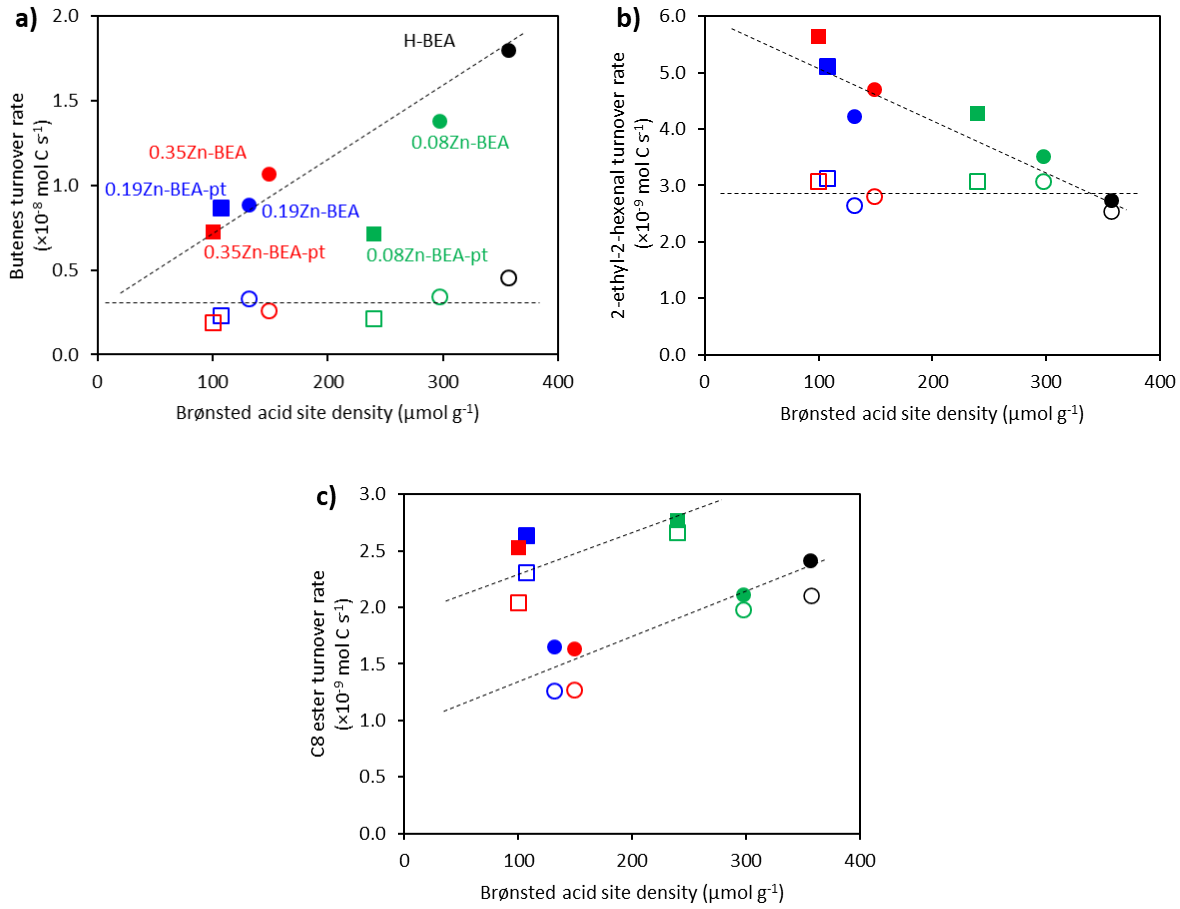

Figure 4.4: (a) Turnover rates of butenes formation (b) turnover rates of 2-ethyl-2-hexenal (c) turnover rates of butyl butanoate from butanal (0.54 kPa) reaction over 100 mg catalyst at 200 °C. Black data; H-BEA, green data; 0.08Zn-BEA, blue data; 0.19Zn-BEA, red data; 0.35Zn-BEA. Square and circle shapes are for pretreated (at 450 °C) and non-pretreated catalysts, respectively. Filled data points are for initial turnover rates calculated using equation (3). None-filled data points are for turnover rates after 4 h TOS.

Xu et al.[37] showed that the co-feeding of water increased the reaction rate of phenol alkylation with propylene on H-BEA at 350 °C. They related the temporary increase in activity to the observed conversion of Lewis acid sites to Brønsted acid sites. This reversible conversion from

the hydration and dehydration events is widely observed in zeolites.[121,122] Moreover, the acid site conversion was well documented for H-BEA where the tetrahedrally coordinated aluminum could revert to octahedrally coordinated aluminum upon exposure to moisture at room temperature.[123] However, these octahedral aluminum sites (Lewis acid) were deemed unstable at temperatures above 102 ^{o}C where they quantitatively revert to the tetrahedral coordination. Because our reaction studies were conducted at a temperature well above 102 ^{o}C and below temperatures where framework dealumination is expected, we would expect the tetrahedrally coordinated aluminum (Brønsted sites) to remain intact without significant influence by the generated water from butanal dehydration. As such, only slightly lower selectivity to butenes across all tested catalysts was observed at 4 h TOS with values of 7.5% for H-BEA, 5.3% for 0.08Zn-BEA, 4.7% for 0.19Zn-BEA, and 4.0% for 0.35Zn-BEA. Therefore, the reduction of the butenes turnover rates for all the catalysts to almost the same value (as noted in **Figure 4.4**a) could be a result of the high extent of catalyst deactivation.

The selectivity to 2-ethyl-2-hexenal (2EH) was seen to increase with the increased loading of Zn with values of 12.7% for H-BEA, 18.2% for Zn/H-BEA 0.08 Zn/Al, and 27.4% for 0.19 Zn/Al as can be seen in **Figure 4.3**. This increased selectivity is in line with the increase in Lewis acidity induced by the Zn ion exchange.[67] The slight decrease in 2EH selectivity to 24.0% for Zn/H-BEA 0.35 Zn/Al could be a result of the formation of ZnO clusters in this higher range of Zn/Al in H-BEA (Zn/Al > 0.26) which are known to be virtually inactive towards condensation products.[124] It is also known that aldol condensation reactions, yielding 2EH as the primary product in our reaction, are catalyzed by both Brønsted and Lewis acid sites in zeolites. In fact, higher selectivity to condensation products could be achieved over Lewis acid sites than on Brønsted acid sites. This was evident from the work of Panov et al.[125] where they showed a

linear correlation between the concentration of Lewis with the turnover rates of acetone condensation to mesityl oxide over HY and USY zeolites and alumina. Because Zn ion exchange proportionally replaces the protons of the exchangeable Brønsted acid sites in H-BEA[67], the linear (inverse) correlation between the turnover rates of 2EH with the Brønsted acid site density suggests strong catalysis of such product with the generated Zn Lewis acid sites. This linear dependence can be clearly seen in **Figure 4.4**b. The activation of the Zn-exchanged zeolites resulted in 2EH selectivities of 27.4%, 32.1%, and 32.5% for 0.08Zn-BEA-pt, 0.19Zn-BEA-pt, and 0.35Zn-BEA-pt, respectively. This relatively high increase in selectivity upon activation is concomitant with the expected coordination changes of Zn from hydrated $Zn(OH)^+$ to either a bridging Zn^{2+} interacting with two aluminum atoms or to two Zn^{2+} bridged by oxygen.[67,103] Activated 0.19Zn-BEA-pt and 0.35Zn-BEA-pt showed almost identical selectivity to 2EH and this is consistent with the findings from Penzien et al. where they observed a constant hydroamination activity of Zn/H-BEA catalysts at Zn/Al > 0.26 where inactive ZnO species start to evolve in this range [126]. As can be seen in **Figure 4.3**b, all tested catalysts showed very similar selectivity (43 – 45%) to 2EH at 4 h TOS. This similarity in catalytic activity could be linked to the reversible conversion of the bridging Zn^{2+} sites to their hydrated form $Zn(OH)^+$ by reacting with the generated water from butanal dehydration reactions. Although $Zn(OH)^+$ species are known to easily dehydrate at elevated temperatures, it is expected that reaction-generated water could still hydrate some of the Zn^{2+}. As can be observed from **Figure 4.4**b, the turnover rates to 2EH for all Zn-exchanged catalysts decreased to a level that almost matched that of H-BEA zeolite after 4 h TOS. This could be a result of both catalyst deactivation due to condensed products blocking the active sites and the hydration of Zn^{2+} sites to a less active $Zn(OH)^+$.

The disproportionation of butanal to butyl butanoate (C_8 ester) is another primary reaction pathway that is commonly observed over acidic, basic, or acid-base bifunctional catalysts.[127] **Figure 4.3**a shows the product selectivity to butyl butyrate with values ranging from 0.8 – 1.1% for all catalysts. As such, the introduction of Zn Lewis sites upon ion exchange didn't seem to notably alter the selectivity of such a product. However, upon pretreatment, Zn-exchanged catalysts showed an increase in selectivity to 1.5 – 1.8%. Unlike the formation of 2EH, this nearly 50% increase in butyl butanoate selectivity on the pretreated Zn-exchanged catalysts was observed even at 4 h TOS (**Figure 4.3**b). These results suggest that butyl butanoate was not catalyzed by the generated Zn Lewis acid sites. This is supported by the notable decrease in the turnover rates of butyl butyrate with the degree of Zn exchange as seen in **Figure 4.4**c. Chin et al.[47] reported a proportional increase in the rates of butanal conversion to butyl butyrate with the number of basic sites in Na-exchanged H-MFI zeolites. Those basic sites included the bi-coordinated oxygen present in the extra-framework alumina and the oxygen atoms conjugate to the Na^+ ions. Therefore, we associate the observed activity to be mainly caused by the basic sites in the zeolites which seem to increase with pretreatment. We also note from **Figure 4.4**c that 0.19Zn-BEA and 0.35Zn-BEA both gave the same turnover rate of butyl butanoate although the latter was expected to contain some basic ZnO clusters. This indicates that these additional ZnO are inactive towards Tishchenko esterification in our reaction system.

4.3.4 Catalyst deactivation assessment

Despite the high activity and tunability of zeolites for the conversion of aldehydes to various products, their microscopic pore confinements and their potential to hinder the diffusion of bulky molecules make them prone to fast deactivation by coke.[52,115] Because our reaction involved significant activity decay over reaction time, it is important to assess this catalyst

deactivation behavior to compare the different catalysts. Unique catalyst deactivation models can often be well described by the simplified rate activity decay equation (4.1) [128,129]:

$$-\frac{da}{dt} = k_d a^d \tag{4.1}$$

$$a = \frac{-r_A}{-r_{A0}} = \frac{rate\ of\ converting\ A\ (deactivated\ catalyst)}{rate\ of\ converting\ A\ (Fresh\ catalyst)} \tag{4.2}$$

Where a is the dimensionless activity of the catalyst defined in equation (4.2), k_d is the catalyst deactivation rate constant (in s^{-1}), and d is the deactivation order which could span a value from 0 to 3. In our reaction analysis, the steady-state conversion of butanal (98%+ product recovery in the gas phase) was obtained roughly after 1 hour of time-on-stream (TOS). Therefore, our deactivation kinetics were conducted based on the catalyst activity at this time (i.e., $a = 1$ at 1 hour TOS). As such, equation (4.3) was used as a modified version of equation (1):

$$-\frac{da}{dt} = a_0 k_d a^d \tag{4.3}$$

Where a_0 represent initial reaction activity ($a_0 > 1$) which could be used to ultimately calculate the initial turnover rate of the desired product. Equation (4.3) can be solved to yield the analytical solution in equations (4.4) and (4.5):

$$a = a_0(1 + (d-1)k_d t)^{\frac{1}{1-d}}\ ;\ d \neq 1 \tag{4.4}$$

$$a = a_0 \exp(-k_d t)\ ;\ d = 1 \tag{4.5}$$

The turnover rates of the three primary products (butenes, 2-ethyl-2-hexenal, and butyl butanoate) were regressed using equation (4.4) to calculate the initial turnover rates, the reaction deactivation order d, and the deactivation reaction constant k. It is worthwhile to note that in order

to minimize the number of independent variables in the estimation process, the estimation was first done on the H-BEA catalyst and the optimal deactivation order values for the particular product were fixed for all other catalysts. **Figure 4.5** shows the turnover rates of these primary products as a function of time-on-stream and **Figure 4.6** shows the calculated catalyst deactivation constants and deactivation orders.

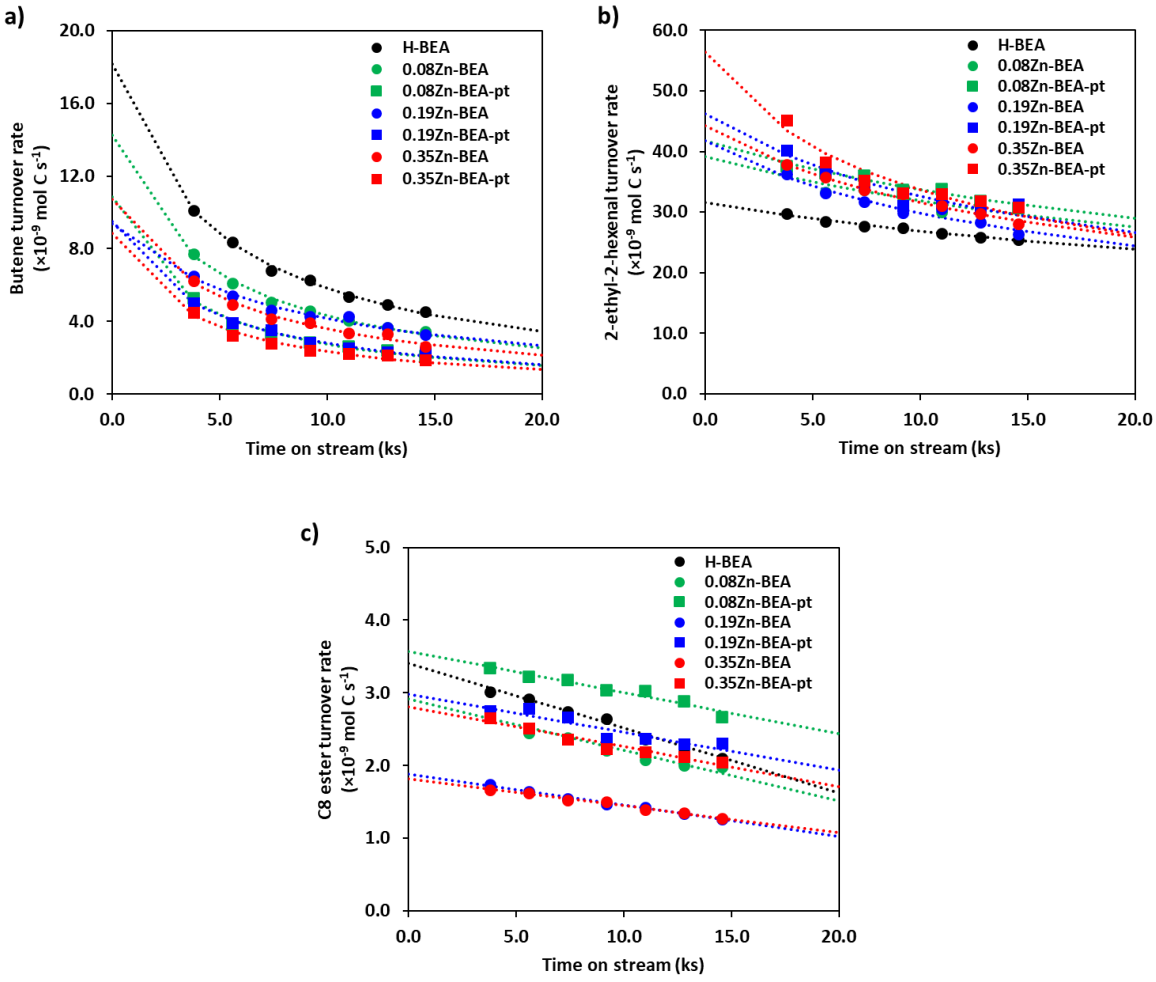

Figure 4.5: Turnover rates of **(a)** Butenes, **(b)** 2-ethyl-2-hexenal, and **(c)** butyl butanoate as a function of time-on-stream (TOS) from butanal (0.54 kPa in He gas) reaction over 100 mg catalyst at 200 °C. Square and circle data points are for pretreated (at 450 °C) and non-pretreated catalysts, respectively. Dotted lines are modeled turnover rates using equation (4.3).

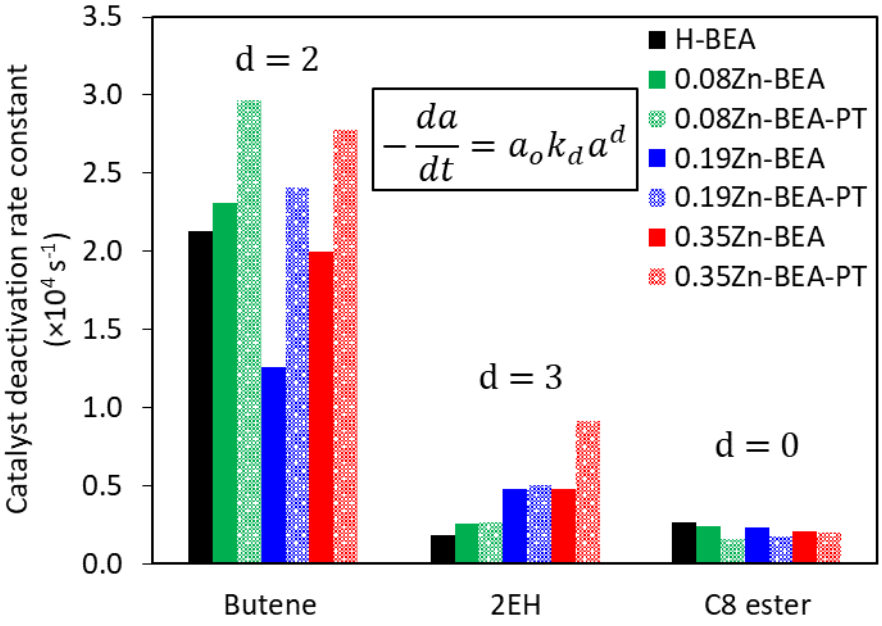

Figure 4.6: Calculated catalyst deactivation rate constants and deactivation orders using equation (4.3) for butanal (0.54 kPa in He gas) conversion over 100 mg catalyst at 200 °C.

As can be observed from **Figure 4.6**, the deactivation orders for butenes and 2EH products were 2 and 3, respectively, whereas C_8 ester showed a zero-order dependence on activity. The order values of 2 and 3 could be indicative of a similar deactivation mechanism (parallel, series, or a mix of the two) for the sites catalyzing these two products.[128] On the other hand, the zero-order deactivation dependence on butyl butanoate formation suggests that such a product is catalyzed by a reactive site that deactivates differently.

Also, from **Figure 4.6**, the large values of the deactivation constants with respect to butenes formation suggest the fast deactivation of Brønsted acid sites, which are responsible for their conversion. In addition, the values of the deactivation constants (although generally higher for activated catalysts) do not show a clear relation with Zn loading. However, the deactivation

constants with respect to the 2EH product increase proportionally with the Zn loading, especially for the activated catalysts (**Figure 4.6**). This clearly implies that the sites catalyzing this product are influenced by both the Zn loading and the temperature pretreatment. Finally, low and almost identical catalyst deactivation constants with regards to butyl butanoate (C_8 ester) suggest that this product is catalyzed by sites that are barely deactivating and hardly influenced by the Zn loading.

4.4 Conclusion

In this study, we showed how Zn/H-BEA containing different species of Zn influences the conversion of butanal into its main three primary products namely, butenes, 2-ethyl-hexenal, and butyl butanoate. The ion exchange with Zn resulted in a decrease in the available Brønsted acid sites as confirmed by 2,6-di-tert-butyl-pyridine titration which entails the replacement of the predominant Brønsted acid sites with Zn Lewis sites. Moreover, the acid site count on Zn/H-BEA zeolites after the thermal treatment showed a 24 - 57 μmol g^{-1} decrease for all Zn-modified catalysts compared with their unmodified versions. This reduction in Brønsted acid sites could be a result of the dehydration of $Zn(OH)^+$ and the coordination with neighboring Brønsted sites. Isopropylamine TPD results suggest that the thermal treatment of H-BEA didn't make notable changes to the concentration of the Brønsted acid sites. However, Zn loading and thermal pretreatment resulted in the reduction of Brønsted acid sites while simultaneously increasing the proportions of isolated Zn^{2+} and $[Zn\text{-}O\text{-}Zn]^{2+}$ sites. The reduction of Brønsted acid sites was reflected in lower selectivities to butenes which are primarily catalyzed by such acid sites. On the other hand, the selectivity to 2-ethyl-2-hexenal (2EH) was seen to increase with Zn loading suggesting the catalyzation of such product with both isolated Zn^{2+} and $[Zn\text{-}O\text{-}Zn]^{2+}$ sites. At higher Zn loadings as in 0.35Zn-BEA-pt, the TPD results show signs of reducing $[Zn - O - Zn]^{2+}$ upon catalyst activation which could be resulting from their conversion into ZnO. The high

deactivation constant for the formation of butenes compared with 2EH suggests the fast deactivation of Brønsted sites in relation to Zn Lewis sites and their comparable deactivation order values of 2 and 3 could be indicative of a similar deactivation mechanism. Unlike the formation of 2EH, the high increase (nearly 50%) in selectivities to butyl butanoate on the pretreated Zn-exchanged catalysts coupled with their zero-order deactivation suggest that such product was not catalyzed by the generated Zn Lewis acid sites. On the other hand, the zero-order deactivation dependence on the rate of butyl butanoate formation suggests that such a product was catalyzed by a reactive site that deactivates differently.

Chapter 5: Kinetic analysis and modeling for butanal conversion over Zn/H-BEA catalysts considering deactivation

5.1 Introduction

Over the years, there has been a growing interest in utilizing bio-oils (sometimes referred to as pyrolysis oils) as either renewable fuels or for the production of a variety of chemicals ranging from food flavoring to biodegradable agricultural fertilizers.[45] Bio-oils are free-flowing dark brown liquids with a notable smokey odor and made of multicomponent mixtures derived from the depolymerization and fragmentation of cellulose, hemicellulose, and lignin.[72] However, inherent properties of bio-oils such as high water content, high viscosity, high oxygen content, and high process corrosiveness caused by acidic compounds are limiting their industrial applications.[130] The high oxygen content of bio-oils, which usually ranges between 45-50wt.%, is the main property that distinguishes them from heavy fossil oils.[131] As such, bio-oils constitute a complex mixture of compounds that include alcohols, organic acids, aldehydes and ketones, and esters. In a step to valorize these compounds and utilize their abundance, research efforts are focused on studying the reactivities of bio-oil constituents such as ethers[28,88], alcohols[79,88,132,133], aldehydes[48,51,117], and ketones[134,135] to shed light on their reaction mechanism and improve their catalytic conversion to valuable products.

Aldehydes and ketones are two of the oxygenated hydrocarbons of interest due to their high concentrations in bio-oils[136] and their ability to react over acidic, basic, acid-base bifunctional catalysts to eliminate oxygen and form new C-C bonds resulting in a diverse range of

products.[10,47,137] Aldol condensation is an important class of reaction as it increases the carbon chain length and its mechanism depends on the catalytic site being acidic or basic. In the basic site mechanism, a proton from the α-carbon of the aldehyde or ketone is extracted from the basic site generating a carbanion which in turn attacks the carbonyl group of the other aldehyde or ketone creating a new C-C bond.[115,138] On the other hand, the reaction on the acidic site starts with an initial keto-enol tautomerization of the aldehyde or ketone to their conjugated enol followed by the nucleophilic attack of the α-carbon in enol to a protonated carbonyl group (by the acid site proton) of another aldehyde or ketone to generate the C-C bond.[51,95,115] Although there are advantages associated with the use of either basic or acidic catalyst sites, the former is generally more prone to deactivation by the presence of organic acids. Shen et al.[117] probed the activity of MgO supported on SiO_2 in converting butanal at 300 and 400 ^oC and observed the rapid deactivation of the catalyst with the co-feed of 1 vol% of butanoic acid with the catalyst almost fully deactivating after 2 h of reaction time. The conversion of aldehydes has also been well studied over Brønsted acid catalysts where it is seen to facilitate the formation of both inter and intra C=C bonds generating olefinic and aldol condensation products, respectively.[47,51] For example, butanal reactions over Brønsted acid sites such as those found in H-MFI zeolites and polyoxometalate clusters at moderate temperatures of 300 ^oC have been identified to follow three main reaction pathways namely 1) the direct dehydration-hydrogenation to yield butene and butadiene, 2) aldol condensation to primarily yield 2-ethyl-hexenal along with other C_8 and heavier aldehydes, and 3) Tishchenko esterification to produce butyl butyrate.[47,95] Besides allowing multiple reaction pathways, zeolites such as H-BEA are deemed to offer exceptional hydride transfer properties as observed by the high selectivity to the highly saturated 2,2,3-trimethylbutane from the conversion of dimethyl ether at 200 ^oC and as revealed by C^{13} labeling

experiments.[28,56,57] The modification of zeolites with transition metals has been recognized as an effective way of generating Lewis acid sites with acid-base pairs bifunctionality to catalyze the conversion of aldehydes and ketones. Lewis et al.[10] demonstrated the high activity of Hf-, Sn-, and Zr-BEA for the cross-aldol condensation of benzaldehyde with acetone to produce benzalacetone with up to 97% selectivity at 90% conversion and 90 ^{o}C reaction temperature. They also revealed how Hf-BEA could maintain productivity with high selectivity to condensation products in the presence of acetic acid impurities at conditions where the base catalyst MgO showed no activity.[10] Kots et al.[85] probed the reactivity of Zr-BEA zeolite for the self-condensation of butanal and reported that BEA zeolite containing open Zr-sites were more active than the ones with closed Zr-sites with both sites giving similar selectivity of 85 wt.% to 2-ethyl-hexenal at 260 ^{o}C and 43 – 46% conversion. Moreover, transition metal exchanged zeolites such as Zn/H-BEA and Zn/H-ZSM5 have demonstrated their hydride transfer ability for the dehydrogenation and aromatization of light alkanes.[25,103] Penzen et al.[67] and Biscardi et al.[103] showed the unique features of Zn-exchanged BEA and ZSM-5, respectively, in tuning the bifunctionality of Brønsted and Lewis acid sites through Zn loading and temperature pretreatment. In their study, the metal loading and temperature pretreatments resulted in Zn species with different reactivities depending on their bonding coordination with the zeolite structure as confirmed by the extended X-ray absorption fine structure (EXAFS) analysis.

The use of reaction kinetic analysis serves as a great tool for catalyst selection and process design. Reaction kinetic studies utilizing power law [12,13] and Langmuir-Hinshelwood-Hougen-Watson (LHHW) [14,15,139] rate expressions have been extensively used to explain catalytic phenomena and predict industrial process performance. Besides these traditional methods being useful, coupling them with deeper chemical intuition and rigorous surface chemistries is desirable

and envisioned to streamline the process of catalyst design. Defined by Domesic et al[16], microkinetics is another reaction kinetic analysis that attempts to incorporate basic surface chemistries involved in the catalytic reaction. Therefore, the model is based on the description of catalytic processes in terms of the information and assumption about active sites and the nature of elementary steps making the reaction scheme. The use of microkinetic analysis is advantageous in that it doesn't require any assumptions regarding the nature of the rate-determining elementary reactions or the abundant species adsorbed on the catalyst surface.[17] Microkinetic modeling has been successfully applied to describe and interpret various reaction systems. [18–22]

In this work, we aim to study the conversion of butanal on Zn-loaded H-BEA zeolite by developing a reaction kinetic model that accounts for catalyst deactivation and describes the reaction and catalyst properties in terms of kinetic and thermodynamic parameters similar to those used in the typical microkinetic analysis. These parameters include adsorbed species binding energies on the catalyst surface, reaction activation energies, fractional coverages of adsorbed species on the catalyst surface, and total acid site concentration of the catalyst. We first derive a simplified reaction sequence for the conversion of butanal on H-BEA by noting the product evolution at different conversion levels. Then, we formulate the kinetic model by calculating the equilibrium and reaction constants for each elementary step along with using appropriate mass balance equations. The kinetic model was first developed for the conversion of butanal on an H-BEA catalyst at 200 ^{o}C and using experiments at different butanal partial pressures, conversions, and times on stream to fit the adjustable parameters in the model. We used H-BEA zeolites with different degrees of Na^{+} ion exchange to vary the concentration of Brønsted acid sites and understand the influence of such acid sites on the reaction sequence. Acid site titration with pyridine as a probe molecule was used to quantify the total acid site concentration on the catalyst

surface (both Brønsted and Lewis acid sites) to be used as an input parameter in the kinetic model. The developed kinetic model was then used to fit the experimental data for the conversion of butanal on Zn/H-BEA catalysts by adjusting the model parameters and using the values from the H-BEA model as initial guesses. Finally, the thermodynamic parameters estimated for each catalyst were compared to gain fundamental insights about the observed reactivities of each catalyst.

5.2 Experimental methods

5.2.1 Catalyst preparation

The primary catalyst considered in this study is the acidic version of HN_4-BEA (Si/Al 12.5) zeolite (Zeolyst International). H-BEA was obtained by calcining NH_4-BEA at 500 ^oC for 4 hours (1 $^oC\ min^{-1}$ rate) in a flow of dry air. Na^+ exchanged BEA samples were prepared by mixing batches of H-BEA into solutions of 0.02, 0.10, and 0.50 M of Na^+ obtained by dissolving sodium chloride (NaCl, Sigma Aldrich). The ion exchange was conducted at 50 ^oC for 2 h after which the solids were separated by centrifugation and washed with batches of de-ionized water (100 ml each) at least 4 times. After that, the samples were dried at 90 ^oC for 24 h and then calcined at 500 ^oC in flowing dry air. The prepared samples were denoted as 0.02Na-BEA, 0.10Na-BEA, and 0.50Na-BEA, respectively. Zn-exchanged zeolites were prepared by suspending three H-BEA samples in 0.03-0.06 M aqueous solutions of zinc acetate ($ZnC_4H_6O_4$, Sigma Aldrich) for 14 – 69 h at 80 ^oC. The samples were then dried at 40 ^oC for 20 h followed by calcination at 500 ^oC for 5 h (0.5 $^oC\ min^{-1}$ rate). The Zn/Al ratio in these catalysts was calculated after digesting the solids in a mixture of concentrated HCl and NHO_3 acids and measuring the concentration of Zn^{2+} and Al^{2+} ions in each sample by inductively coupled plasma–optical emission spectroscopy (ICP-OES; Avio 200 ICP Optical Emission Spectrometer, Perkin Elmer). The three samples were denoted based on their

Zn/Al ratios as 0.08Zn-BEA, 0.19Zn-BEA, and 0.35Zn-BEA. When applicable, some of these catalysts were temperature pre-treated in He gas (UHP >99.999%, Praxair) at 450 ^{o}C for 1 h before the reaction. These catalysts were denoted as 0.08Zn-BEA-PT, 0.19Zn-BEA-PT, and 0.35Zn-BEA-PT, respectively. All the prepared catalysts were pelletized, crushed, and sieved to 60-80 US mesh size (177 – 250 μm agglomerate diameter) to minimize the effects of transport artifacts on reaction kinetics data.

5.2.2 Catalyst acid site titration with pyridine

A mixture of pyridine (99.8%, Sigma Aldrich) in isopropanol (95.5%, Sigma Aldrich) having a molar ratio of 1:250 was used to titrate the total catalyst acid sites (Brønsted and Lewis acid sites). In a typical titration experiment and using the same setup for the reaction studies mentioned in section 2.3, the titrant mixture is fed into a gas-mixing vaporization zone heated at 130 ^{o}C and mixed with He gas (UHP >99.999%, Praxair) resulting in a stream containing 11.4 kPa isopropanol and 45.6 Pa titrant. The turnover rates of isopropanol dehydration over the tested catalysts were measured while simultaneously calculating the cumulative pyridine adsorption rate. The titrant uptake was calculated from the difference between the concentration of the titrant in the feed and the gas outlet. The titration experiment was considered complete when the concentration of isopropanol in the effluent gas becomes steady for one hour.

5.2.3 Reactivity measurements

The turnover rates of butanal over the prepared catalysts were measured in a stainless-steel reactor with a 5.0 mm inner diameter. The tested catalysts (0.01 – 100 mg) were loaded in the reactor and held in the reaction zone by two plugs of quartz wool with a negligible pressure drop across the fixed bed. The reactor was heated in a furnace consisting of a ceramic shell heater (Applied Test Systems) in a stainless-steel shell. The reactor temperature was controlled by a

PID controller (Applied Test Systems) through a K-type Omega thermocouple attached to the outer wall of the reactor where the middle of the catalyst bed was located. Liquid butanal feed (98.0% >, Sigma Aldrich) was introduced at a 1.0 - 5.0 μL min^{-1} flow rate to a liquid vaporization zone, which was maintained at 10 ^{o}C above the boiling point of the liquid, through a syringe pump (New Era Pump Systems, Inc.) using a 1.0 mL gas-tight syringe. The vaporized liquid was wept to the catalyst bed for reaction by a 50 ml min^{-1} flow of He gas stream which was regulated by a mass flow controller (mks GE50A). The product gas streams were analyzed by an online GC/MS (7890B/5977 MSD Agilent Technologies) equipped with an HP-5ms column (30 m and 0.25 mm ID). All the gas lines downstream of the reactor were heated to 180 ^{o}C by electrical heating tapes to avoid condensation of reaction products.

Before the reaction, the vaporized liquid feed was stabilized by flowing the feed stream through a reactor-bypass line while the tested catalyst sample was heated to the reaction temperature at a 10 ^{o}C min^{-1} heating rate. The temperature pre-treated samples were heated to 450 ^{o}C (10 ^{o}C min^{-1}) for 1 hour under a 20 ml min^{-1} He purge then cooled to the reaction temperature before starting the reaction. After stabilizing both the feed flow and reactor temperature, the He purge into the catalyst bed was stopped and the vaporized feed was directed to the catalyst bed through a 3-way valve to start the reaction and analyze the product gas with GC/MS.

5.3 Development of the kinetic model

5.3.1 Reaction sequence

The reaction of butanal on a Brønsted acid catalyst starts with the adsorption of the molecule on the site through their oxygen to form a hydrogen-bonded complex as observed by

both quantum chemical calculations, IR, and NMR results for the H/D exchange on H-ZSM-5 zeolite.[26,53,54] This adsorption causes weakening in the C=O bond evidenced by the lower vibrational shifts observed in the IR experiments.[26] As the proton transfers from the Brønsted acid site to the carbonyl oxygen of the aldehyde, the neighboring framework oxygen of the catalyst attacks its alpha hydrogen forming an enol. The formed enol then attacks a nearby protonated aldehyde forming a new C-C bond which upon dehydration evolves a larger condensation product.[55] Aside from the aldol condensation, butanal could also undergo a dehydration step by the removal of a water molecule to form 1,3-butadiene or a hydrogenation-dehydration step to yield butenes.[95] The disproportionation of butanal to butyl butanoate through Tishchenko esterification is another primary reaction pathway that is commonly observed over acidic, basic, or acid-base bifunctional catalysts.[47,127] Butyl butyrate could also convert to 4-heptanone upon the removal of H_2 and CO to eventually form heptane isomers following a hydrogenation-dehydration step. [47,117,127]

In our study, we examined the conversion of butanal on H-BEA zeolite at 200^{o}C and varying conversions to note the product selectivity changes and determine the reaction sequence based on product evolution. Because the reaction resulted in a wide range of products, the selectivities of the different products were lumped based on their structural and chemical similarity as shown in **Figure 5.1**a and b. As can be observed from **Figure 5.1**a, 2-ethyl-hexenal had the highest product selectivity at low butanal conversions indicating that it is a primary reaction product. The high selectivity to butenes at low butanal conversion (**Figure 5.1**a) along with the fact that butenes preserve the four-carbon chain length of butanal suggests that it was also a primary product in the reaction. In **Figure 5.1**b, butyl butyrate shows the highest selectivity at low butanal conversion which tends to decrease with higher conversion. In addition, heptenes and C_7

esters products started to evolve at slightly higher conversions than observed with butyl butyrate (**Figure 5.1**b). These two observations suggest that butyl butyrate is a primary reaction product while heptenes and C_7 esters are secondary. Similarly, the increasing selectivity of C_{10}+ aromatics with butanal conversion (**Figure 5.1**a) indicates that they result from secondary condensation reactions.

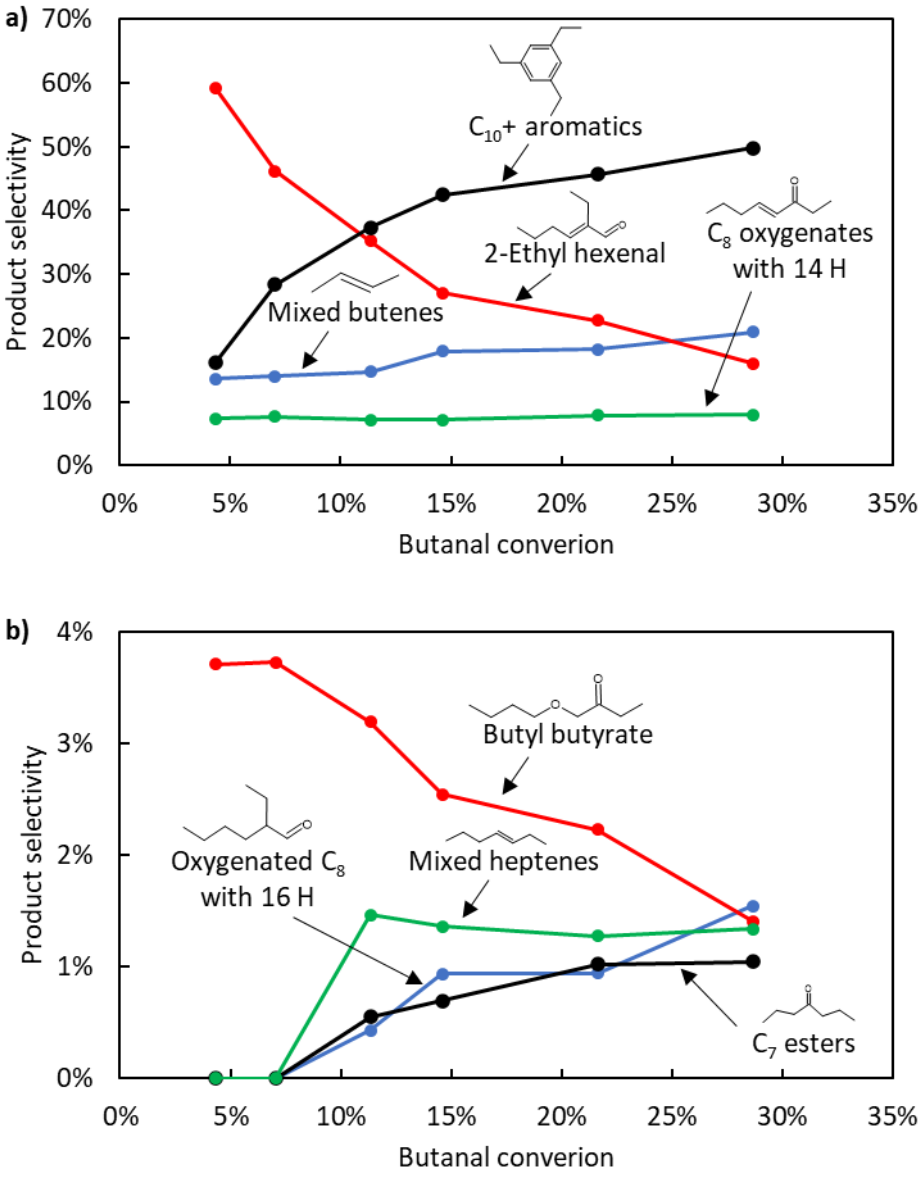

Figure 5.1: Selectivity of the products at different conversions of butanal over H-BEA catalyst at 200°C. Butanal pressure was 0.54 kPa in 50 ml min^{-1} He gas and catalyst weights were 10 –

100 mg. The shown structure of every product/product lump represents the most dominant compound.

Based on the abovementioned literature findings and the trends of selectivity evolution from our conversion variation experiments, a reaction sequence for butanal conversion over H-BEA catalyst was suggested as shown in **Figure 5.2**. To simplify the modeling of such a system, the reaction products were lumped into four categories 1) mixed butenes resulting from the dehydration-hydrogenation of butanal 2) mixed C_8 oxygenates resulting from aldol condensation 3) butyl butyrate, C_7 oxygenates, and mixed heptenes resulting from Tishchenko esterification 4) C_{10}+ mixed aromatics and oxygenated aromatics resulting from the cyclization of condensed products. These product lumps were used to formulate a simplified reaction sequence consisting of 9 elementary steps as shown in **Table 5-1**. As an approximation, the most abundant compound in each category was selected to represent each reaction lump in the elementary steps considered. More specifically, 2-ethyl-hexenal, butyl butyrate, 1,3,5-triethyl benzene, and 2-butene were used to represent aldol condensation products, esterification products, aromatics, and butenes lumps, respectively.

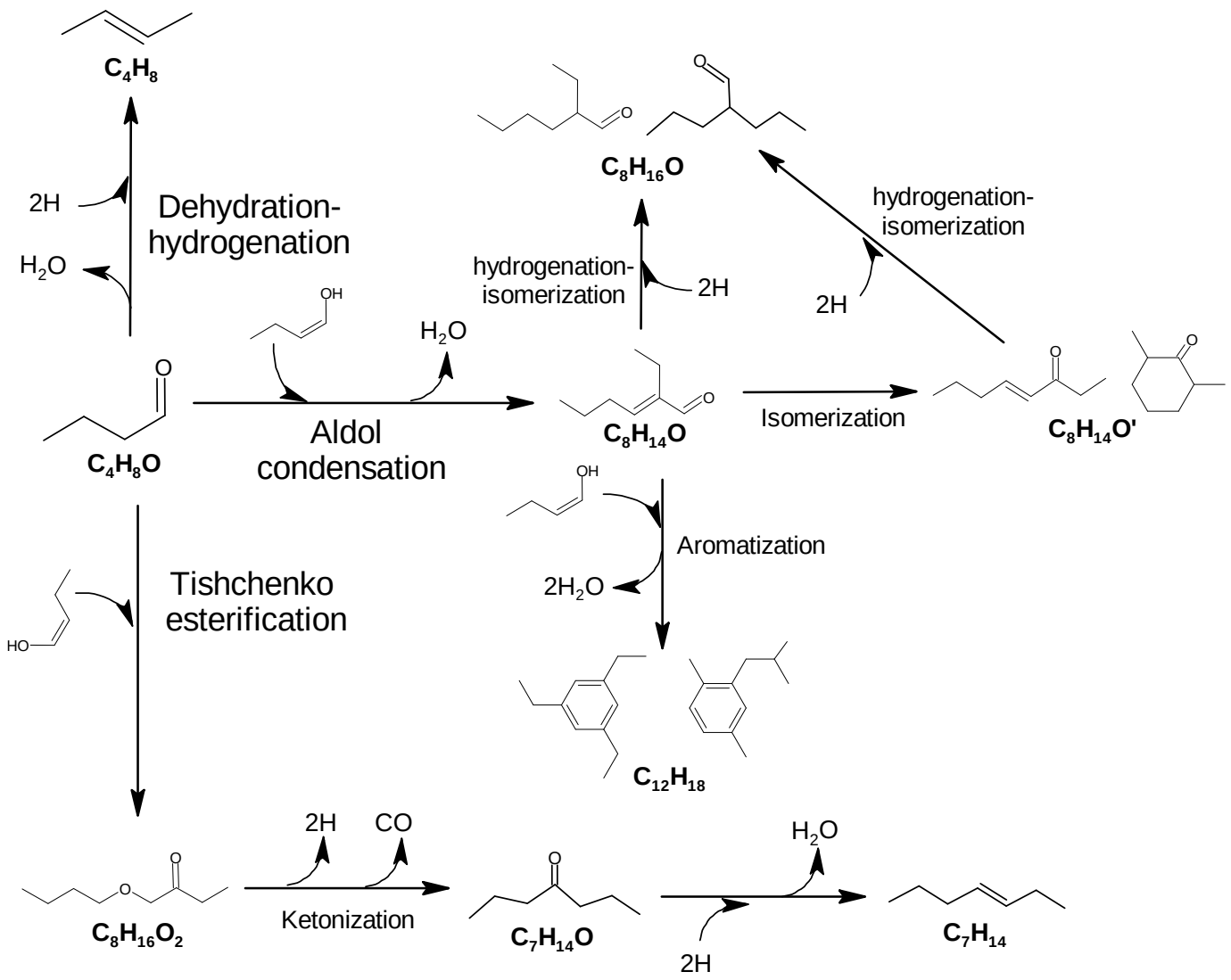

Figure 5.2: Proposed reaction sequence based on the selectivity evolution of different products from the conversion of butanal on H-BEA catalyst.

Table 5-1: Elementary steps used to model the conversion of butanal on H-BEA. C_4H_8O stands for butanal, C_4O_8 for 2-butene, $C_8H_{14}O$ for 2-ethyl hexenal, $C_8H_{16}O$ for butyl butyrate, and $C_{12}H_{18}$ for 1,3,5-triethyl benzene. * represents a vacant surface acid site and $C_xH_xO_x$* represents a molecule-adsorbed acid site.

Reaction step	Surface reactions
1	$C_4H_8O + * \leftrightarrow C_4H_8O*$
2	$C_4H_8O* + H_2 \leftrightarrow C_4H_8* + H_2O$
3	$C_4H_8 + * \leftrightarrow C_4H_8*$
4	$C_4H_8O* + C_4H_8O \leftrightarrow C_8H_{14}O* + H_2O$
5	$C_8H_{14}O + * \leftrightarrow C_8H_{14}O*$
6	$C_4H_8O* + C_4H_8O \leftrightarrow C_8H_{16}O_2*$
7	$C_8H_{16}O_2 + * \leftrightarrow C_8H_{16}O_2*$
8	$C_8H_{14}O* + C_4H_8O \leftrightarrow C_{12}H_{18}* + 2\,H_2O$
9	$C_{12}H_{18} + * \leftrightarrow C_{12}H_{18}*$

As seen in **Table 5-1**, the elementary steps 2, 4, 6, and 8 were all assumed to follow the Eley-Rideal reaction where an adsorbed aldehyde reacts with a gas phase butanal to form the C-C bond and increases the carbon chain length. Produced water from the dehydration events in reactions 2, 4, and 8 was expected to have a low impact on the turnover rates of butanal due to its expected low pressures (at low conversions) and the fact that our reaction temperatures were well above 100 ^oC below which water adsorption is expected to influence the catalyst acidity. [125] Therefore, in our reaction sequence, water was assumed to form without molecular adsorption on the catalyst surface and for simplicity, a similar assumption was used for molecular hydrogen.

5.3.2 Model parameterization

5.3.2.1 Thermodynamic parameters

The model was parameterized in terms of either the forward or reverse rate constants of every elementary. These reaction constants were related to the thermodynamic equilibrium constant through equation (5.1):

$$K_{i,eq} = \frac{k_{i,for}}{k_{i,rev}} \tag{5.1}$$

Where $K_{i,eq}$ is the equilibrium constant $k_{i,for}$ is the forward rate constant, and $k_{i,rev}$ is the reverse rate constant of elementary step i. The first step was to calculate the thermodynamic equilibrium constant of each of the 9 steps using equation (5.2):

$$K_{i,eq} = \exp\left(-\frac{\Delta G^o{}_i}{k_B T}\right) = \exp\left(\frac{\Delta S^o{}_i}{k_B}\right)\exp\left(-\frac{\Delta H^o{}_i}{k_B T}\right) \tag{5.2}$$

Where $\Delta G^o{}_i$, $\Delta S^o{}_i$, and $\Delta H^o{}_i$ are the standard Gibbs free energy, entropy, and enthalpy changes, respectively. k_B is Boltzmann's constant and T is the reaction's temperature. The standard enthalpy of change and standard entropy of change for each elementary reaction were calculated using equations (5.3) and (5.4), respectively.

$$\Delta H_i = \sum\nolimits_{products} H_p - \sum\nolimits_{reactants} H_r \tag{5.3}$$

$$\Delta S_i = \sum\nolimits_{products} S_i - \sum\nolimits_{reactants} S_i \tag{5.4}$$

The standard enthalpy and entropy of the gaseous species used in equations (5.3) and (5.4) were obtained from standard reference books.[140] On the other hand, the standard enthalpies of

adsorbed species were calculated by correcting the enthalpy of the corresponding gas species with a binding energy term using equation (5.5):

$$H_{i,surface} = H_{i,gas} + BE_i \tag{5.5}$$

Where BE_i is the binding energy of the adsorbed species which was used as an adjustable parameter in our model. The standard entropies of adsorbed species were corrected by subtracting the vibrational entropy from the standard entropy of the gas species and correcting with a retained entropy factor using equation (5.6):

$$S_{i,surface} = F_{loc}\left(S_{i,gas} - S_{i,trans}\right) \tag{5.6}$$

Where $S_{i,surface}$ and $S_{i,gas}$ are the standard entropy of the adsorbed species and gas species, respectively. F_{loc} is the fraction of the local entropy retained by the surface species. It was assumed that all adsorption species were characterized by the same fraction F_{loc} which was used as an adjustable parameter in our model. $S_{i,trans}$ is the translational entropy of the gaseous species which is defined in equation (5.7):

$$S_{i,trans} = R\left[\ln\left(\left(\frac{2\pi m k_B T}{h^2}\right)^{\frac{3}{2}}\frac{k_B T}{P}\right) + \frac{5}{2}\right] \tag{5.7}$$

Where R is the gas constant, m is the mass of species of interest, h is Plank's constant, and P is the pressure.

5.3.2.2 Kinetic parameters

For the adsorption and desorption steps 1, 3, 5, 7, and 9, (**Table 5-1**) the forward reaction rate constants were defined in the adsorption direction using collision theory as in equation (5.8):

$$k_{ads} = \frac{\theta \exp\left(-\frac{E_{ads}}{RT}\right)}{\sqrt{2\pi m k_B T}} A_{site} \quad (5.8)$$

Where θ is the species sticking probability on the catalyst surface which could adequately be assumed to be equal to 1.[141] E_{ads} is the adsorption's activation energy and because there is no bond formation or breaking involved, it is generally assumed to be of little kinetic significance.[18,22] A_{site} is the area occupied per site with a value of 10^{-19} m^2 per site as a good approximation for a typical molecular cross-sectional area.[22] For the surface reactions 2, 4, 6, and 8, the forward rate constants were defined in the way the reactions were written in **Table 5-1** and using equation (5.9):

$$k_{i,for} = A_i \, exp\left(-\frac{E_{a,i}}{RT}\right) \quad (5.9)$$

Where A_i is the preexponential factor and $E_{a,i}$ is the activation energy of the surface reaction *i*. A value of 10^3 for the preexponential factor corresponding to a typical Eley-Rideal reaction was assumed for all surface reactions.[142]

5.3.3 Modeling approach

5.3.3.1 Model equations

The conversion of butanal over the considered acid catalysts was modeled as a steady-state plug flow reactor (PFR). The kinetic model was constructed by solving 7 differential equations for the rate of change of molar flow rates with the catalyst weight along the reactor, 5 algebraic equations for the steady-state balance of adsorbed species, and 1 site balance equation. Briefly, the mass balance of gaseous species is written as equation (5.10):

$$\frac{dF_i}{dw} = \rho_s \sum r_i \quad (5.10)$$

Where F_i is the molar flow rate of the gaseous species in mol s^{-1}, w is the weight of the catalyst in g, ρ_s is the catalyst acid site density in mol (g catalyst)$^{-1}$ which was obtained from pyridine titration experiments, and r_i is the turnover frequency of species i in s^{-1}. Because H_2 gas is a reactant in reaction 2 (**Table 5-1**) and its concentration was not measured in our experiments, H_2 rate of generation in the reaction was related to the rate of aromatics formation through equation (5.11):

$$r_{H_2} = \alpha r_{C_{12}H_{18}} \tag{5.11}$$

Where r_{H_2} is the rate of formation of H_2 gas, α is a model adjustable constant, and $r_{C_{12}H_{18}}$ is the rate of aromatics formation. The value of α was chosen such that the experimental gaseous flow rates were fitted with negligible H_2 in the outlet gas. In this case, r_{H_2} becomes the rate of consumption of H_2 which should necessarily be equal to the rate of butenes formation. The mole balance for the adsorbed surface species is written as equation (5.12):

$$\rho_s \sum r_i = 0 \tag{5.12}$$

Where θ_i is the fractional coverage of the adsorbed species onto the catalyst surface. Finally, the site balance equation considers the fractions of vacant sites, sites occupied by adsorbed species, and the fraction of unavailable sites due to catalyst deactivation. The site balance is written as equation (5.13):

$$1 = \theta_V + \theta_d + \sum \theta_i \tag{5.13}$$

Where θ_V, θ_d, and θ_i are the fraction of vacant acid sites, deactivated sites, and adsorbed species i, respectively.

5.3.3.2 Catalyst deactivation model

The conversion of butanal on H-BEA zeolite at 200 ^{o}C resulted in continuous catalyst deactivation even after 4 hours of reaction time. As seen in **Figure 5.3**, butanal conversion dropped from above 30% to just below 10% during the first 4 hours. This deactivation behavior is commonly observed with aldol condensation reactions of aldehydes on acid catalysts due to the heavily condensed products and the coke adsorbing on the catalyst sites. [86,143] To reflect this catalytic phenomenon in our kinetic model, the catalyst deactivation was considered by adding a time-dependent term θ_d in equation (5.13) to account for the fraction of deactivated acid sites. θ_d was assumed to have an exponential dependence on time as in equation (5.14):

$$\theta_d = \exp\left(-k_d P^o_{C_4H_8O} t\right) \tag{5.14}$$

Where k_d is the catalyst deactivation constant and was used as an adjustable parameter in the model, $P^o_{C_4H_8O}$ is the partial pressure of butanal in the feed, and t is the time on stream.

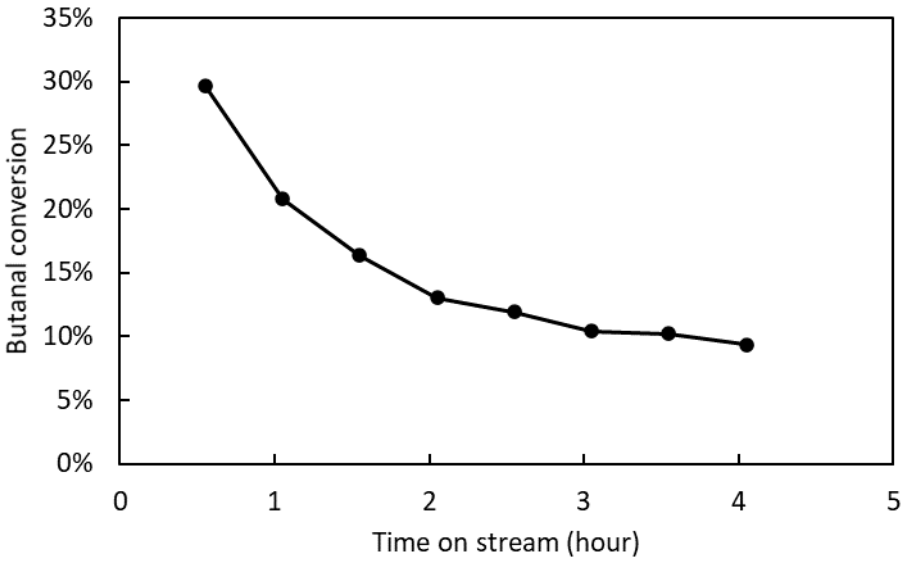

Figure 5.3: Butanal conversion on H-BEA as a function of time on stream at 200 ^{o}C. Butanal pressure was 0.54 kPa in 50 ml min^{-1} He gas and the catalyst weight was 100 mg.

5.3.3.3 Model solution and parameter estimation

The solution of the differential-algebraic equations along with the estimation of the adjustable parameters was performed using Athena Visual Studio engineering software.[144] A total of 12 parameters (5 BE_i's, 4 $E_{a,i}$'s, F_{loc}, k_d, and α) were adjusted to fit the experimental molar flow rates of butanal and all gaseous products. At first, the parameter estimation was performed on the experiments of butanal conversion over H-BEA catalyst at 200 ^{o}C, 0.54 - 2.94 kPa butanal partial pressures, and varying times on stream. Then, the estimated parameters for H-BEA catalyst were used as initial guesses to fit the data of butanal conversion on the other Na/H-BEA and Zn/H-BEA catalysts at 200 ^{o}C and 0.54 kPa butanal partial pressure. F_{loc} was estimated to be equal to 0.92 from fitting the experimental data of H-BEA and this value was assumed to be constant during the estimation of all other modified catalysts. This assumption was considered reasonable knowing that the conversion of oxygenates could be kinetically modeled assuming the same F_{loc} for different solid acid catalysts.[145] In addition, the experiments used to fit the adjustable parameters were limited to 200 ^{o}C to alleviate a temperature-dependent deactivation behavior and avoid undesirable secondary reactions which could result in an increased modeling complexity. As such, the kinetic and thermodynamic intuitions gained from the experiments on different catalysts at a particular temperature are expected to provide valuable insights and starting guide for a wider range of reaction conditions.

5.4 Results and discussion

5.4.1 Acid site titration with pyridine

Acid site titration was chosen as the technique of choice to determine the total acid site concentration of H-BEA, Na/H-BEA, and Zn/H-BEA zeolites (both Brønsted and Lewis acid sites). The advantage of using acid site titration techniques is the ability to probe the acidity of the

catalyst at normal operating conditions as opposed to other chemisorption techniques which could operate at conditions that are very far from relevant.[60] As a strong base molecule, pyridine was used to titrate the acidity of the zeolites and the number of acid sites was determined assuming a 1:1 adsorption stoichiometry. **Figure 5.4**a and b show the pyridine adsorption profile on all the tested catalysts and **Table 5-2** shows the calculated acid site densities. As can be observed from **Table 5-2**, Na-exchanged catalysts showed a clear acid site concentration reduction as expected from the neutralization of the protons of the Brønsted acid sites by the Na^+ ions.[51] On the other hand, the pyridine uptake was higher for the zeolites exchanged with Zn^{2+} indicating higher acid site concentrations. This increase in acidity was caused by the formation of Lewis acid sites as a result of the Zn^{2+} ion exchange.[67] The calculated acid concentration values (**Table 5-2**) were used as input parameters for the acid site density ρ_s in our kinetic model.

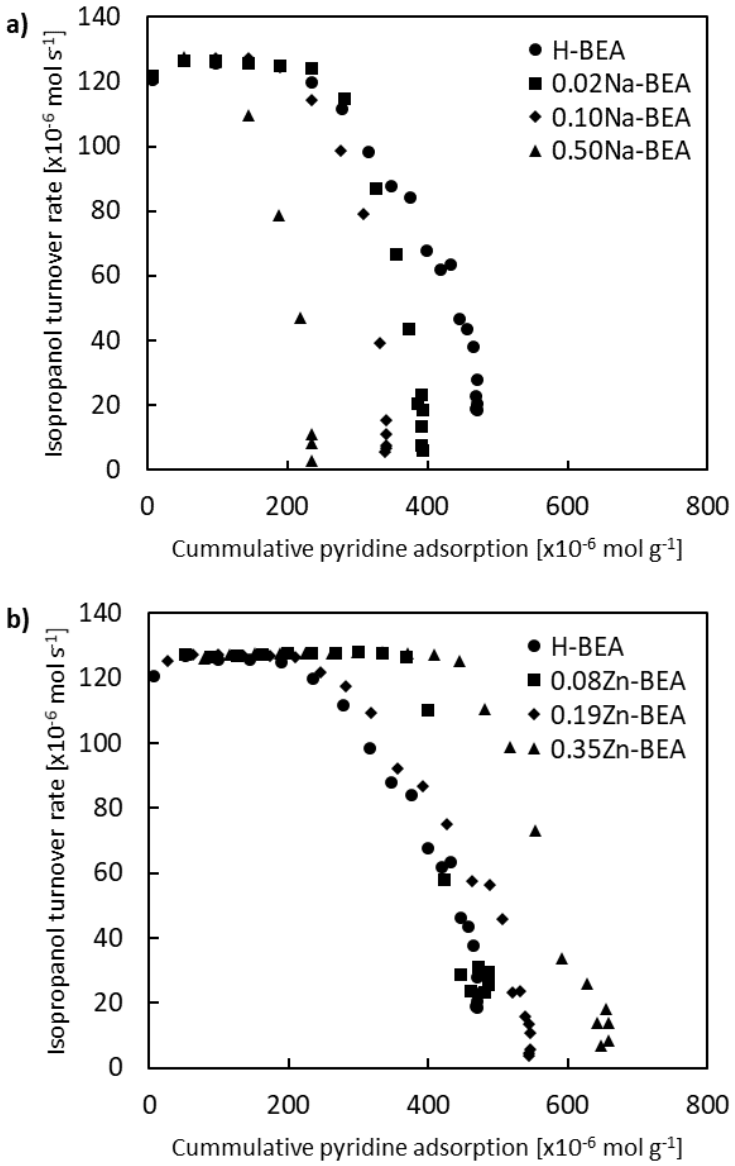

Figure 5.4: Pyridine uptake by H-BEA and a) Na/H-BEA zeolites or b) Zn/H-BEA zeolites at 200 ^{o}C. The titration was performed with 11.4 kPa isopropanol and 45.6 Pa pyridine in He gas mixture 20 mg of catalyst.

Table 5-2: Total acid site densities calculated from the pyridine titration experiments

Catalyst	Total catalyst acidity (μmol g^{-1})
H-BEA	472
0.02Na-BEA	392
0.10Na-BEA	341
0.50Na-BEA	235
0.08Zn-BEA	488
0.19Zn-BEA	546
0.35Zn-BEA	659

5.4.2 Comparing experimental and model results for butanal conversion on H-BEA

The turnover rates of products from the conversion of butanal on H-BEA at 200 ^{o}C and varying feed partial pressures were compared with the experimental values to ensure proper model prediction and parameter estimation. **Figure 5.5**a-e show the parity plots for the conversion of butanal over the H-BEA catalyst. The coefficient of determination (R^2) values of 0.887 - 0.952 in **Figure 5.5**a-e indicates the ability of the model to capture the trends of the turnover rates for all product lumps at varying conditions and times on stream.

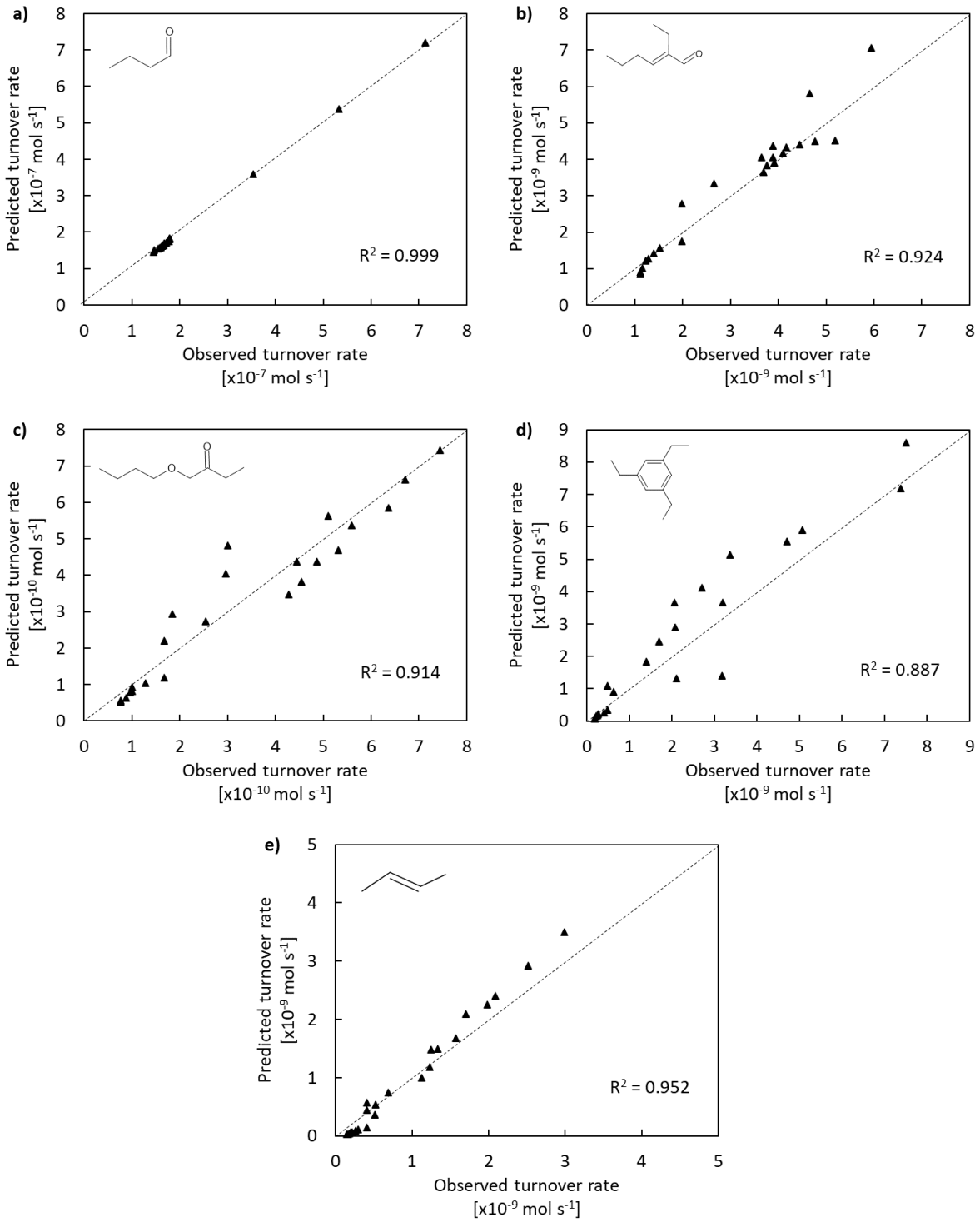

Figure 5.5: Parity charts comparing the experimental and model-predicted turnover rates of a) butanal feed, b) 2-ethyl-2-hexenal product lump, c) butyl butyrate product lump, d) C_{10}+ aromatics lump, and e) butenes. Butanal conversion rates were measured at 200 ^{o}C, 0.54 – 2.94 kPa butanal partial pressure in He, and 10 - 100 mg catalyst weight. The displayed structure on figures b - e indicates the most abundant species in the product lump.

5.4.3 Turnover rates of different products

5.4.3.1 Aldol condensation products

The ion exchange with Na^+ reduced the turnover rates of aldol condensation products compared with H-BEA (**Figure 5.6**b). This is expected due to the reduction of total acid sites within the catalyst as observed in **Table 5-2**. However, Na^+ is also known to catalyze the aldol condensation in acidic catalysts such as MFI zeolites.[51] This catalyzation by Na^+ is clearer when comparing initial rates normalized by the number of acid sites (**Figure 5.7**a) where higher turnover frequencies were obtained at higher Na^+ loadings. As seen in **Figure 5.7**a, the observed turnover frequencies of aldol condensation products were 9.68×10^{-5} s^{-1} for H-BEA, 9.21×10^{-5} s^{-1} for 0.02Na-BEA, 1.04×10^{-4} s^{-1} for 0.10Na-BEA, and 1.55×10^{-4} s^{-1} for 0.50Na-BEA.

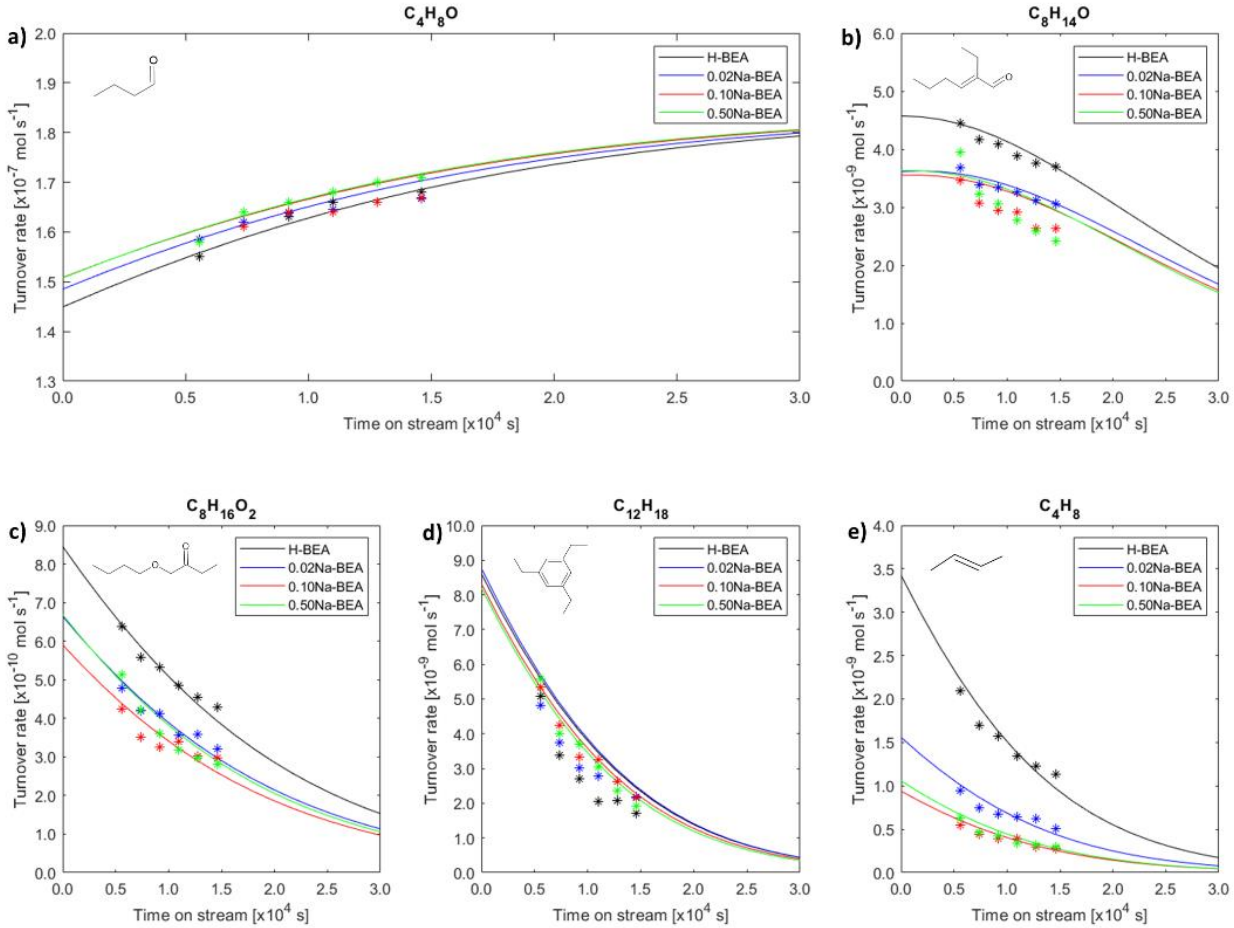

Figure 5.6: Predicted and experimental flow rates of a) butanal, b) aldol condensation products, c) esterification products, d) aromatics, and e) butenes resulting from the conversion of butanal on H-BEA and Na/H-BEA catalysts. Reactions were performed with 0.54 kPa butanal partial pressure in He, 100 mg catalyst weight, and 200 ^{o}C temperature. Experimental data are shown as stars (*) and modeled results are shown as solid lines

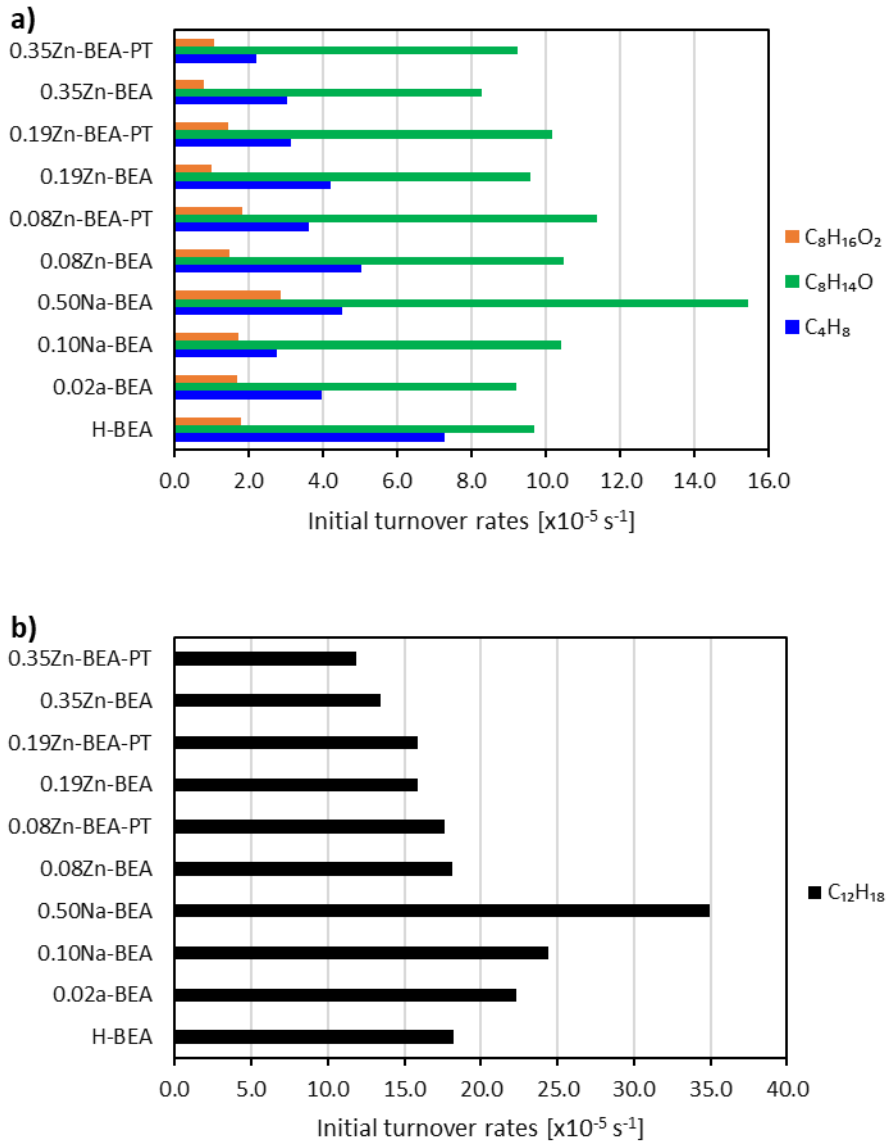

Figure 5.7: Initial turnover rates per acid site (zero time on stream) for the conversion of butanal on H-BEA, Na/H-BEA, and Zn/H-BEA predicted from the kinetic model.

Zn-loaded catalysts appear to increase the aldol condensation rates compared to unexchanged H-BEA (**Figure 5.8**b) as expected from the higher acid site contents. The ion exchange with Zn^{2+} is known to produce different acidic sites which include Zn^{2+} sites bridging the oxygen of two Al tetrahedra and the $[Zn - O - Zn]^{2+}$ sites bridging two aluminum tetrahedra

with the latter dominating at higher Zn/Al ratios.[67] As seen in **Figure 5.7**a, the observed turnover frequencies of aldol condensation products were 1.05×10^{-4} s^{-1} for 0.08Zn-BEA, 9.58×10^{-5} s^{-1} for 0.19Zn-BEA, and 8.27×10^{-5} s^{-1} for 0.35Zn-BEA. Because the turnover rates of aldol condensation products were observed to slowly fade away with increased Zn^{2+} content, it is expected that the main Zn^{2+} sites catalyzing the conversion to aldol condensation products are Zn^{2+} sites bridging the oxygens of two Al tetrahedra. However, the temperature-pretreated 0.80Zn-BEA-PT, 0.19Zn-BEA-PT, and 0.35Zn-BEA-PT showed 9%, 6%, and 12% higher turnover frequencies compared with the non-pretreated ones, respectively. This could be a result of the conversion of the hydrated $Zn(OH)^{+}$ sites, which are known to be present in Zn-exchanged zeolites and could easily be dehydrated upon heating[103], to a more active dehydrated Zn^{2+} site. This in turn suggests that $Zn(OH)^{+}$ sites are less active than their dehydrated forms.

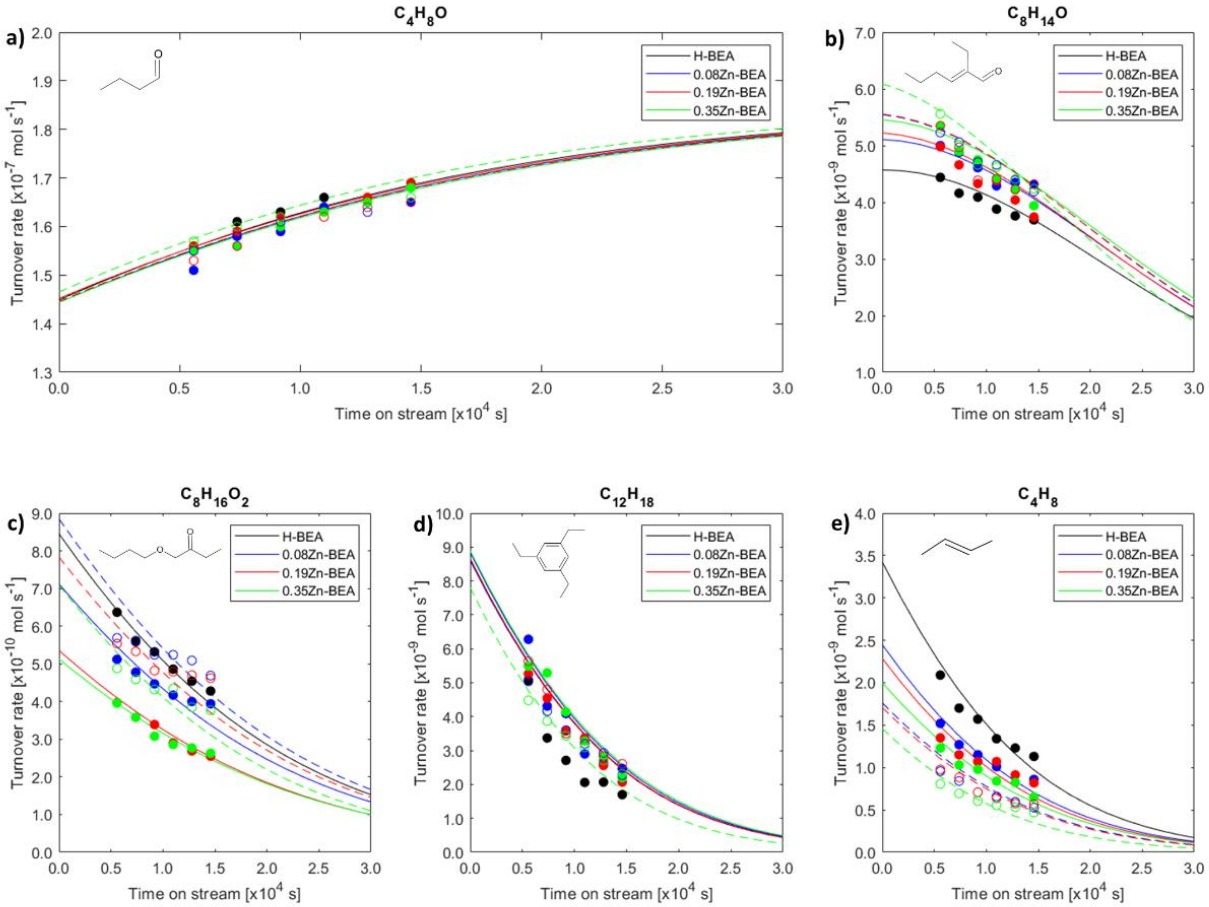

Figure 5.8: Predicted and experimental flow rates of a) butanal, b) aldol condensation products, c) esterification products, d) aromatics, and e) butenes resulting from the conversion of butanal on H-BEA and Zn/H-BEA catalysts. Reactions were performed with 0.54 kPa butanal partial pressure in He, 100 mg catalyst weight, and 200 ^{o}C temperature. Experimental data are shown as filled circles (for the none pretreated catalysts) and empty circles (for the temperature pretreated catalysts). The modeled results are shown as solid lines.

5.4.3.2 Tishchenko esterification products

The turnover rates of Tishchenko esterification products were seen to decrease on Na-exchanged zeolites similar to what was observed with aldol condensation products (**Figure 5.6**c). Unlike the aldol condensation products, the turnover frequencies of esterification products (**Figure 5.7**a) showed similar values of 1.79×10^{-5} s^{-1} for H-BEA, 1.69×10^{-5} s^{-1} for 0.02Na-BEA, and 1.73×10^{-5} s^{-1} for 0.10Na-BEA. The similarity in these turnover frequencies clearly indicates that products like butyl butyrate were not catalyzed by Na^+ and their turnover rates were merely governed by the availability of acid sites. However, the higher turnover frequency of 2.85×10^{-5} s^{-1} observed over 0.50Na-BEA could be attributed to esterification products turning over non-acidic sites which might have formed upon ion exchange with higher Na^+ loading.

On the Zn-loaded zeolites, the turnover rates of esterification products were seen to decrease with the Zn^{2+} loading (**Figure 5.8**c). As observed in **Figure 5.7**a, the turnover frequencies of esterification products proportionally decreased with Zn loading with values of 1.46×10^{-5} s^{-1} for 0.08Zn-BEA, 1.44×10^{-6} s^{-1} for 0.19Zn-BEA, and 7.78×10^{-6} s^{-1} for 0.35Zn-BEA. In addition, the temperature-pretreated samples 0.80Zn-BEA-PT, 0.19Zn-BEA-PT, and 0.35Zn-BEA-PT showed 24%, 46%, and 38% higher turnover frequencies than those observed over their non-pretreated versions, respectively. However, these increases in rates were much higher than the rates observed for aldol condensation products suggesting differences in catalyzation sites. Although some acid site properties were expected to change upon the thermal pretreatment, these changes could also include increasing the catalyst basicity with basic sites. These basic sites could include lattice oxygen atoms bridging two Al atoms, tricoordinated with three Al atoms, and terminal OH groups.[146] Basic sites of such sort and those present in metal oxides are known to catalyze Tishchenko-type esterification reactions.[47,117]

5.4.3.3 Aromatic products

As observed in **Figure 5.6**d, the turnover rates of aromatics over Na-BEA catalyst slightly increase with increased Na^+ loading. By examining **Figure 5.7**b, the turnover frequencies of aromatics over the Na-exchanged were seen to proportionally increase with Na^+ loading with values of 1.82×10^{-4} s^{-1} for H-BEA, 2.23×10^{-4} s^{-1} for 0.02Na-BEA, 2.44×10^{-4} s^{-1} for 0.10Na-BEA, and 3.49×10^{-4} s^{-1} for 0.50Na-BEA. This is consistent with the turnover trend for aldol condensation products shown in **Figure 5.7**a as they represent the intermediate steps before aromatics formation. Similarly, the turnover rates of aromatics over Zn-loaded catalyst showed a slight increase proportional to the Zn^{2+} loading (**Figure 5.8**d). On the contrary, the turnover frequencies of aromatics (**Figure 5.7**b) tended to decrease with Zn^{2+} loading with values of 1.81×10^{-4} s^{-1} for 0.08Zn-BEA, 1.59×10^{-4} s^{-1} for 0.19Zn-BEA, and 1.35×10^{-4} s^{-1} for 0.35Zn-BEA. These trends were similar to those observed with aldol condensation products. However, the pretreated catalysts 0.08Zn-BEA-PT and 0.35Zn-BEA-PT showed 3% and 12% reductions in turnover frequencies compared to their non-pretreated versions, respectively, while 0.19Zn-BEA-PT and 0.19Zn-BEA showed almost the same turnover frequency. The reduction in turnover frequencies of aromatics upon pre-treatment could be explained by the loss of some Brønsted acid sites during the dehydration of $Zn(OH)^+$ species into bridging Zn sites which are known to occur over Zn/H-BEA zeolite.[67]

5.4.3.4 Direct dehydration-hydrogenation to butenes

The turnover rates of butenes were seen to decrease with Na^+ loading as depicted in **Figure 5.6**e and this is expected knowing that Na^+ replaces the protons on the zeolite surface (Brønsted acids sites) and that the direct dehydration-hydrogenation of aldehydes is known to be predominantly catalyzed by Brønsted acid sites that are present on acidic catalysts.[51,95] The

turnover frequencies of butenes formation over Na-exchanged zeolites were also seen to decrease with Na loading with values of 7.25×10^{-5} s^{-1} for H-BEA, 3.97×10^{-5} s^{-1} for 0.02Na-BEA, and 2.75×10^{-5} s^{-1} for 0.10Na-BEA. This result is anticipated realizing that the turnover frequencies are calculated by normalizing the molar flow rates by the total acid sites which include both Brønsted and Lewis acids sites. In addition, it is inferred from the reduction of turnover frequencies with Na^+ loading that the distribution of the acid sites was shifting towards weaker acid sites. This shift in acid site distribution is typical for Na^+ exchanged BEA zeolites evident from the observed shift in NH_4-TPD peaks to lower desorption temperatures compared with unexchanged H-BEA.[147] Similar behavior was observed with Zn-loaded zeolites where butenes turnover rates were observed to decrease with Zn-loading (**Figure 5.8**e). In addition, the turnover frequencies of butenes shown in **Figure 5.7**a tended to decrease with Zn^{2+} loading with values of 5.52×10^{-5} s^{-1} for 0.08Zn-BEA, 4.19×10^{-5} s^{-1} for 0.19Zn-BEA, and 3.03×10^{-5} s^{-1} for 0.35Zn-BEA. Moreover, the temperature pretreated 0.80Zn-BEA-PT, 0.19Zn-BEA-PT, and 0.35Zn-BEA-PT showed 28%, 25%, and 27% lower turnover frequencies compared with non-pretreated ones, respectively. This reduction could be potentially caused by the coupling of $Zn(OH)^+$ species with acidic OH groups in Brønsted acid sites to form water and a Zn^{2+} cation intersecting with two aluminum sites.[103]

5.4.4 Degree of rate control

One of the powerful tools to determine the rate-limiting steps in a reaction network is the use of Campbell's degree of rate control (DRC) as written in equation (5.15) [148,149]:

$$X_{RC,i} = \frac{k_i}{r}\left(\frac{\partial r}{\partial k_i}\right)_{k_{j\neq i},\, K_i} \tag{5.15}$$

Where $X_{RC,i}$ is defined as the relative increase in the net rate r to the relative increase in the rate constant k_i of the reaction step i while keeping the equilibrium constant of that step K_i and the

reaction constants of all other elementary steps $k_{j\neq i}$ constant. When calculated for a particular elementary step, a positive value means that increasing k_i will increase the net rate r and when $X_{RC,i}$ approach a value of 1, step *i* is termed a rate-limiting step (RLS).[149] The opposite is true when the DRC is negative where *i* becomes an inhibiting step. As depicted in **Figure 5.9**, the $X_{RC,i}$ values on the rate of butanal conversion where 0.52 for aldol condensation reactions, 0.04 for esterification reactions, and 0.31 for aromatics formation reactions. $X_{RC,i}$ values for all other reactions were negligible which means that they had little to no influence on butanal conversion rates. The result indicates that aldol condensation is the rate-limiting step in our reaction scheme.

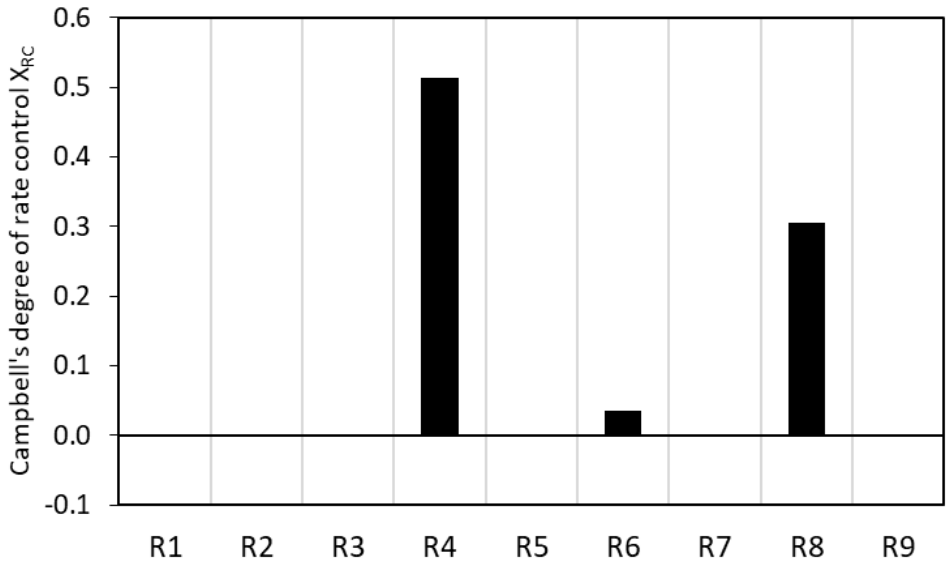

Figure 5.9: Campbell's degree of rate control for the conversion of butanal on H-BEA catalyst. Rx represents reaction number "x" from the reaction sequence in **Table 5-1**.

5.4.5 Comparing activation energies of reaction steps

The activation energy for the formation of aldol condensation products was seen to decrease with lower acid site densities (**Figure 5.10**a). Compared with 79.1 kJ mol^{-1} for the H-BEA catalyst, the activation energies were 78.7 kJ mol^{-1} for 0.02Na-BEA, 78.6 kJ mol^{-1} for

0.10Na-BEA, and 77.5 kJ mol^{-1} for 0.50Na-BEA. This reduction in activation energy was behind the observed increase in turnover frequencies of aldol condensation products over Na-loaded zeolites (**Figure 5.7**a). On Zn-loaded catalysts, the activation energy of aldol condensation reactions (**Figure 5.10**d) was seen to initially decrease to 78.6 kJ mol^{-1} for 0.08Zn-BEA then increase with higher metal loads to 79.2 kJ mol^{-1} for 0.19Zn-BEA and to 79.6 kJ mol^{-1} for 0.35Zn-BEA catalysts. In addition, the activation of the Zn-loaded zeolites resulted in a slight increase of 0.12 and 0.36 kJ mol^{-1} in activation energy for 0.08Zn-BEA-PT and 0.35Zn-BEA-PT, respectively, with 0.19Zn-BEA-PT showing almost no change relative to its none pretreated version. This trend in activation energy was clearly reflected in the turnover frequencies of aldol condensation formation observed in **Figure 5.7**a where 0.08Zn-BEA with the lowest activation energy barrier shows the highest turnover frequency compared with H-BEA and other Zn-loaded catalysts. The lower activation energy observed with 0.08Zn-BEA compared to H-BEA (although they had almost the same acid site density) and to samples with higher Zn^{2+} loading suggests that isolated Zn^{2+} species connecting two Al tetrahedra were more favorable in catalyzing aldol condensation products than other forms of Zn^{2+} species.

Figure 5.10b shows the activation energy for the esterification products where a slight increase in activation energy was observed with lower acid site concentrations going from 89.9 kJ mol^{-1} for H-BEA to 90.4 kJ mol^{-1} for 0.10Na-BEA. However, 0.50Na-BEA showed a reduction in activation energy to 88.7 kJ mol^{-1}. This off-trend reduction in activation energy suggests that esterification products were catalyzed differently at such a higher Na^{+} loading and as will be explained in the following sections. This observation was also in line with the observed higher turnover frequency of esterification products over 0.50Na-BEA (**Figure 5.7**a) compared with other Na-loaded catalysts. On Zn-loaded catalysts, the activation energy for esterification reactions

(**Figure 5.10**e) proportionally increased with Zn^{2+} with values of 90.3 kJ mol^{-1} for 0.08Zn-BEA, 92.0 kJ mol^{-1} for 0.19Zn-BEA, and 92.7 kJ mol^{-1} for 0.35Zn-BEA. In addition, the pretreated samples showed reductions in the activation energies compared to none pretreated samples with values of 89.6 kJ mol^{-1} for 0.08Zn-BEA-PT, 90.6 kJ mol^{-1} for 0.19Zn-BEA-PT, and 91.7 kJ mol^{-1} for 0.35Zn-BEA-PT. These activation energy trends were well correlated with the activities of these catalysts in catalyzing esterification products where increasing the Zn^{2+} content resulted in lower turnover frequencies which tend to increase when the catalyst was pretreated (**Figure 5.7**a). Furthermore, and contrary to what was noted with Na-loaded catalysts, the activation energy for esterification reactions shown in **Figure 5.10**e generally followed the site acidity trends but with the none pretreated samples falling slightly above the acidity trend. Similar to aldol condensation products, the activation energies for the formation of aromatics (**Figure 5.10**c) proportionally decreased with lower acid site density with values going from 81.5 kJ mol^{-1} for H-BEA to 77.7 kJ mol^{-1} for 0.50Na-BEA. As seen in **Figure 5.10**f, the activation energies for the formation of aromatics on Zn-loaded catalysts also correlated well with the increase in acid site density with higher Zn^{2+} content. The activation energy values were 81.8 kJ mol^{-1} for 0.08Zn-BEA, 82.3 kJ mol^{-1} for 0.19Zn-BEA, and 83.3 kJ mol^{-1} for 0.35Zn-BEA. Unlike the aldol condensation products, the activation energy increase even at low Zn^{2+} loading suggests that aromatics formation was less favorable on Zn^{2+} Lewis acid sites. Pretreating the catalysts resulted in marginal increases of 0.11 – 0.30 kJ mol^{-1} in the activation energy of aromatics similar to what was observed with the formation of aldol condensation products. Besides all other products, the activation energies of butenes were all low with values less than 10^{-5} kJ mol^{-1}. This suggests that butenes formation was readily activated within our model given the estimated pre-exponential factors.

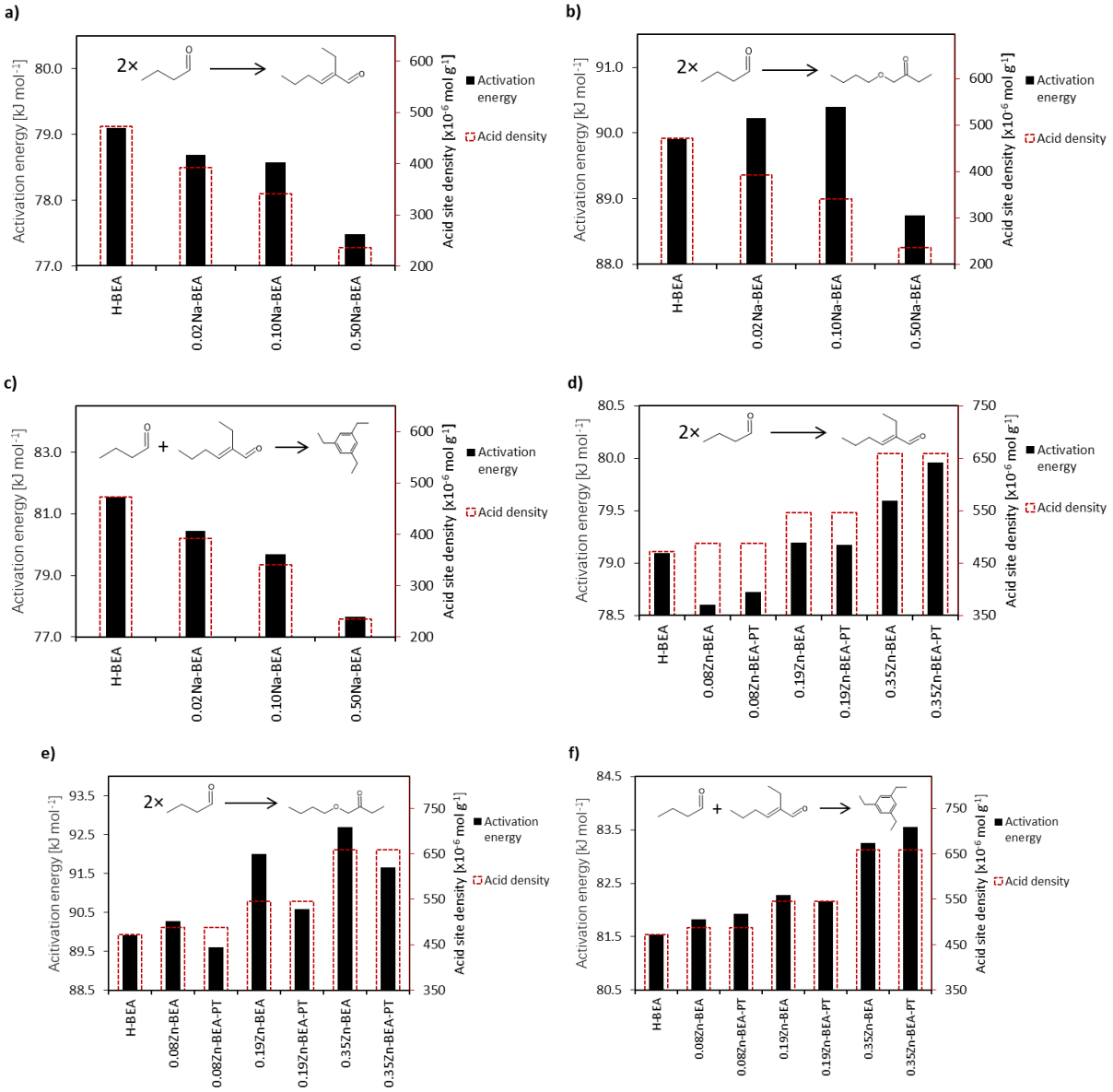

Figure 5.10: Comparing activation energies for forming a) aldol condensation products on Na/H-BEA catalysts, b) Tishchenko esterification products on Na/H-BEA catalysts, c) aromatic reactions on Na/H-BEA catalysts, d) aldol condensation products on Zn/H-BEA catalysts, e) Tishchenko esterification products on Zn/H-BEA catalysts, and f) aromatic reactions on Zn/H-BEA catalysts.

5.4.6 Binding energies and fractional surface coverages of adsorbed species

Figure 5.11a shows the binding energies of butanal on the Na-loaded catalysts. As can be observed in **Figure 5.11**a, the binding energy of butanal initially decreased from 66.2 kJ mol^{-1} for H-BEA to 65.8 kJ mol^{-1} for 0.02Na-BEA then increased with higher loading of Na^+ to 65.9 kJ mol^{-1} for 0.10Na-BEA then to 66.1 kJ mol^{-1} for 0.50Na-BEA. The decrease in butanal binding energy with lower loading of Na^+ was most likely attributed to the reduction in the acid site concentration. With higher Na^+ loading, the increase in binding energy is more likely induced by the Na^+ cations as their catalyzation to condensation products becomes more apparent at higher loadings. As illustrated in **Figure 5.11c**, Zn-loaded catalysts showed similar trends where increasing the Zn^{2+} loading initially decreased the binding energy of butanal to 65.8 kJ mol^{-1} for 0.08Zn-BEA then gradually increased it to 66.0 kJ mol^{-1} for 0.19Zn-BEA then to 66.2 kJ mol^{-1} for 0.35Zn-BEA. Upon pre-treatment, all Zn-loaded catalysts showed an increase in binding energy to the same value of 66.1 – 66.2 kJ mol^{-1}. The binding energies of aldol condensation products (**Figure 5.11**b) were proportionally decreasing with the decrease in total acid sites with values of 93.2 kJ mol^{-1} for H-BEA, 92.8 kJ mol^{-1} for 0.10Na-BEA, and 92.0 kJ mol^{-1} for 0.50Na-BEA. The similarity in binding energies on H-BEA and 0.02Na-BEA (with the lowest Na^+ loading) suggests that the total acid site density had negligible impact on the binding energy of aldol condensation products and that the lower energies observed with 0.10Na-BEA and 0.50Na-BEA were potentially a result of Na^+ interactions with the adsorbed species. The binding energy of aldol condensation products on Zn-loaded catalysts denoted in **Figure 5.11**d showed a minor initial decrease in butanal binding energy to 93.0 kJ mol^{-1} for 0.08Zn-BEA which gradually increased with higher metal loadings to 93.1 kJ mol^{-1} for 0.19Zn-BEA and to 93.7 kJ mol^{-1} for 0.35Zn-BEA. However, and unlike the case with butanal adsorption, the catalyst pre-treatment resulted in a reduction in the binding energies

compared to their untreated versions with values of 93.0 kJ mol^{-1} for 0.08Zn-BEA-PT, 92.8 kJ mol^{-1} for 0.19Zn-BEA-PT, and 93.1 kJ mol^{-1} for 0.35Zn-BEA-PT. The binding energies of butenes, esterification, and aromatic products on all tested catalysts were found to be less than -10^{-3} kJ mol^{-1}.

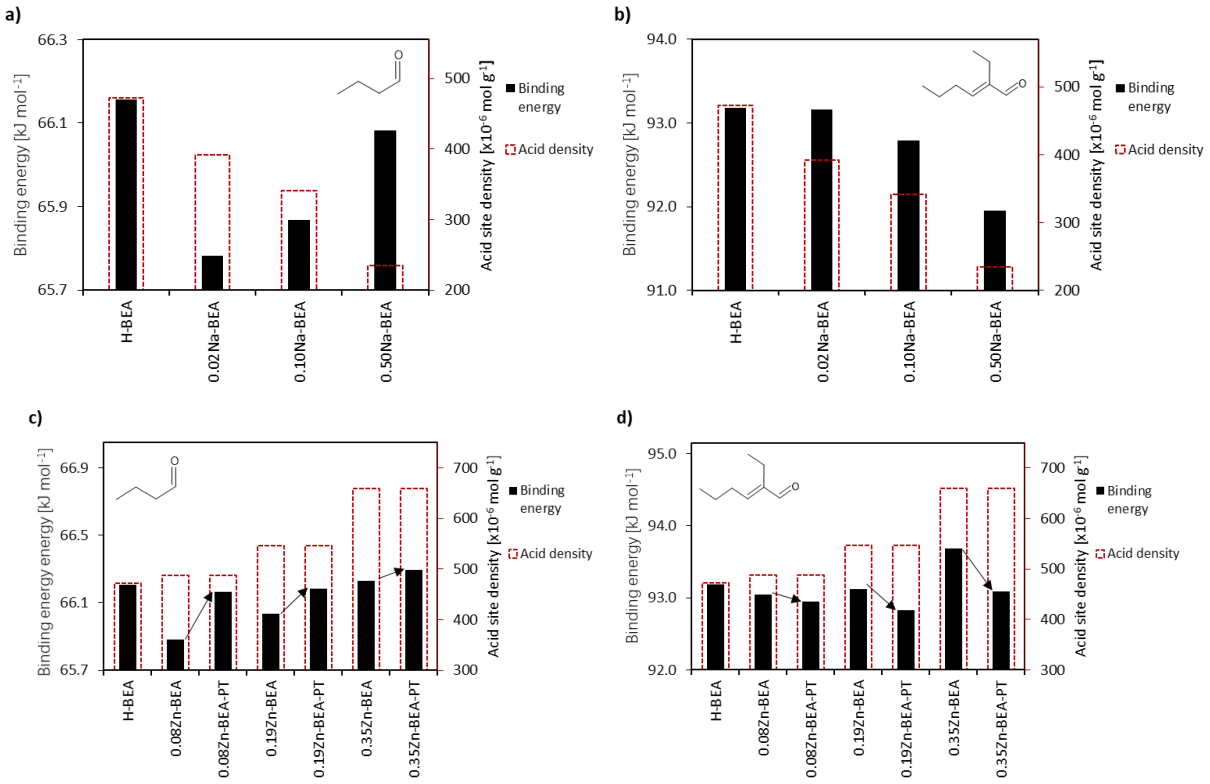

Figure 5.11: Comparing binding energies of a) butanal on Na/H-BEA catalysts, b) aldol condensation products on Na/H-BEA catalysts, c) butanal on Zn/H-BEA catalysts, and d) aldol condensation products on Zn/H-BEA catalysts. Black arrows indicate how binding energy changed upon catalyst activation.

To understand the influence of the binding energy changes on the kinetics of butanal conversion, the turnover frequencies of various products were calculated at varying binding energies of butanal and aldol condensation products and the results were plotted in **Figure 5.12**. As can be observed from the results in **Figure 5.12**a, the model predicts that increasing the

catalyst's surface binding energy to butanal increases the turnover rate of aldol condensation and to a lesser extent the turnover rate of esterification products. This observation is also reflected in **Figure 5.12**c which shows that butanal covers the entire catalyst surface as its binding energy approaches 100 kJ mol^{-1}. The model also suggests that the binding energies of butanal on H-BEA catalyst are near the optimal values for the highest turnover rates of aromatics and butenes products (at constant binding energies of other species). As expected, lowering the binding energy of butanal results in a reduction in the turnover rates of all products due to the inability of the molecule to adsorb for reaction. This can be noted in **Figure 5.12**c where the catalyst surface becomes vacant as the binding energy of butanal approaches -40 kJ mol^{-1}. **Figure 5.12**b shows the predicted turnover frequencies of different products over the H-BEA catalyst at different binding energies of aldol condensation products. As can be inferred from **Figure 5.12**b, increasing the catalyst's binding energy to aldol condensation products results in a reduction in their turnover rates. This was due to the limited product desorption caused by strong surface interaction with aldol condensation products. This was apparent from **Figure 5.12**d where aldol condensation became the most dominant surface species as their adsorption energy approaches -100 kJ mol^{-1}. This reduction in the turnover frequency of aldol condensation products was coupled with an increase in butenes and aromatics turnover frequencies. On the other hand, the turnover frequencies of aldol condensation products increase as their binding energies approach -40 kJ mol^{-1}. This was concomitant with a reduction in both aromatics and butenes as their formation was dependent on the activation of aldol condensation products on the catalyst surface.

By analyzing the binding energy trends discussed earlier for the different catalysts (**Figure 5.12**a-d), it can be observed that Na^{+}, Zn^{2+}, and Brønsted acid sites on the catalyst surface all increase the apparent binding energy of butanal resulting in more conversion to aldol condensation

products. At the same time, having more Zn^{2+} and Brønsted acid sites on the catalyst surface increases the binding energy of aldol condensation making desorption from the catalyst surface more difficult. This mixed influence by Zn^{2+} was the reason behind the lower turnover frequencies observed experimentally with higher loading of Zn^{2+}. On the contrary, the ion exchange with Na^{+} lowers the binding energy of aldol condensation products which results in their higher turnover frequencies. This anticipated increase in turnover rates was observed experimentally with Na-BEA catalysts (**Figure 5.7**a). The activation of Zn^{2+} species on the H-BEA catalysts resulted in higher turnover frequencies of aldol condensation products due to the simultaneous increase and reduction in butanal and aldol condensation products' binding energies, respectively. Such binding energy variations make Zn-BEA-PT more favorable in catalyzing aldol condensation products while limiting the formation of aromatics (**Figure 5.7**b) by increasing the energy barrier for their formation (**Figure 5.10**f).

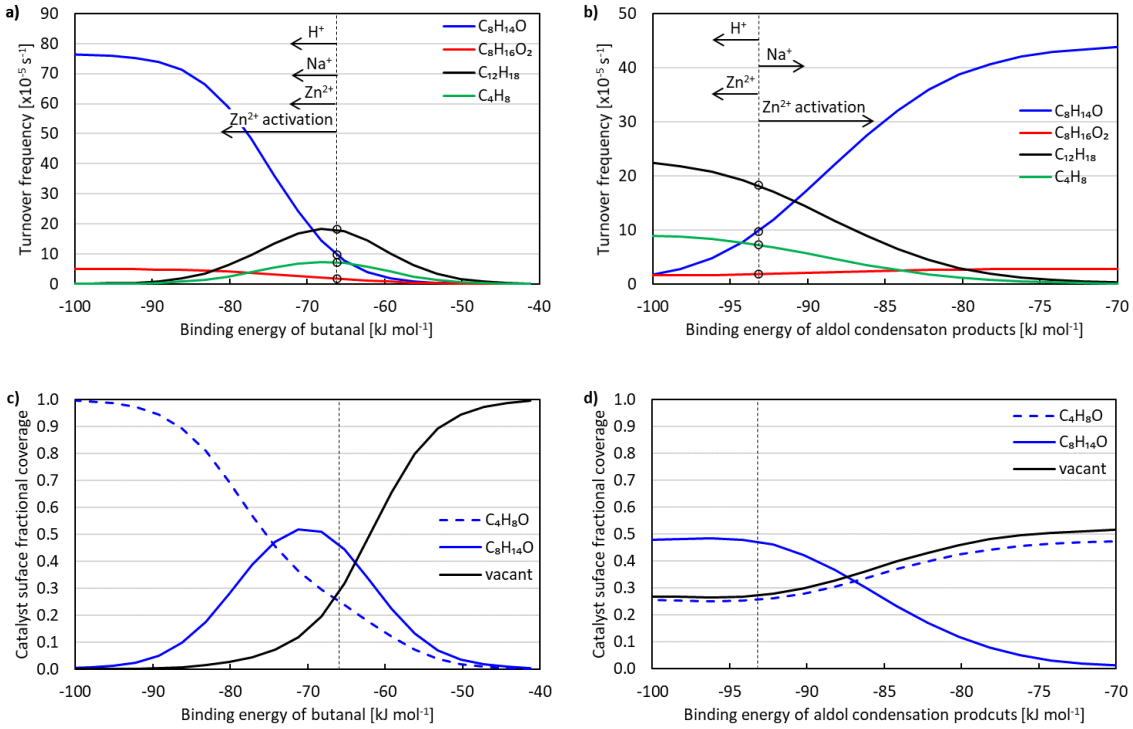

Figure 5.12: Model-predicted turnover frequencies of various products over H-BEA catalyst as a function of a) butanal binding energy (at -93.2 kJ mol^{-1} aldol condensation BE) and b) aldol condensation binding energy (at -66.2 kJ mol^{-1} butanal BE). The fractional coverages of adsorbed species are shown in c) as a function of butanal binding energy and in d) as a function of aldol condensation binding energy. The dotted black line indicates the binding energy value estimated on the H-BEA catalyst. the black solid arrows indicate the direction in which the binding energies would move when Brønsted acid sites and metal loadings are increased.

5.5 Conclusion

The conversion of butanal over H-BEA catalysts produce a wide range of products which could be divided into four product lumps namely, aldol condensation, Tishchenko esterification, aromatization, and dehydration-hydrogenation products. The kinetic model of Na/H-BEA and Zn/H-BEA catalysts explained how changes in Brønsted acid site and metal concentrations play part in altering the activation energies of surface reactions and the binding energies of adsorbed species. The turnover rates of aldol condensation and aromatic products were largely influenced by changes in surface species binding energies induced by Brønsted acid site concentration and

Zn^{2+} metal loading. Zn^{2+} metal loading varied the apparent binding energies of both butanal and aldol condensation products whereas Brønsted acid site concentration only varied the binding energy of butanal. However, and unlike the formation of aldol condensation products, the activation energy for the formation of aromatic products strongly correlated with total acid site concentration on the catalyst surface irrespective of the type of acid site type or Zn^{2+} metal coordination. The catalyzation of aldol condensation and aromatic products with Na^{+} was explained by the simultaneous increase and reduction in butanal and aldol condensation product binding energies with loading, respectively. The predicted turnover rates of esterification products and their responses to changes in catalyst surface energies suggest that they were more likely catalyzed by nonacidic sites. Finally, while butenes formation from the direct dehydration-hydrogenation of butanal is readily activated with negligible apparent energy barrier, it is heavily dependent on the availability of hydrogen from donating species such as aromatics.

Chapter 6: Reactivity study of butanal with isobutane co-feed on H-BEA modified with Zn^{2+} cations

6.1 Introduction

Aromatics such as benzene, toluene, and xylenes (BTX) are important building blocks for the production of numerous industrial products.[150,151] Conventionally, high yields of BTX aromatic compounds are produced from the naphtha reforming process which uses a metal-acid bifunctional catalyst consisting of metals like Pt and Ru on alumina supports.[152] Proper integration of these metallic and acidic functionals is paramount for promoting dehydrogenation, hydrogenation, isomerization, and cyclization reactions to optimize catalyst performance and stability.[153,154] Research on metal-acid catalysts and their optimum combination has encouraged more on-purpose methods for producing aromatics such as the aromatization of methane[155,156], C_2+ alkanes[157–159] and oxygenated hydrocarbons taken from renewable sources such as biomass[94,160]. These catalysts are preferably made of metal-loaded zeolites owing to their acid site turnability and higher resistance to deactivation compared with metal oxide supports such as alumina.[158]

In particular, the modification of zeolites with transition metals has been observed to enhance the dehydrogenation and cracking of light alkanes resulting in higher aromatic yields.[155,156,161,162] The influence of transition metals on the activation of light alkanes could be seen through the work of Sun et al.[162] where they noted the reduction in the apparent activation energies of both cracking and dehydrogenation of isobutane from 121.7 kJ mol^{-1} to 65.7 kJ mol^{-1} and from 123.4 kJ mol^{-1} to 52.5 kJ mol^{-1}, respectively, on Zn/HZSM-5 compared with

acidic HZSM-5. The higher dehydrogenation ability observed over Zn-loaded zeolites is a result of the strong C-H bond activation by Zn species as confirmed by the faster and less energetic exchange rate (more than two orders of magnitude faster with around 52 kJ mol^{-1} lower activation energy) between zeolitic hydrogen on Zn/H-BEA and deuterated methane compared with the rate of exchange on H-BEA.[98,163] Besides light alkanes, the modification of zeolites with transition metals could also enhance the hydrogenolysis reactions of oxygenates to produce aromatics and water. For example, Ausavasukhi et al.[64] showed that metal-impregnated Ga/ZSM-5 enhanced the incorporation of hydrogen to produce water and toluene from benzaldehyde instead of exclusively producing benzene and CO in the case of none modified ZSM-5. In another study, Yu et al.[94] demonstrated how ZSM-5 impregnated with different transition metals could enhance the aromatization of isobutyl alcohol with Zn/HZSM-5 giving the highest yield of 60 wt% aromatics. Recently, Nash et al.[66] showed how incorporating Zn onto Cu-BEA boosts the research octane number (RON) of gasoline produced from DME conversion by generating more olefins through dehydrogenation events.

Although zeolites make great catalysts for the formation of aromatics from alkanes and oxygenated hydrocarbons, there are some pitfalls in treating each of these reactants individually. For instance, light alkanes generally require high reaction temperatures to initial oligomerization to aromatics whereas oxygenated hydrocarbons could readily convert to diverse and heavy products that could result in quick catalyst deactivation even at temperatures well below those required for alkane aromatization.[48] The co-feeding of light alkanes with oxygenates has received a particular research interest as a way to mitigate catalyst deactivation and to advantageously harness the distinctive chemistries of alkanes and oxygenates. Some studies showed that co-feeding butanes with methanol or DME resulted in prolonged catalytic life of

ZSM-5 and higher yields of olefins (compared with feeding methanol alone) while simultaneously approaching an autothermal reaction condition from the exothermic and endothermic conversion of alkanes and methanol, respectively[36,50] Song et al.[164] investigated the performance of ZSM-5/ZSM-11 impregnated with Zn for the conversion of methanol with n-butane co-feed at 510 ^{o}C and showed how the metal modification could improve the catalyst stability and raise the selectivity to aromatics from 26 to 41%. Aside from having the metal itself, the activity of the catalyst is highly dependent on the metal incorporation method. For example, Penzien et al.[67] showed how different loadings of Zn prepared by ion exchange could result in different Zn Lewis acidic species which include 1) Zn exchanged to two tetrahedral aluminum sites, 2) Zn exchanged to one tetrahedral aluminum as $Zn(OH)^{+}$, 3) two aluminum-bonded Zn sites bridged by oxygen, and 4) ZnO clusters located at the outer surface or inside the catalyst pores. Variations in the reactivities of these sites were apparent from their distinctive interactions with probe molecules such as isopropylamine and acetonitrile.[67] Furthermore, reactivities of various Zn species resulting from different preparation methods were also recognized in the conversion of some alkanes and oxygenates.[103,159,160,165,166]

The forgoing research findings underline the superior ability of zeolites loaded with transition metals such as Zn in the aromatization of light alkanes and biomass-derived oxygenates. They also highlight the advantages of co-feeding alkanes with oxygenates and how it leads to enhanced aromatization and higher catalyst stability. However, much of the research attention on aldehydes, ketones, and alcohols focused on their individual conversions with alkane co-feeding studies centering mostly on methanol. In this chapter, we investigate the deoxygenation and aromatization of butanal (a model compound representing the oxygenates that constitute nearly 60wt% of bio-oils) with isobutane co-feeding on Zn/H-BEA zeolite with different metal loadings.

Ion exchange was used as a technique of choice for metal loading owing to its ability to generate more active Zn species at exchangeable hydroxyl sites on H-BEA.[160] Temperature-programmed-desorption (TPD) of isopropylamine was used to quantify the proportions of Brønsted and different Zn Lewis acid sites on the catalysts. This work aims to identify the proper loading and proportions of Zn sites on H-BEA zeolite which result in enhancing the deoxygenation reaction of butanal, increasing the selectivity to aromatics, and improving the catalyst stability. This was accomplished by studying the reactivities of butanal and isobutane separately and by constructing simplified reaction sequences which were used to explain their collaborative chemistries in the co-feeding experiments.

6.2 Experimental methods

6.2.1 Catalyst preparation

H-BEA was obtained by calcining NH_4-BEA (Si/Al 12.5, Zeolyst International) at 500 ^oC for 4 hours (1 $^oC\ min^{-1}$ rate) in a flow of dry air. Zn/H-BEA samples were prepared by mixing 1 g of H-BEA in 0.003 – 0.03 M and 40 ml solutions of zinc nitrate (98% Sigma Aldrich) while mixing at 80 ^oC for 2 hours. The solids were then centrifuged and washed three times with deionized water (100 ml each) before drying at 90 ^oC for 24 hours. The samples were then calcined at 500 ^oC for 4 h (0.5 $^oC\ min^{-1}$ rate). Each sample was then labeled as *m*Zn-BEA where *m* represents the Zn/Al ratio of that catalyst. For Example, 0.15Zn-BEA designates a Zn/H-BEA catalyst with Zn/Al equal to 0.15.

6.2.2 Catalyst characterization

The concentration of Zn in the loaded catalysts was determined by inductively coupled plasma–optical emission spectroscopy (ICP-OES; Avio 200 ICP Optical Emission Spectrometer,

Perkin Elmer). The analysis was performed on the Zn solutions before and after the ion exchange and the metal concentration difference was used to calculate the metal loading in each catalyst. The Zn/Al ratios were calculated by taking the ratio of the calculated Zn concentration to the theoretical Al concentration obtained from the known Si/Al ratio of the H-BEA catalyst. Temperature-programmed-desorption of isopropylamine (> 99.5%, Sigma Aldrich) was used to determine the concentration of Brønsted and Zn Lewis acid sites in all catalysts. In every TPD experiment, 20 mg of catalyst was saturated with a stream of isopropylamine gas (2.75 kPa in He) at 40 ^{o}C for 1 hour. The catalyst was then purged with 20 ml min^{-1} of He gas (UHP >99.999%, Praxair) for 1 hour to strip off weakly adsorbed isopropylamine. After that, the reactor temperature was raised from 40 ^{o}C (at 5 ^{o}C min^{-1} rate) to 680 ^{o}C while monitoring the reactor effluent gases with a GC-MS. The total amounts of desorbed propylene were quantified from the MS signals at 41 m/z.

6.2.3 Catalyst testing

The turnover rates of converted products from the reaction of butanal and isobutane over the prepared catalysts were measured in a stainless-steel reactor with a 5.0 mm inner diameter. 20 – 50 mg of catalysts were loaded and held in the reaction zone between two plugs of quartz wool. The reactor was heated in a furnace (Applied Test Systems) consisting of a ceramic shell heater enclosed in a stainless-steel shell. The reactor temperature was controlled by a PID controller (Applied Test Systems) connected to a K-type Omega thermocouple which was attached to the outer wall of the reactor where the middle of the catalyst bed was located. Liquid butanal feed (>98.0%, Sigma Aldrich) was introduced at a 1.0 μL min^{-1} flow rate using a 1.0 mL gas-tight syringe and a syringe pump (New Era Pump Systems, Inc.) into a vaporization zone which was maintained at 10 ^{o}C above the boiling point of the liquid. The vaporized liquid was wept to the

catalyst bed for reaction by a 50 ml min^{-1} flow of He (UHP >99.999%, Praxair) gas stream which was regulated by a mass flow controller (GE50A, mks). Before the reaction, each catalyst was heated from room temperature to 450 ^{o}C for 1 hour (10 ^{o}C min^{-1} ramp) while purging with 20 ml min^{-1} He gas before cooling down to the desired reaction temperature. Gaseous reaction products were analyzed by an online GC/MS (7890B/5977 MSD, Agilent Technologies) equipped with an HP-5ms column (30 m and 0.25 mm ID). All the gas lines downstream of the reactor were heated to 180 ^{o}C by electrical heating tapes to avoid condensation of reaction products. For the experiments that test the reactivity of isobutane, mixtures of 0.44 – 1.32 kPa isobutane (high purity, Gas Innovations) in He gas were fed into the catalysts at 300 – 400 ^{o}C temperatures to elucidate the reactivity of the light alkane and calculate the apparent activation energies for the primary products. Butanal and i-butane co-feeding experiments were performed using 0.54 kPa butanal in a volumetric mixture of 1:5 i-butane to He gas (50 ml min^{-1} total flow) at 200 and 300 ^{o}C. Before every run, the composition of the gaseous feeds was stabilized by flowing the gas mixtures through a reactor-bypass line. After stabilizing both the feed composition and reactor temperature, the He gas purge into the catalyst bed was stopped and the feed mixture was directed to the catalyst bed through a 3-way valve to start the reaction and analyze the product gas with GC-MS.

6.3 Results and discussion

6.3.1 Isopropylamine temperature-programmed-desorption (TPD)

The reactive desorption of isopropylamine has been used to quantify the amounts of Brønsted and Zn Lewis acid sites. Isopropylamine adsorbs on Brønsted acid sites forming isopropyl ammonium ion which reacts in a narrow desorption temperature range via Hoffmann elimination reaction to yield propylene and ammonia.[63] Isopropylamine TPD has been widely used as a technique to quantify Brønsted sites on metal-loaded zeolites such as BEA and ZSM-

5.[64–66] Although such an analytical technique was known for its selectivity to Brønsted acid sites in zeolites, Lewis acid sites generated by the incorporation of Zn metal on zeolites were also observed to catalyze the decomposition of isopropylamine. [67,68] Because the decomposition of isopropylamine during TPD on the different acid sites is temperature-specific due to differences in metal-amine interaction strengths, quantifying the desorbed propylene at these temperatures could be used to compute the concentration of the corresponding acid sites catalyzing the reaction. For example, Penzien et al.[67] observed that the TPD of isopropylamine on Zn/H-BEA samples with different Zn/Al ratios resulted in propylene desorbing at three different temperatures. In their analysis, they attributed the desorption peaks at 347, 394, and 476 ^{o}C to Brønsted acid sites, Lewis acid sites formed by Zn incorporation on vicinal aluminum $[Zn\text{-}O\text{-}Al]^{2+}$, and Lewis acid sites formed by pairs of Zn cations with bridging oxygen $[Zn\text{-}O\text{-}Zn]^{2+}$, respectively. **Figure 6.1** shows the amounts of propylene and isopropylamine desorbed from each catalyst.

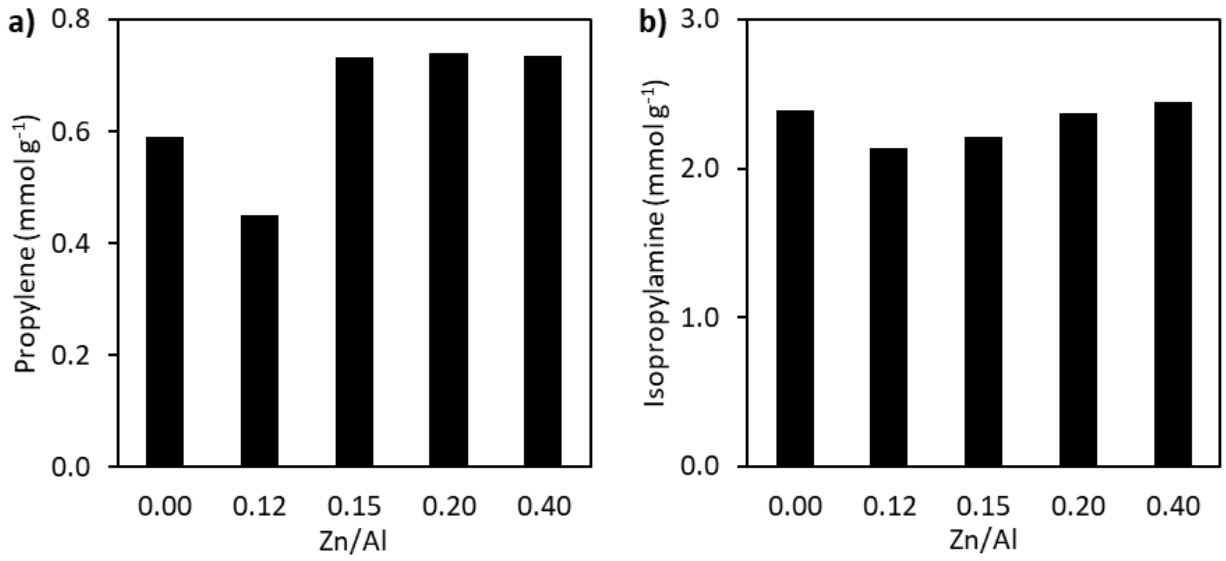

Figure 6.1: Results of isopropylamine TPD experiments showing a) total propylene and b) total isopropylamine desorbed from all catalysts. 20 mg of catalyst samples were saturated with isopropylamine (2.75 kPa in He) at 40 ^{o}C for 1 hour, purged with 50 ml min^{-1} He for 1 hour, then heated from 40 to 680 ^{o}C at 5 ^{o}C min^{-1} heating rate.

Figure 6.1a shows the quantified amounts of propylene desorption at the different TPD temperatures which can be used to quantify the total Brønsted and Zn Lewis acid sites on the samples. As can be inferred from **Figure 6.1**a, the amounts of propylene desorbed from each sample were 590 μmol g^{-1} for H-BEA, 450 μmol g^{-1} for 0.12Zn-BEA, 732 μmol g^{-1} for 0.15Zn-BEA, 739 μmol g^{-1} for 0.20Zn-BEA, and 735 μmol g^{-1} for 0.40Zn-BEA. The high amounts of propylene desorption from the samples with high Zn loading were due to the proportional increase of the Lewis sites from Zn incorporation.[67] Although there doesn't seem to be a direct relationship between the acidity of the catalysts and the unreacted isopropylamine from TPD, the consistency of desorption amounts could give hints about the uniformity of the porous structures and other weaker acidic sites. **Figure 6.1**b shows isopropylamine desorption amounts which ranged between 2135 – 2450 μmol g^{-1}.

In our TPD experiments, propylene desorption profiles could be deconvoluted into three peaks as can be seen in **Figure 6.2**. **Figure 6.3** shows propylene desorption amounts for all three peaks. The total amounts of propylene from peak 1, which corresponds to Brønsted acid sites, was seen to decrease from 423 μmol g^{-1} on H-BEA to nearly a constant amount of 201 – 211 μmol g^{-1} on all Zn/H-BEA catalysts. This result is consistent with Penzien et al.[67] reports which showed that above 0.02 Zn/Al, isolated Brønsted acid sites on H-BEA cannot stabilize the exchange with Zn^{2+} cations resulting in a constant residual Brønsted acidity. Desorbed propylene from peak 2 which correspond to $[Zn\text{-}O\text{-}Zn]^{2+}$ sites was seen to increase with the Zn loading with values of 5 μmol g^{-1} on H-BEA, 29 μmol g^{-1} on 0.12Zn-BEA, 233 μmol g^{-1} on 0.15Zn-BEA, 297 μmol g^{-1} on 0.20Zn-BEA, and 270 μmol g^{-1} on 0.40Zn-BEA. Similarly, propylene desorbing from peak 3 which corresponds to isolated $[Zn\text{-}O\text{-}Al]^{2+}$ species was seen to increase with Zn loading with values of 7 μmol g^{-1} on H-BEA, 74 μmol g^{-1} on 0.12Zn-BEA, 75 μmol g^{-1} on 0.15Zn-BEA, 68

μmol g^{-1} on 0.20Zn-BEA, and 87 μmol g^{-1} on 0.40Zn-BEA. The sudden rise in propylene desorption in peak 3 compared to peak 2 with lower Zn loadings (Zn/Al < 0.12) is typical for the quick exchange of Zn into neighboring Al pairs as the preferable exchange sites.[67] On the other hand, the nearly steady propylene desorption amounts at peak 2 (for Zn/Al > 0.20) and at peak 3 (for Zn/Al > 0.12) suggest the conversion of Zn into other less reactive species which are not visible in isopropylamine TPD. These species could include ZnO nanoclusters which are known to exist on zeolites impregnated with Zn.[103,156,161] While extended X-ray absorption fine structure (EXAFS) results on ion-exchanged Zn/H-ZSM-5 (0.10 – 0.19 Zn/Al)[103] and Zn/H-BEA (0.08 and 0.53 Zn/Al)[67] revealed the absence of ZnO, higher exchange ratios of H-BEA (Zn/Al > 0.26) already showed evidence of possible existence of ZnO species as revealed by the additional desorption peak in acetonitrile TPD experiments.[67] Therefore, we conclude that our samples had increasing amounts of both $[Zn\text{-}O\text{-}Al]^{2+}$ and $[Zn\text{-}O\text{-}Zn]^{2+}$ with Zn loading up to the ratio Zn/Al 0.20 and that further increase mostly contributed to the formation of new ZnO species while only marginally increasing the $[Zn\text{-}O\text{-}Al]^{2+}$ site density as observed from **Figure 6.3**.

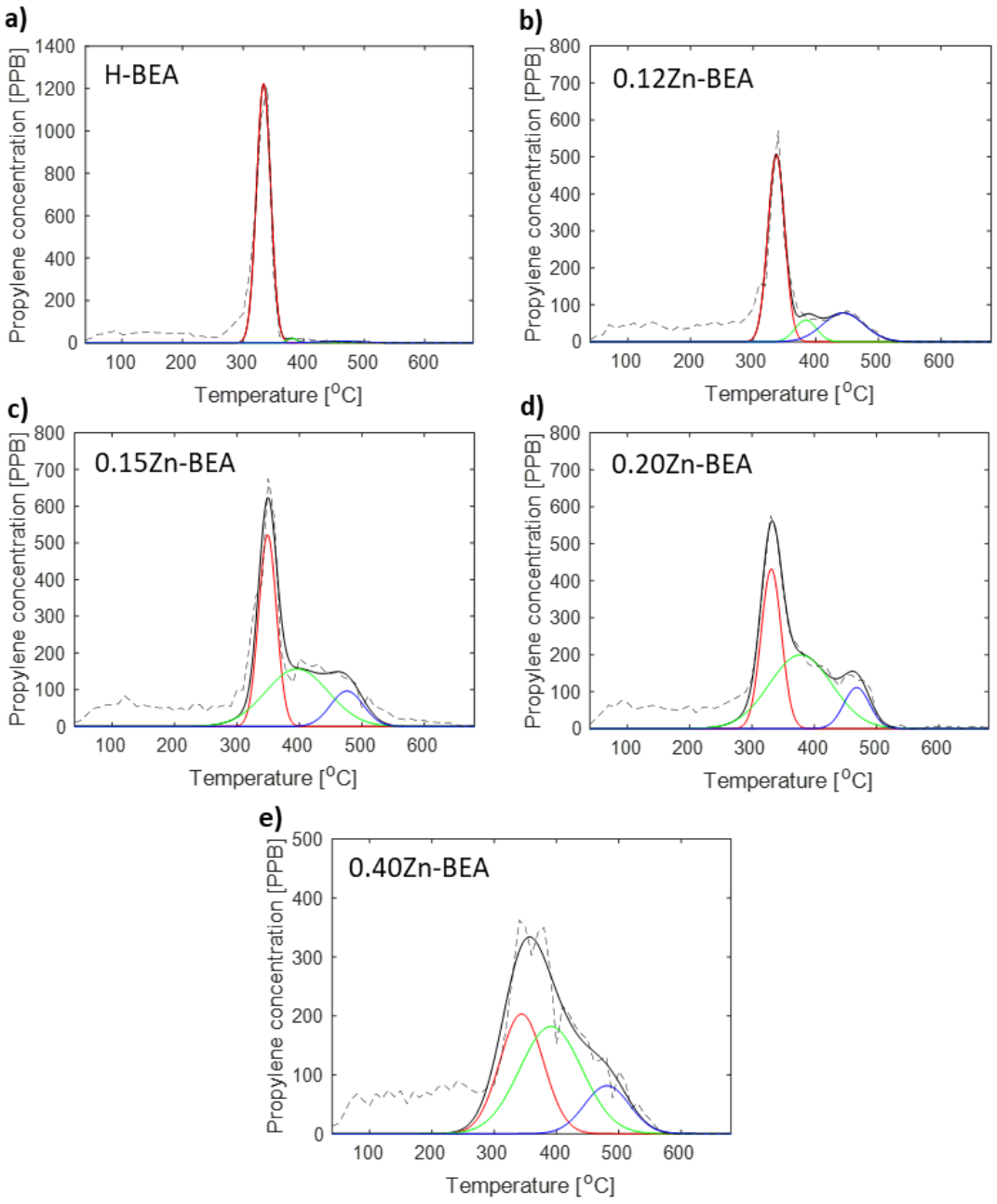

Figure 6.2: Propylene TPD profiles and their deconvoluted peaks for a) H-BEA, b) 0.12Zn-BEA, c) 0.15Zn-BEA, d) 0.20Zn-BEA, and e) 0.40Zn-BEA catalysts.

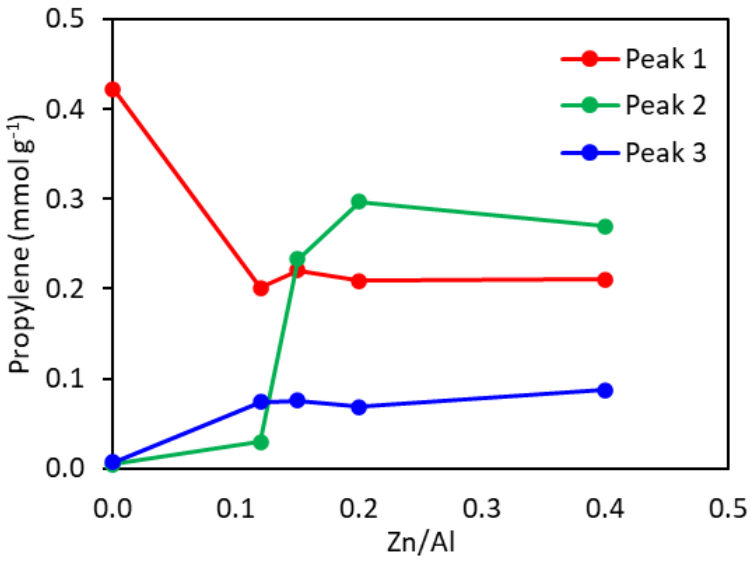

Figure 6.3: Amounts of desorbed propylene calculated from the three peaks shown in **Figure 6.2**.

6.3.2 Butanal reaction at 200 ºC

The conversion of butanal with and without isobutane co-feed was first explored on all prepared catalysts at 200 ºC with initial conversions kept lower than 17% to drive the product composition away from the thermodynamic equilibrium.[92] This was done to approach transient reaction conditions and to elucidate the influence of isobutane co-feed on the rates of the C_8 oxygenates and aromatics. Because butanal reaction over all tested catalysts involved continuous catalyst deactivation even after 2 hours of time-on-stream (TOS) as shown in **Figure 6.4**, the deactivation behavior of each catalyst was compared by fitting the conversion as a function of TOS to calculate the initial conversion and the deactivation constant. Equation (6.1) shows a first-order deactivation model derived from the Levenspiel deactivation model on solid catalysts.[128]

$$x = x_0 \exp(-kt) \tag{6.1}$$

Where x is the conversion at time t, x_0 is the initial conversion at t = 0, and k is the deactivation constant. As compared in **Figure 6.5**a, the initial conversion of butanal was seen to decrease with the co-feeding of isobutane with the conversions dropping from 16.3 to 12.9% on H-BEA and from 12.1 to 8.0% on 0.40Zn-BEA catalysts. The changes in conversions were much less pronounced on middle-range Zn-loaded catalysts where the conversions changed from 11.4 to 11.8% on 0.12Zn-BEA, from 11.6 to 10.2% on 0.15Zn-BEA, and from 12.0 to 11.6% on 0.20Zn-BEA. As illustrated in **Figure 6.5**b, the calculated deactivation constants from equation (1) markedly decreased with isobutane co-feeding from 4.78×10^{-3} to 2.96×10^{-3} min^{-1} on H-BEA, from 3.45×10^{-3} to 2.10×10^{-3} min^{-1} on 0.15Zn-BEA, and from 5.11×10^{-3} to 1.86×10^{-3} min^{-1} on 0.40Zn-BEA. On the contrary, isobutane co-feeding resulted in a slight increase in the deactivation constant from 2.71×10^{-3} to 3.03×10^{-3} min^{-1} on 0.12Zn-BEA and from 3.60×10^{-3} to 4.12×10^{-3} min^{-1} on 0.20Zn-BEA samples. These trends in conversion and deactivation were reflected in the turnover rates of C_8 oxygenates (mainly 2-ethyl-2-hexenal) and C_{12} aromatics as the two main products after 2 hours of TOS as presented in **Figure 6.6**. The co-feeding of light alkanes with oxygenated feeds such as methanol has been shown to attenuate catalyst deactivation and coke formation.[36] This is due to the active participation of the olefins in the catalytic cycle as Mier et al.[50,167] showed that co-feeding n-butane with methanol resulted in an order of magnitude increase in the kinetic constant for generating olefins to 3.94 mol g^{-1} h^{-1} compared with only 0.166 mol g^{-1} h^{-1} for the cracking of n-butane alone. As can be observed from **Figure 6.6**, all the tested catalysts showed reductions in the turnover rates of C_8 oxygenates and C_{12} aromatics with isobutane co-feed after 2 hours of TOS compared with feeding butanal alone. The only exception was the 0.15Zn-BEA catalyst which showed an increase in both C_8 oxygenates and C_{12} aromatics with isobutane co-feed. In fact, 0.15Zn-BEA resulted in the highest turnover rates with values of

1.20 µmol min^{-1} for C_8 oxygenates and 2.06 µmol min^{-1} for C_{12} aromatics. This result is anticipated given the high stability and initial conversion on 0.15Zn-BEA compared with other catalysts as seen in **Figure 6.5**a and b. Although 0.15Zn-BEA and 0.40Zn-BEA had similar total acidity concentrations from the TPD experiment (732 – 735 mmol g^{-1}), their characteristic activity and deactivation behavior suggests clear distinctions in acid site type and distribution. The TPD results revealed that 0.15Zn-BEA and 0.40Zn-BEA had comparable site proportions corresponding to Brønsted and $[Zn\text{-}O\text{-}Al]^{2+}$ sites. However, 0.15Zn-BEA showed a larger proportion of the $[Zn\text{-}O\text{-}Zn]^{2+}$ sites resulting from the higher Zn loading (270 µmol g^{-1} compared with 233 µmol g^{-1}). Because 0.15Zn-BEA showed a favorable conversion to aromatics over other catalysts and both 0.15Zn-BEA and 0.40Zn-BEA had the lowest catalyst deactivation constants, these two catalysts were selected for further catalytic screening as discussed below.

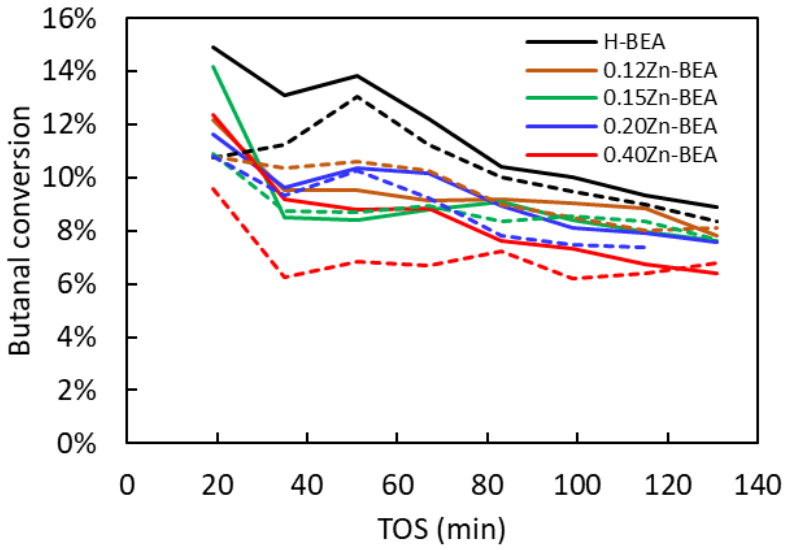

Figure 6.4: Butanal conversion over different catalysts at 200 °C and 0.96 min^{-1} WHSV (with respect to butanal). The solid lines are for butanal feed at 0.54kPa with He gas. The dotted lines are for butanal with isobutane co-feed at 0.54 kPa butanal with isobutane and He gas mixture (1:5 isobutane to He volume basis)

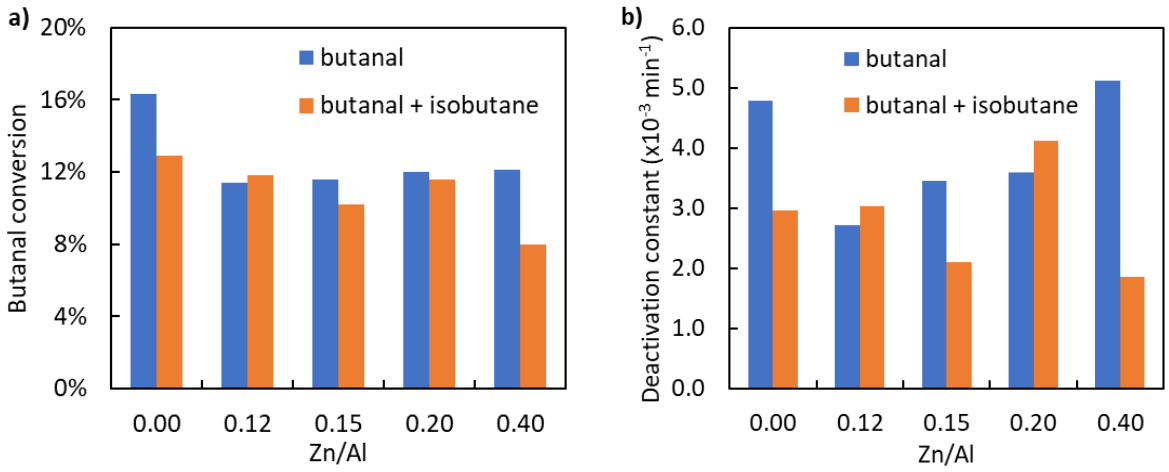

Figure 6.5: a) The initial butanal conversions x_o and b) the catalyst deactivation constants k calculated from fitting equation (6.1) to conversion versus TOS data.

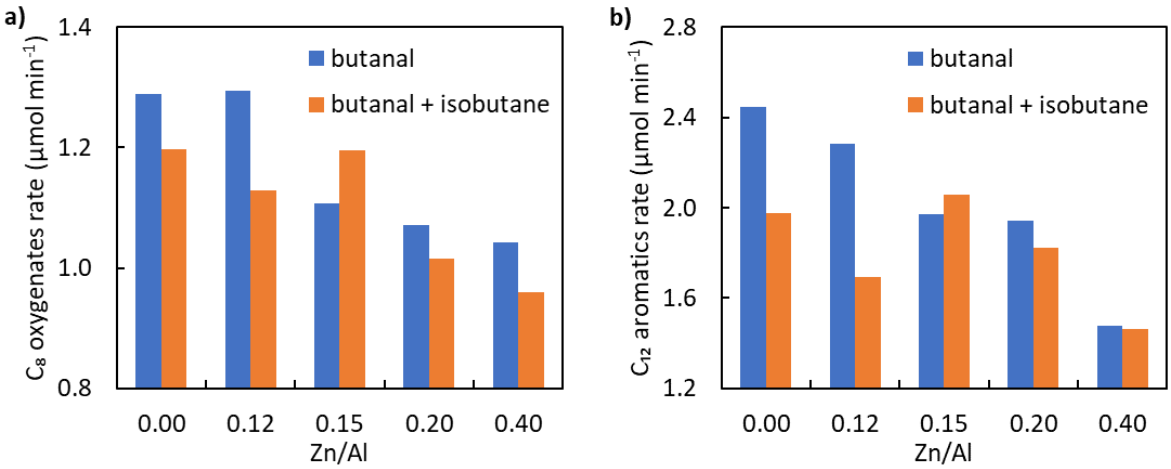

Figure 6.6: The turnover rates of a) C_8 oxygenates and b) C_{12} aromatics from the conversion of butanal over BEA zeolites with different Zn/Al ratios at 200 ^oC and 2 hours TOS.

6.3.3 Isobutane reaction

To study the conversion of isobutane and determine its minimum activation temperature, isobutane was reacted over H-BEA, 0.15Zn-BEA, and 0.40Zn-BEA at different temperatures. Our results indicated that the reaction at 200 ^oC and 0.7 – 1.3 kPa isobutane partial pressures did not result in measurable products and that only at temperatures near 300 ^oC we started to see some

converted products. Accordingly, 300 ^{o}C was chosen as the minimum reaction temperature for the isobutane reaction investigation. **Figure 6.7** shows the selectivity of products from the conversion of isobutane at 300 ^{o}C, 350 ^{o}C, and 400 ^{o}C. Based on the product evolution with temperature changes, a simplified reaction sequence was generated and is shown as Scheme 6.1. It is worth mentioning that isomerization reactions were embedded within each reaction step and that the molecules shown in Scheme 6.1 represent the most dominant isomer of each product. Isobutane first dehydrogenates to isobutene (R-1 in Scheme 6.1) which then oligomerizes with another isobutene molecule to form a C_8 olefin (R-2 in Scheme 6.1). Dehydrogenation and oligomerization to C_8 olefins were also confirmed by ^{13}C labeling and NMR experiment of isobutane on Zn-exchanged H-BEA and H-ZSM-5 zeolites.[159] The C_8 olefin shown in Scheme 6.1 was considered a transition molecule (labeled with a star *) because it was not detected in the gas products of this reactivity investigation. At 300 ^{o}C, this C_8 transition molecule then quickly undergoes cracking into propylene and pentene (R-3 in Scheme 6.1) and where pentene could hydrogenate to pentane (R-4 in Scheme 6.1). The fast tendency for cracking on Brønsted acid zeolites could also be realized from the DFT calculations on ZSM-5 which showed that the activation energies for the dehydrogenation and cracking of isobutane were virtually the same with less than 1.4 kJ/mol difference.[168] Although hydrogenolysis to methane and alkenes is likely to occur with light alkanes [25], Gabrinko et al.[166] showed that the reaction constant for isobutane dehydrogenation was an order of magnitude higher than the direct hydrogenolysis to methane and propylene at 290 ^{o}C on Zn-exchanged H-BEA. In addition, the carbon-based ratios of C_3 olefin to C_5 alkane in our reaction products (at 0.43 kPa isobutane and 300 ^{o}C) ranged from 0.4 – 0.6 which were very close to the theoretical value 0.6 for the cracking of C_8 olefins. This confirms the limited hydrogenolysis in our reaction and that the majority of propylene was produced from the rapid

cracking of C_8 olefins. At 350 ^oC, xylene started to form through the dehydrogenation of the C_8 transition molecule in reaction R-5 of Scheme 6.1. Also, at the same temperature, the generated propylene could oligomerize with butenes to yield toluene after dehydrogenation (R-6 in Scheme 6.1). Experiments on Zn^{2+}/H-BEA[166] agree with our finding and that xylenes and toluene were the two major aromatization products of isobutane with the latter dominating. Increasing the temperature to 400 ^oC resulted in further oligomerization and dehydrogenation of xylenes and toluene with butenes resulting in the generation of C_{12} and C_{11} naphthenes (R-7 and R-8 in Scheme 6.1), respectively.

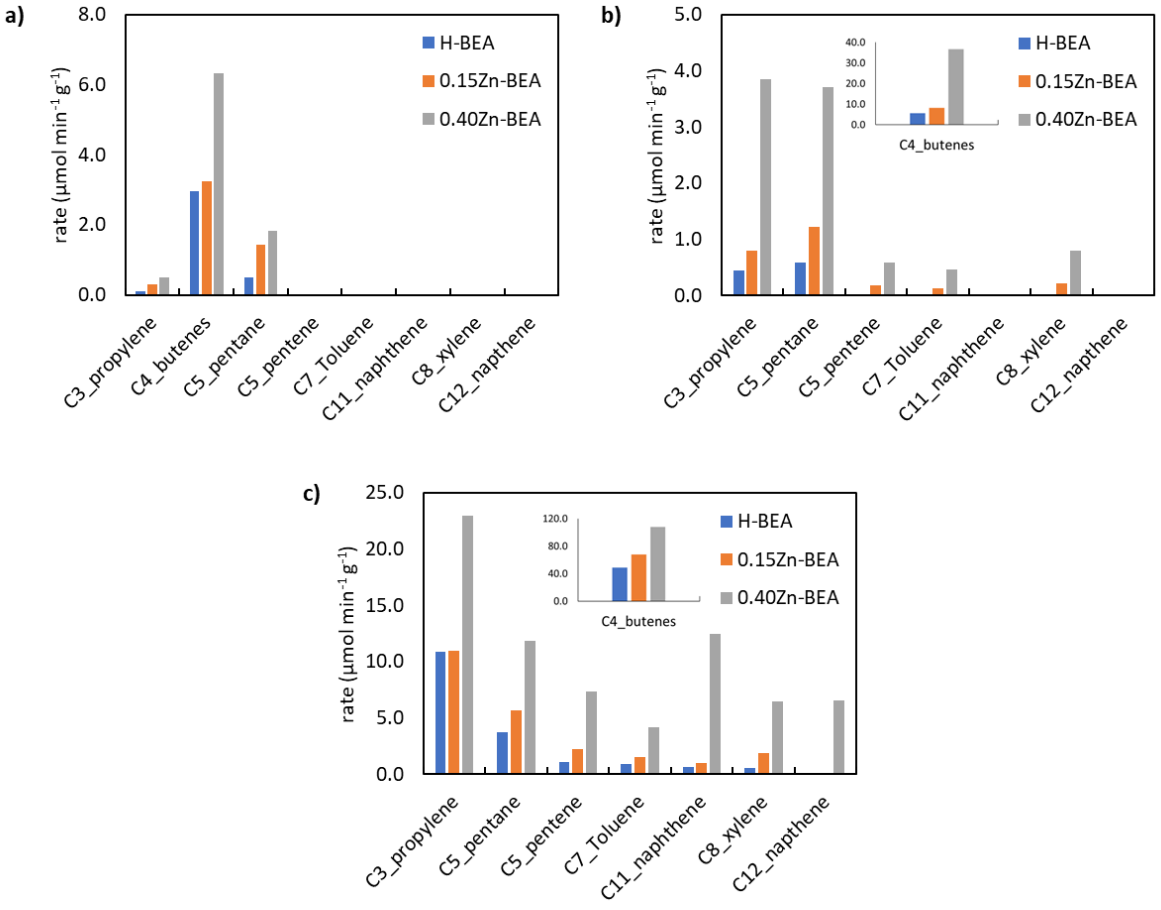

Figure 6.7: Turnover rates of different products from the conversion of isobutane over H-BEA, 0.15Zn-BEA, and 0.40Zn-BEA a) at 300 ^oC, b) at 350 ^oC, and c) at 400 ^oC. Reaction conditions: 1.32 kPa isobutane in He gas and 1.92 min^{-1} WHSV (isobutane basis).

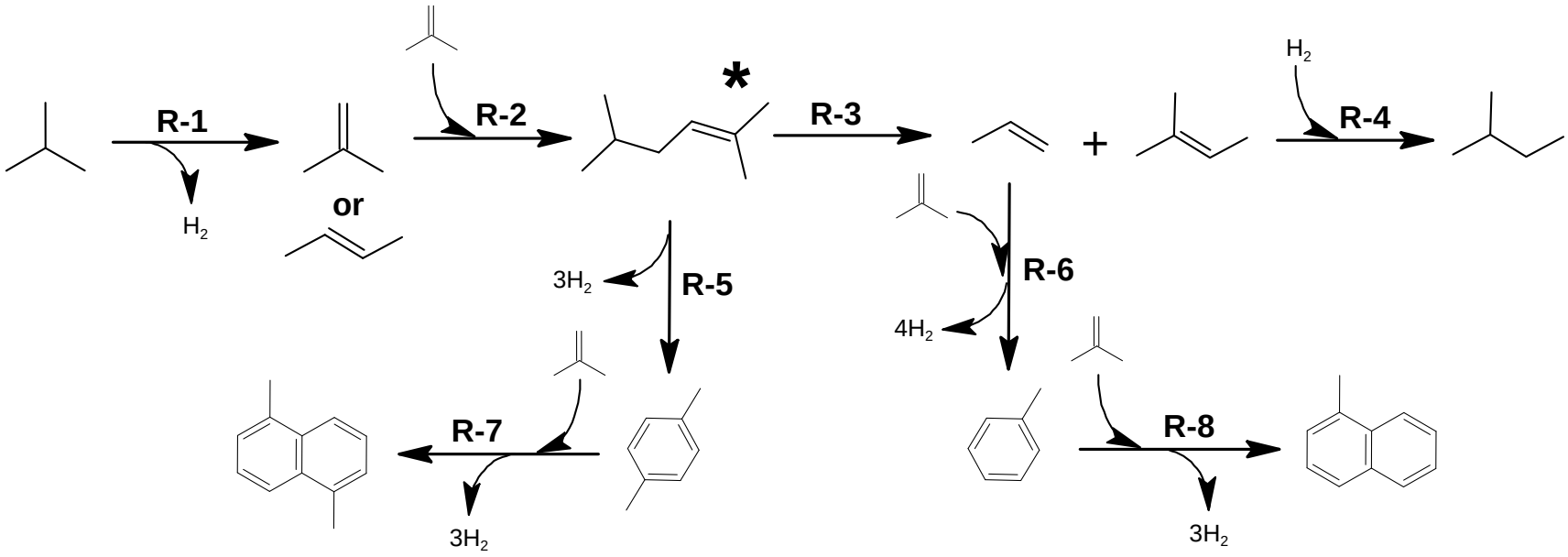

Scheme 6.1: Suggested reaction sequence for the conversion of isobutane over H-BEA and Zn/H-BEA zeolites at 300 – 400 ^{o}C.

Figure 6.8 shows the activation energies for the formation of butenes, propylene, and pentane which were determined from the first-order reaction constants. As a first reactive step, the apparent activation energies for the dehydrogenation of isobutane (R-1 in Scheme 6.1) were 87.3, 91.0, and 79.0 kJ mol^{-1} for H-BEA, 0.15Zn-BEA, and 0.40Zn-BEA, respectively (**Figure 6.8**a). Zn species in zeolites such as H-BEA has been widely confirmed to reduce the activation barrier for the C-H bond activation in alkanes resulting in a similar decrease in their apparent activation energy for dehydrogenation.[98,162,165,166] This result shows that 0.40Zn-BEA sustains a more favorable dehydrogenation ability compared with the other two catalysts. The enhanced dehydrogenation was also reflected in the higher turnover rates of butenes formation over 0.40Zn-BEA compared with the other catalysts as depicted in **Figure 6.7**. The activation energy for the formation of propylene (a combination of butenes oligomerization in R-2 and creaking to olefins in R-3 of Scheme 6.1) increased proportionally with the Zn loading with values of 182.1 kJ mol^{-1} on H-BEA, 152.9 kJ mol^{-1} on 0.15Zn-BEA, and 125.5 kJ mol^{-1} on 0.40Zn-BEA as shown in **Figure 6.8**b. These energy trends suggest the enhancement of the oligomerization and cracking ability of Zn species in the zeolite compared with the unloaded H-BEA. Because BEA zeolite is known to retain both $[Zn\text{-}O\text{-}Zn]^{2+}$ and $[Zn\text{-}O\text{-}Al]^{2+}$ species at Zn/Al loadings higher than or equal to 0.15[67], it is anticipated that both of these species are responsible for enhancing the rate of propylene and pentene formation which is evident from their higher rates over 0.15Zn-BEA and 0.40Zn-BEA. However, because 0.40Zn-BEA is expected to contain a larger proportion of the former Zn site in addition to some ZnO clusters (quantitative TPD analysis in **Figure 6.3**) and the fact that such catalyst maintains the lowest energy barrier, we expect the $[Zn\text{-}O\text{-}Zn]^{2+}$ and ZnO sites to be the main contributor to such oligomerization and cracking enhancement. The potential dehydrogenation and aromatization enhancements caused by ZnO were confirmed in the work of

Gabrienko et al.[166] where they observed lower activation energies for the dehydrogenation and aromatization of isobutane on H-BEA modified with ZnO clusters compared with H-BEA modified with Zn^{2+} cations. The energy-favorable dehydrogenation and aromatization shown by the 0.40Zn-BEA are clearly displayed by the higher rates of xylene and toluene (**Figure 6.7**b and c) as well as the fact that it was the only catalyst that produced C_{12} naphthenes at measurable rates (**Figure 6.7**c). It turns out that 0.40Zn-BEA was more selective to xylene (R-5 in Scheme 6.1) than to toluene (R-6 in Scheme 6.1) with a ratio of toluene to xylene molar rates (carbon based) equal to 0.70. On the other hand, 0.15Zn-BEA having a higher activation energy for dehydrogenation gave a ratio of toluene to xylene of 1.30. The lower ratio observed on 0.40Zn-BEA compared with 0.15Zn-BEA capitalizes on the dehydrogenation ability of the former where the dehydrogenation of the C_8 olefin (R-5 in Scheme 6.1) became faster than its cracking and oligomerization (R-3 and R-6 in Scheme 6.1). This clearly indicates that the milder dehydrogenation ability of 0.15Zn-BEA (**Figure 6.8**a) coupled with its enhancement in oligomerization made it more selective to toluene. It is well known that Zn concentration in zeolites play an important role in aromatization as Zn species favor the direct aromatization of oligomers compared with Brønsted acid sites which are mainly responsible for their isomerization and cracking.[169] **Figure 6.8**c shows the activation energies for the hydrogenation of pentene to pentane (R-4 in Scheme 6.1) where H-BEA showed the highest activation energy of 120.6 kJ mol^{-1} compared to 0.15Zn-BEA and 0.40Zn-BEA catalysts which had lower activation energies of 54.6 and 54.1 kJ mol^{-1}, respectively. This result suggests the low ability of H-BEA catalyst for hydrogenation and H_2 incorporation into unsaturated olefins compared with the Zn-loaded catalysts. Because in our reaction conditions no C_9 aromatics were formed, we conclude that C_5 olefins had nearly no contribution to the oligomerization of isobutene. Therefore, the ratio of C_5 olefins to C_5 alkanes was used to gain more

insights on the hydrogenation ability of the 0.15Zn-BEA and 0.40Zn-BEA catalysts and to discriminate their similarity in activation energy. The calculated C_5 olefins to C_5 alkanes rate ratios at 400 ^oC were 0.91 for 0.15Zn-BEA and 0.73 for 0.40Zn-BEA. The lower olefin ratio over 0.40Zn-BEA proves the higher hydrogenation ability in such catalyst with higher Zn loading. Since 0.40Zn-BEA is expected to contain higher concentrations of $[Zn\text{-}O\text{-}Zn]^{2+}$ and ZnO sites, we could argue that such species are responsible for lowering the activation energy and increasing the oligomerization rates to aromatics.

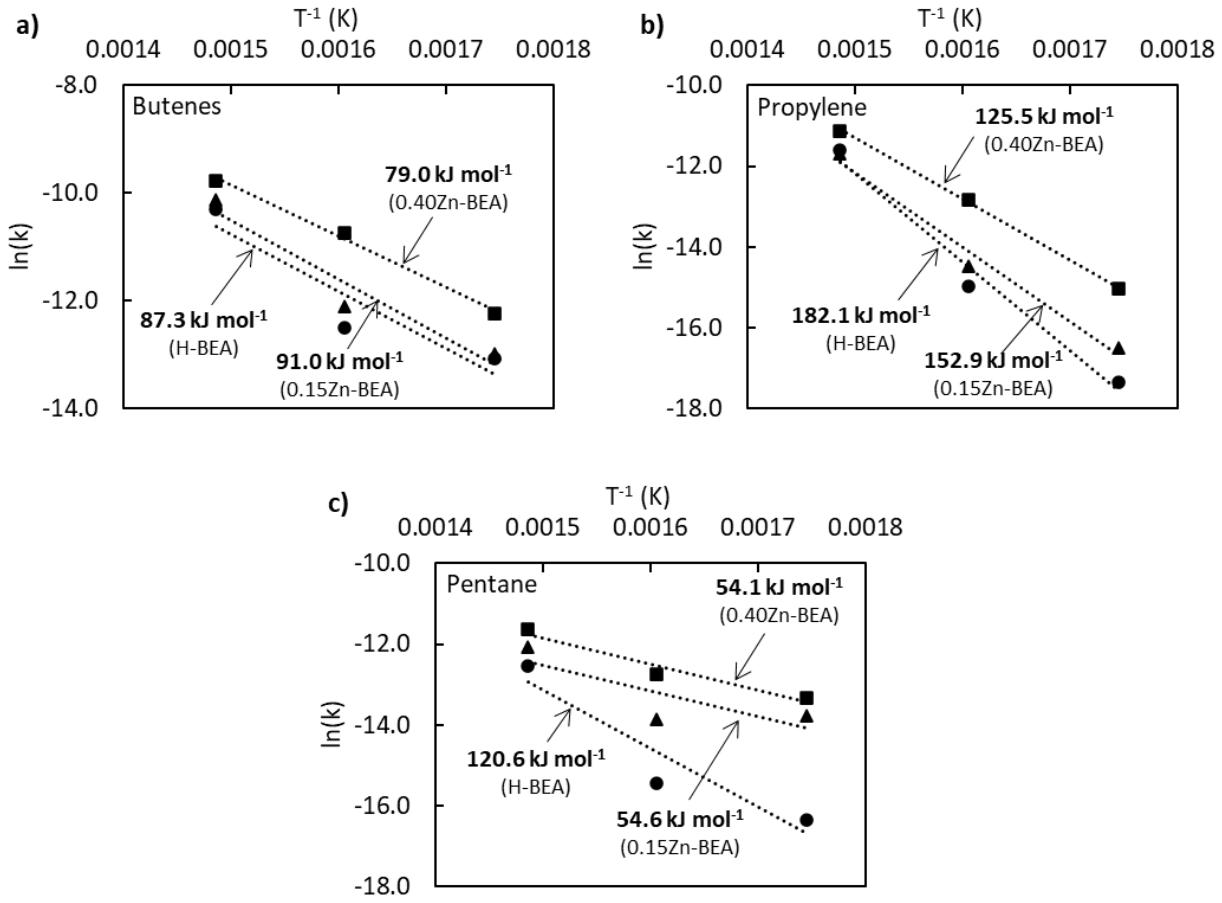

Figure 6.8: The activation energies for a) butenes formation (R-1 in Scheme 6.1), b) propylene formation (R-3 in Scheme 6.1), and c) pentane formation (R-4 in Scheme 6.1) from the reaction of isobutane on different catalysts. Reaction conditions: 0.66 - 1.32 kPa isobutane in He gas, 1.92 min^{-1} WHSV (isobutane basis), and 300 – 400 ^oC temperature range.

6.3.4 Butanal reaction with isobutane co-feed

6.3.4.1 Butanal reaction at 300 ºC

After studying isobutane reactivity and observing that 300 ^{o}C was the near minimum activation temperature, this temperature was chosen to re-evaluate the reactivity of butanal with isobutane co-feed. First, butanal alone was reacted on all prepared catalysts to note down the reaction sequence before attempting the reaction with the isobutane co-feed. Scheme 6.2 shows the proposed reaction sequence based on our experiments and the knowledge about butanal conversion over Brønsted acid site catalysts.[85,95]

As noted in Scheme 6.2, butanal conversion starts by undergoing three distinctive reactions namely, the aldol condensation to C_8 oxygenate (R-1), the direct dehydrogenation-dehydration to butenes (R-2), and the esterification to C_8 ester (R-3).[47,95,117] The formed C_8 condensate could dehydrate to a C_8 olefin (R-6 in Scheme 6.2) which could then crack into butenes or propylene and pentene (R-8 and R-10 in Scheme 6.2).[170] At the same time, the C_8 condensate could further undergo condensation-dehydration with butanal to yield a higher C_{12} oxygenate (R-4 in Scheme 6.2) which could dehydrate to C_{12} aromatics (R-13 in Scheme 6.2) then dehydrogenate to form naphthenes (R-17 in Scheme 6.2).[47] The C_{12} condensate could also undergo dehydration and cracking to yield two C_6 olefins (R-11 in Scheme 6.2). On the other hand, the C_8 esterification product could undergo deoxygenation and dehydrogenation through the removal of CO and H_2 to yield a C_7 ketone (R-5 in Scheme 6.2).[117] This C_7 ketone could react with another butanal molecule which upon dehydration could yield C_{11} aromatics (R-9 in Scheme 6.2). Concurrently, C_7 ketone could also lose H_2 and dehydrate to form C_7 olefin (R-7 in Scheme 6.2).[47,117] C_7 olefin could then oligomerize with another C_4 or C_3 olefin (from reactions R-2, R-8, and R-10 in Scheme 6.2) and upon dehydrogenation yields C_{11} (R-16 in Scheme 6.2) and C_{10} (R-14 in Scheme

6.2) aromatics. The C_{11} aromatics could then dehydrogenate to C_{11} naphthenes (R-22 in Scheme 6.2) and the dehydrogenation of C_{10} aromatics could yield C_{10} naphthenes (R-20 in Scheme 6.2). **Figure 6.9** shows the selectivities of different products from the conversion of butanal and butanal with the isobutane co-feed over different catalysts. As can be observed from **Figure 6.9**a, the overall selectivity to alkanes slightly decreased with the Zn loading from 1.2% on H-BEA to 0.4% on 0.40Zn-BEA catalyst. The higher amount of Brønsted acid sites on H-BEA, compared with Zn-loaded catalysts, increases the cracking reactions as in R-8, R-10, and R-11 of Scheme 6.2 resulting in the formation of more C_5 and C_6 alkanes. This was also evident from isopropyl alcohol conversion results[94] showing 43% yield to alkanes (from cracking reactions) on ZSM-5 compared with just 18% on Zn/ZSM-5.

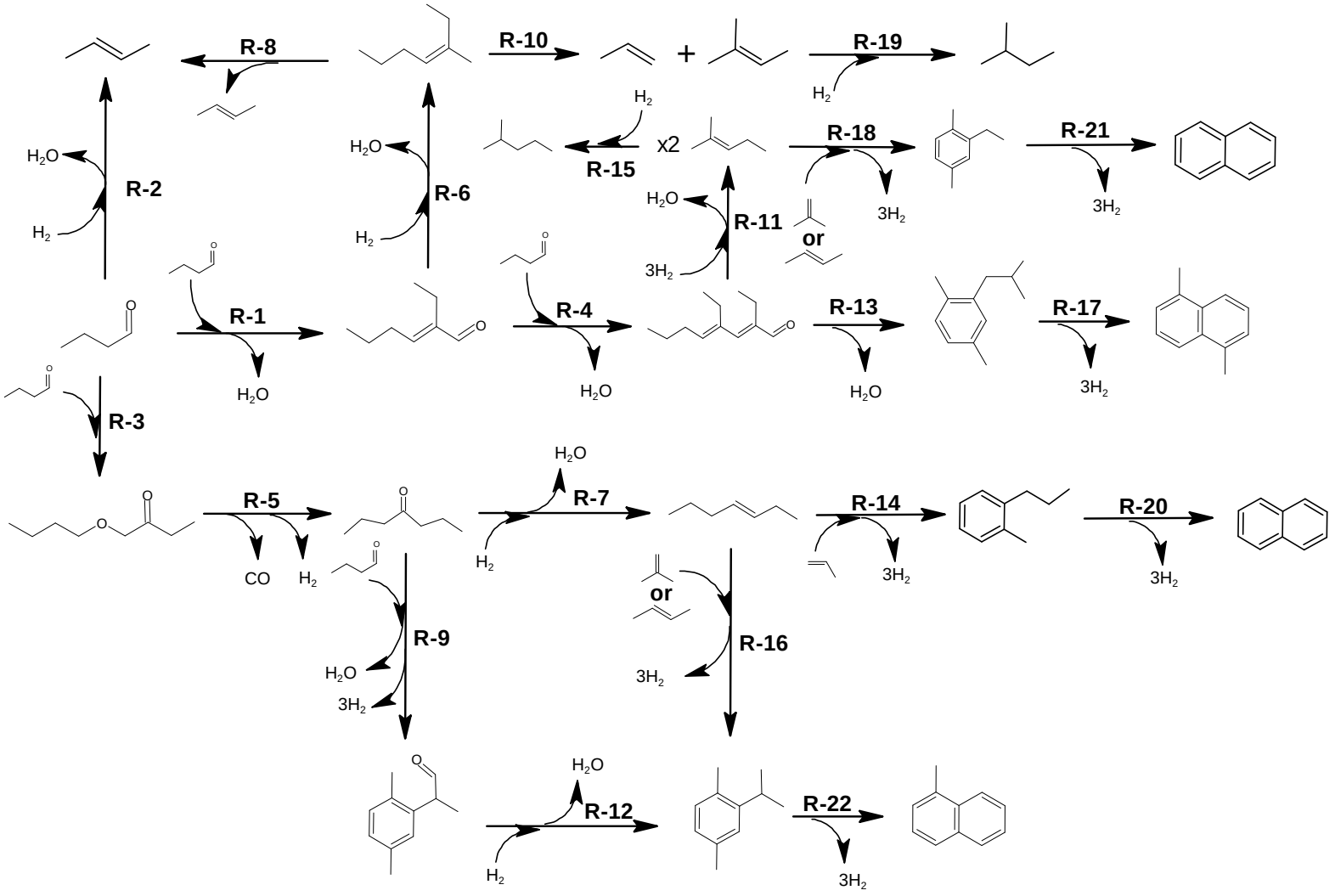

Scheme 6.2: Proposed reaction sequence of butanal conversion over H-BEA and Zn-exchanged BEA zeolites at 300 ^{o}C

The overall selectivity to olefins increased from 36.6% on H-BEA, to 42.9% on 0.15-BEA, and to 39.7% on 0.40Zn-BEA. This shows that the 0.15 Zn/Al ratio had a favorable olefin formation compared with the other catalysts. A close analysis of all olefinic species in **Figure 6.9**b reveals that the selectivities to C_3, C_5, and C_8 olefins proportionally decreased with Zn loading with values going from 5.5% (H-BEA) to 4.2% (0.40Zn-BEA) for C_3 olefin, from 3.7 to 2.9% for C_5 olefins, and from 0.5 to 0.2% for C_8 olefins. These decreasing trends suggest that Zn sites facilitate the condensation of C_8 species (R-4 in Scheme 6.2) while simultaneously limiting the competing C_8 dehydration reaction (R-6 in Scheme 6.2). Indeed, analysis of the C_6 olefins (**Figure 6.9**b) shows their proportional increase in selectivity from 1.5% on H-BEA to 2.1% on 0.40Zn-BEA. In addition, evidence of the enhancement of the condensation reaction R-4 is noted from the proportional increase in selectivity to C_{12} oxygenates and C_{12} aromatics (R-13 in Scheme 6.2) as observed in **Figure 6.9**c and d. Besides all olefins, C_7 olefins notably showed a proportional increase in selectivity with Zn with values of 4.2% on H-BEA, 8.8% on 0.15Zn-BEA, and 9.9% on 0.40Zn-BEA. These increasing trends are indicative of the Zn species augmenting the esterification route of butanal (R-3, R-5, and R-7 in Scheme 6.2) which eventually produces the C_7 olefin. All tested catalysts showed high selectivity to butenes with 0.15Zn-BEA showing the highest value of 23.3% compared with H-BEA and 0.40Zn-BEA which had almost the same selectivity of 21.0%.

As presented in **Figure 6.9**c, the overall selectivity to oxygenated products was seen to increase with Zn loading from 7.3% on H-BEA to 9.8% on 0.15Zn-BEA, and to 8.4% on 0.40Zn-BEA. A close examination of the oxygenated species reveals that the main products driving the higher selectivity over 0.15Zn-BEA were the C_7 and C_8 oxygenates. This result agrees with our kinetic modeling work (Chapter 5) which showed that BEA catalysts with a higher concentration

of isolated Zn sites compared with $[Zn\text{-}O\text{-}Zn]^{2+}$ sites (Zn/Al near 0.08) had lower activation energies for C_8 aldol condensation and C_8 esterification products. The selectivity to C_7 ketone (R-5 in Scheme 6.2) was 2.5% on H-BEA, 3.1% on 0.15Zn-BEA, and 1.7% on 0.40Zn-BEA. Similarly, the selectivity to C_8 oxygenated products was 1.5% on H-BEA, 2.5% on 0.15Zn-BEA, and 2.2% on 0.40Zn-BEA. The observed reduction in selectivity for the C_7 and C_8 oxygenates over 0.40Zn-BEA compared with 0.15Zn-BEA could be a result of the former favoring the condensation of the C_7 and C_8 oxygenates with butanal to form longer condensed products. Our kinetic results (Chapter 5) showed that BEA catalysts with high Zn/Al ratios had higher binding energy for C_8 condensation products which in turn could facilitate their condensation with another butanal molecule to form larger oxygenates. This is in fact reflected in 0.40Zn-BEA giving the highest selectivities to C_{11} and C_{12} oxygenates (1.9% for C_{11} and 2.3% for C_{12} oxygenates) compared with H-BEA (1.3% for C_{11} and 1.6% for C_{12} oxygenates) and 0.15Zn-BEA (1.7% for C_{11} and 1.9% for C_{12} oxygenates).

Figure 6.9d shows the overall selectivity to aromatics which increases with the Zn loading from 24.1% on H-BEA to 27.1% on 0.15Zn-BEA and to 26.7% on 0.40Zn-BEA. The notable trend is observed with the selectivity of C_{12} aromatics (R-13 in Scheme 6.2) which constituted the majority of the aromatics with selectivity values of 11.8% on H-BEA, 15.1% on 0.15Zn-BEA, and 16.7% on 0.40Zn-BEA. Again, this result emphasizes the higher condensation and dehydration ability of the catalysts with higher Zn loading (seen in reactions R-1 and R-4 in Scheme 6.2) resulting in more production of C_{12} aromatics. As seen in **Figure 6.9**e, the overall selectivity to naphthenes first decreased from 25.7% on H-BEA to 15.8% on 0.15Zn-BEA and to 20.3% on 0.40Zn-BEA. The lowest selectivity observed over 0.15Zn-BEA was also coupled with the highest selectivity to C_{11} naphthenes (6.6%) among other catalysts as observed in **Figure 6.9**e. Because

0.15Zn-BEA catalyst also gave high selectivity to both C_7 oxygenates and C_7 olefins, we associate the increased production of C_{11} naphthenes to the enhanced condensation and dehydration of the C_7 oxygenates (R-9 in Scheme 6.2) as well as the oligomerization of C_7 olefins with C_4 olefins (R-16 in Scheme 6.2).

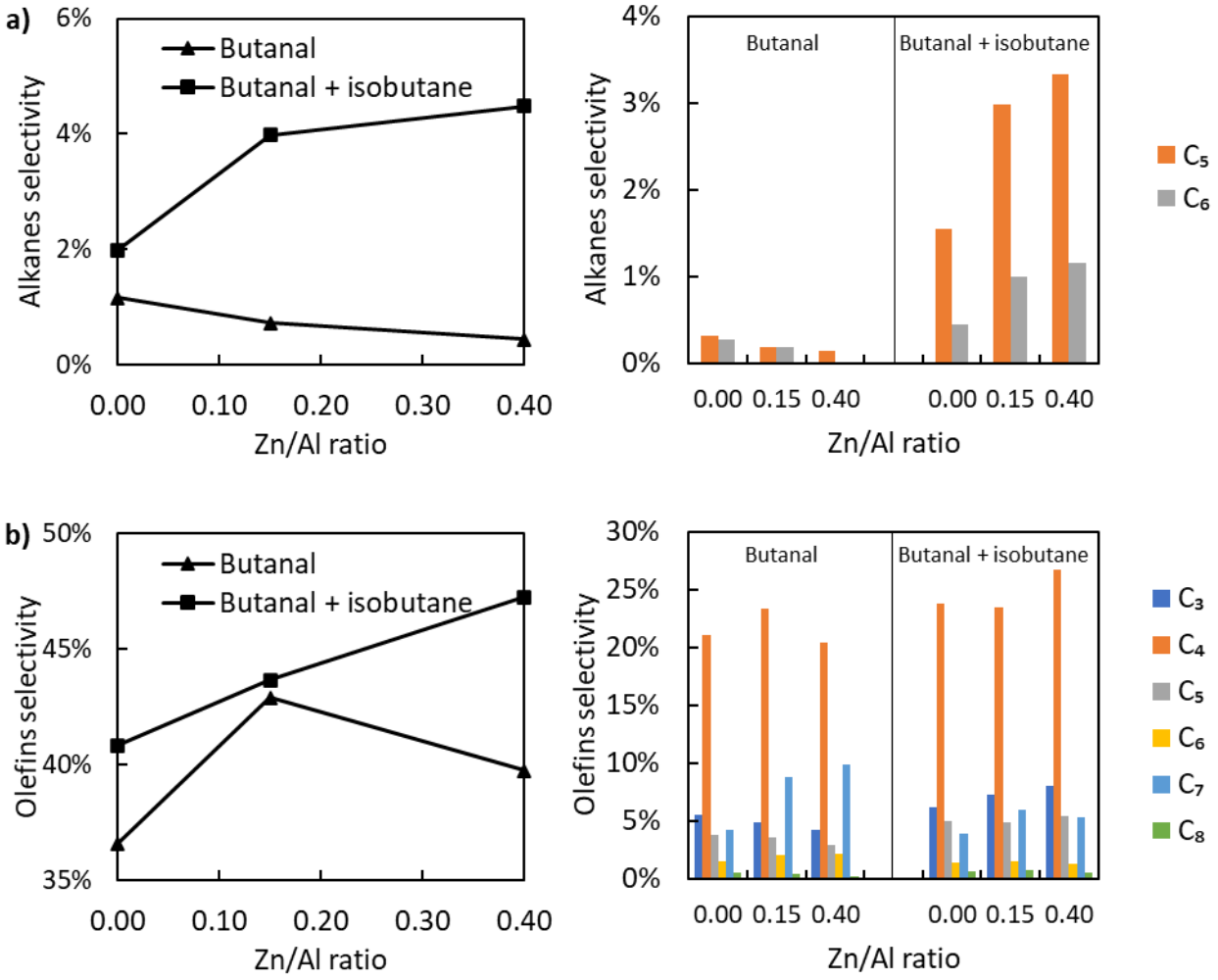

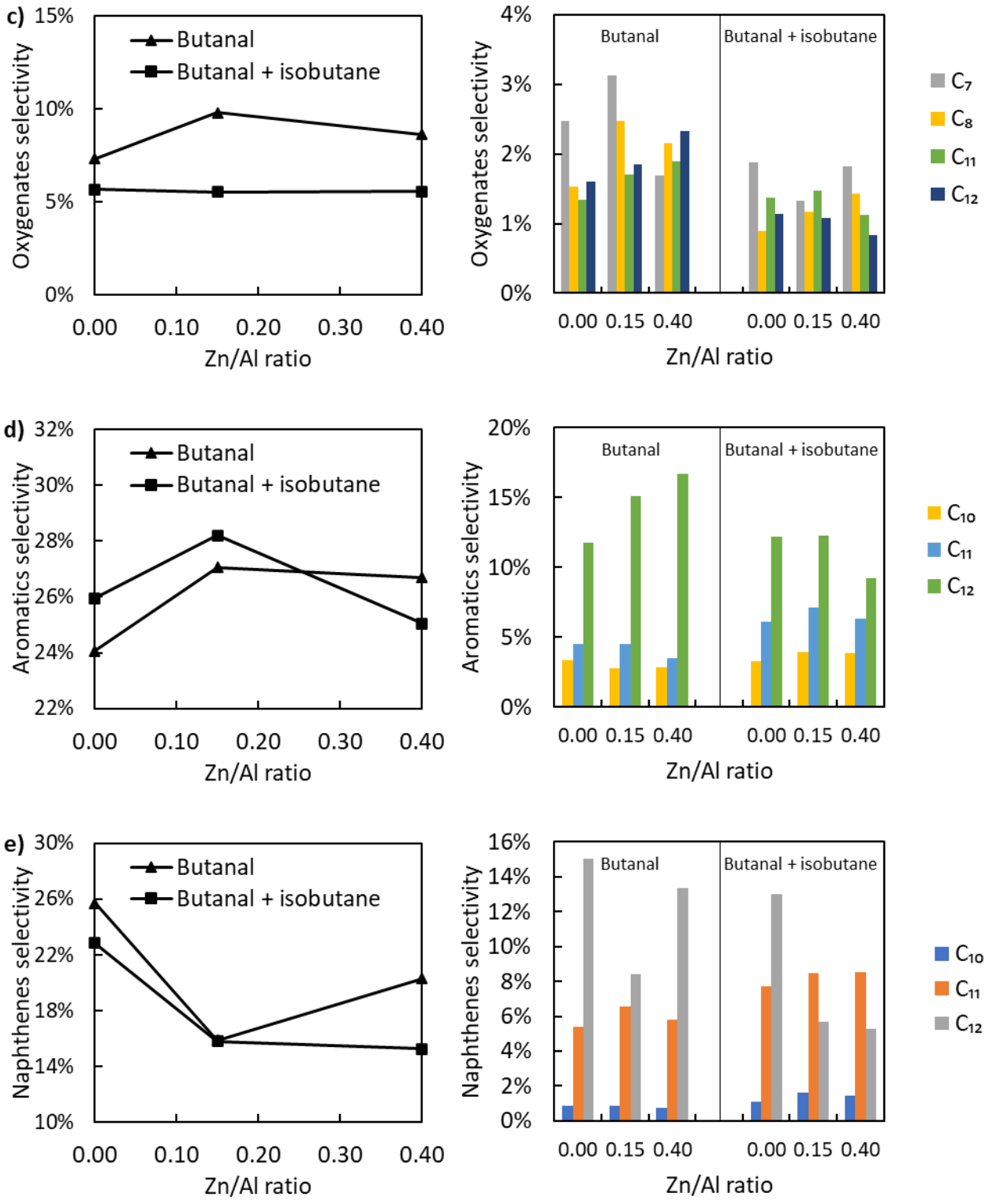

Figure 6.9: Selectivities (carbon-based) to a) alkanes, b) olefins, c) oxygenates, d) aromatics, and e) naphthenes from the conversion of butanal and butanal with isobutane co-feed over BEA zeolite with different Zn loadings. Reaction conditions: 300 °C temperature, 0.54 kPa butanal in

He (butanal reaction) or in 1:5 isobutane to He molar basis (butanal with isobutane co-feed reaction).

6.3.4.2 Butanal reaction with isobutane co-feed at 300 ºC

Figure 6.9a shows that isobutane co-feeding with butanal increased the overall selectivity to alkanes with values of 2.0% on H-BEA, 4.0% on 0.15Zn-BEA, and 4.5% on 0.40Zn-BEA. The increased selectivity was due in part to the availability of hydrogen from the dehydrogenation events of isobutane which could saturate the olefins generated from butanal conversion. This is evident by noting the increase in C_6 alkanes which were products from butanal conversion but not from isobutane as our investigative experiments showed in **Figure 6.7**a. Another reason for the increased selectivity to alkanes is the production of more C_5 alkanes mostly from the conversion of isobutane. The selectivity to olefins with isobutane co-feed increased over all catalysts with values of 40.8% on H-BEA, 43.7% on 0.15Zn-BEA, and 47.2% on 0.40Zn-BEA. Unlike butanal conversion, the co-feeding with isobutane resulted in a proportional increase in the selectivity to C_3 olefin with Zn loading from 6.2% on H-BEA to 8.1% on 0.40Zn-BEA. The selectivities to C_4, C_5, and C_8 olefins over all catalysts also increased with isobutane compared with feeding butanal alone. This was primarily caused by the dehydrogenation of isobutane and its oligomerization and cracking to C_3 and C_5 olefins (R-1, R-2, and R-3 in Scheme 6.1). Conversely, the selectivity to the other olefins C_6 and C_7 decreased with isobutane co-feed over all catalysts. For example, the selectivity to C_6 olefins decreased to 1.4% on H-BEA, to 1.5% on 0.15Zn-BEA, and to 1.3% on 0.40Zn-BEA. Similarly, the selectivity to C_7 decreased to 3.9% on H-BEA, to 5.9% on 0.15Zn-BEA, and to 5.2% on 0.40Zn-BEA.

The overall selectivity to oxygenates for all tested catalysts decreased with the isobutane co-feed from 7.3 – 9.8% to 5.5 – 5.7 % as seen in **Figure 6.9**c. The lower selectivity to oxygenates

with the isobutane co-feed suggests the enhancement of the dehydration and deoxygenation ability of butanal irrespective of the catalyst used. More notably, the selectivity to C_7 oxygenate over 0.15Zn-BEA was 1.3% compared with 1.9% for H-BEA and 1.8% for 0.40Zn-BEA. The lower selectivity to C_7 oxygenate over 0.15Zn-BEA was also matched with high selectivities to C_7 olefins with isobutane co-feed as noted earlier (R-7 in Scheme 6.2) and to C_{11} aromatics (R-16 in Scheme 6.2). This highlights the observed ability of the 0.15Zn-BEA catalyst to efficiently oligomerize the C_7 olefins with C_4 olefins to produce C_{11} aromatics without excessive dehydrogenation to C_{11} naphthenes (R-22 in Scheme 6.2) which was observed with the 0.40Zn-BEA catalyst. The overall selectivity to aromatics increased with the isobutane co-feed from 24.1 to 26.0% on H-BEA and from 27.1 to 28.2% on 0.15Zn-BEA. However, the selectivity to aromatics decreased from 26.7 to 25.0% over 0.40Zn-BEA with isobutane co-feed. In general, isobutane co-feeding increased the selectivities to C_{10} and C_{11} aromatics in reactions R-18 and R-16 due to the oligomerization of butenes with C_6 and C_7 olefins, respectively. This is reasonable considering that isobutane alone could not make such aromatic products on all the tested catalysts at 300 ^oC (**Figure 6.7**a) and that our co-feeding experiments used a much higher isobutane partial pressure (16.1 kPa compared with 0.4 – 1.3 kPa for the case of isobutane conversion experiments) which increases the concentration of butenes in the gas as well as their oligomerization with other olefins produced from the butanal conversion. Except for H-BEA which showed almost unchanged selectivity to C_{12} aromatics (R-13 in Scheme 6.2), the selectivities to C_{12} aromatics decreased with the isobutane co-feed from 15.1% to 12.3% on 0.15Zn-BEA and from 16.7% to 9.2% on 0.40Zn-BEA. These selectivity trends also matched those of C_{12} oxygenates as shown in **Figure 6.9**c. The higher selectivities to C_6 alkane and C_{10} aromatics (R-15 and R-18 in Scheme 6.2) on 0.15Zn-BEA and 0.40Zn-BEA suggests the increased rate of the dehydration and cracking reaction (R-11 in Scheme

6.2) on the expense of the dehydration and cyclization (R-13 in Scheme 6.2) resulting in a reduction in C_{12} aromatics. 0.40Zn-BEA showed the highest selectivity to C_6 alkanes which reflects its high hydrogenation ability in the presence of hydrogen from isobutane dehydrogenation and as expected from the lowest activation energy barrier for hydrogenation reaction (**Figure 6.8**c).

The selectivity to naphthenes decreased from 25.7% to 22.8% over H-BEA, from 15.9% to 15.8% over 0.15Zn-BEA, and from 20.3% to 15.3% over 0.40Zn-BEA. This observed decrease was expected due to the availability of hydrogen from isobutane dehydrogenation events and the shift of reaction equilibria to more saturated products. This is apparent, for example, by noticing the selectivity increase to C_6 alkanes with isobutane co-feed. Similar to aromatics, isobutane co-feed increased the selectivity to C_{10} and C_{11} naphthenes but decreased the selectivity to C_{12} naphthenes. The high selectivity to naphthenes observed over H-BEA even with isobutane co-feed explains the higher deactivation extent observed over this catalyst compared with the Zn-loaded ones (deactivation constants in **Figure 6.5**b) as these naphthene species could become coke precursors that blocks the active sites of the catalyst.[36] Because 0.15Zn-BEA showed the highest selectivity to C_7 olefins (R-7 in Scheme 6.2), C_{11} aromatics (R-16 in Scheme 6.2), and C_{10} naphthenes (R-20 and R-21 in Scheme 6.2), this indicates its superior ability to oligomerize the isobutane-produced C_3 and C_4 olefins with the butanal-produced C_6 and C_7 olefins. The high oligomerization ability of 0.15Zn-BEA was also manifested in its low selectivity to C_4 olefins (23.4%) which was even lower than H-BEA (23.8%) even though the former gave higher selectivity to butenes with the two feeds when run separately. The high tendency for 0.15Zn-BEA to produce C_4 and C_7 olefins from butanal coupled with its high oligomerization ability was the reason behind its overall higher selectivity to aromatics compared with other catalysts. The lower selectivity to aromatics observed over 0.40Zn-BEA was due to the combined effect of the higher

extent of hydrogenation leading to more saturated alkanes before forming aromatic oligomers and the high dehydrogenation ability resulting in the dehydrogenation of aromatics into their respective naphthenes.

6.4 Conclusion

The co-feeding of isobutane with butanal has proven to be an effective method for tailoring product selectivity and mitigating catalyst deactivation. The reaction analysis suggests a strong correlation between the Zn/Al ratio and the reactivity of each ion-exchanged H-BEA. the ion exchange with Zn resulted in samples with increasing amounts of both $[Zn\text{-}O\text{-}Al]^{2+}$ and $[Zn\text{-}O\text{-}Zn]^{2+}$ up to a loading of 0.20 Zn/Al and that further increase mostly contributed to the formation of new ZnO species while only marginally increasing $[Zn\text{-}O\text{-}Al]^{2+}$ sites. Zn/H-BEA with 0.15 and 0.40 Zn/Al showed the lowest deactivation behavior among all tested catalysts. The prominent deactivation behavior, which was particularly noticed with H-BEA, was attributed to its fast condensation, deoxygenation, and dehydrogenation of butanal to heavy naphthenes which becomes coke precursor eventually blocking the acid sites. The exceptional ability of Zn/H-BEA with 0.15 Zn/Al to generate C_7 and C_6 olefins from butanal and to effectively oligomerize them with C_3 and C_4 olefins formed from isobutane made it highly selective to aromatics. On the other hand, the higher Zn loading as in 0.40 Zn/Al results in an excessive catalytic dehydrogenation and hydrogenation ability which in turn results in the successive dehydrogenation of aromatics into naphthenes and the saturation of butanal-generated olefins thereby limiting their oligomerization into aromatics.

Chapter 7: Appendices

7.1 Supplementary information relating to Chapter 3

7.1.1 Checking the repeatability of pyridine titration experiments

To assess the repeatability of the pyridine titration experiments, the H-BEA sample was run multiple times using the same titration conditions. **Figure 7.1** shows two experiments for the titration of H-BEA with the samples giving loading capacities of 472 and 469 μmol g^{-1}. The nearly identical saturation curves shown in **Figure 7.1** and the 0.6% error in calculating the loading capacity of H-BEA suggest the high repeatability of our setup in performing these experiments.

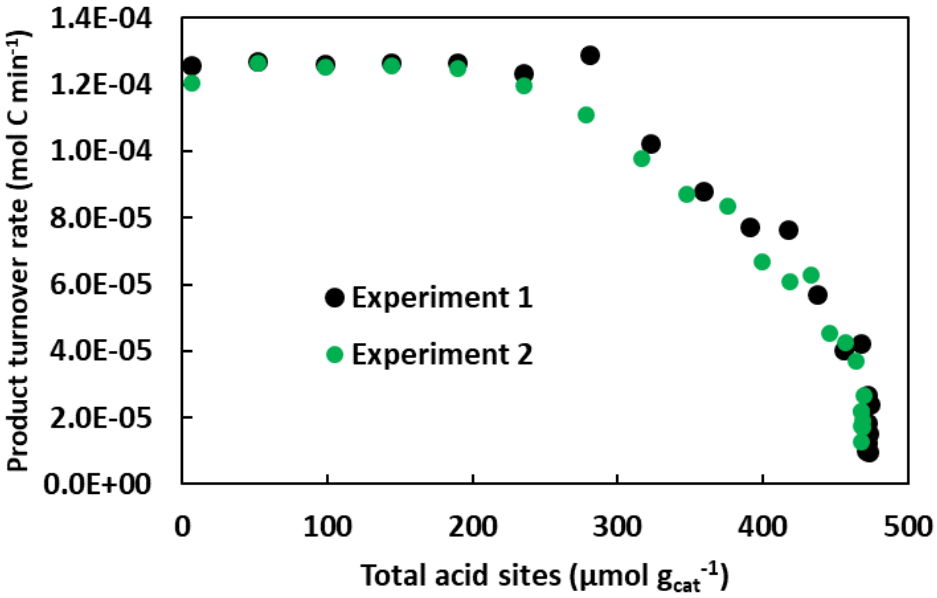

Figure 7.1: H-BEA acid site titration experiments using pyridine at the same conditions.

7.1.2 Isopropylamine temperature-programmed-desorption (TPD) method and calculations

7.1.2.1 MS calibration

The MS signal at 44 m/z was calibrated using predetermined concentrations of isopropylamine made by vaporizing the liquid into He gas. The area of the response generated by the 44 m/z signal was used to calculate the response factor flowing Equation 7.1 which is shown graphically as a slope in **Figure 7.2**. Multiplying this response factor by the response area of the MS at 44 m/z was then used to calculate the concentration of IPA in the outlet gas.

$$IPA\ response\ factor = \frac{IPA\ feed\ concentration\ (mol\ ml^{-1})}{MS\ response\ area\ at\ 44\ m/z\ (a.u.)} \tag{7.1}$$

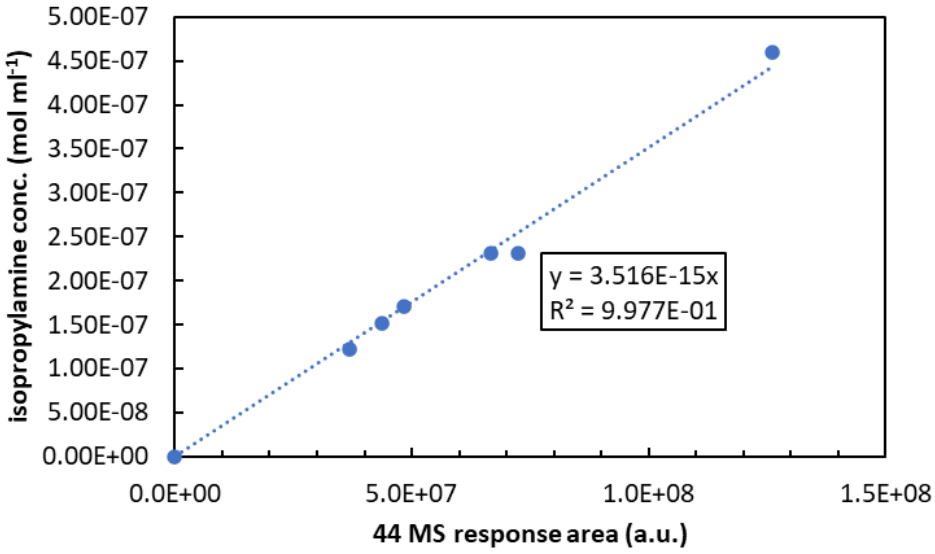

Figure 7.2: Graphical calculation of isopropylamine response factor from the MS signal at 44 m/z.

To calibrate the MS for 41 m/z signal (propylene), a continuous flow of IPA with known concentration was reacted for 20 mg of H-BEA zeolite at 450 ^{o}C to convert the majority of IPA to propylene. After reaching a steady state composition following 41 and 44 m/z signals, the

difference in IPA concentration in the feed and the gas product was used to calculate the concentration of propylene in the outlet gas as in equation (7.2). This calculated concentration of propylene was used to define the response factor for the 41 m/z signal according to equation (7.3):

$$propylene\ conc.in\ the\ gas = IPA\ conc.in\ the\ feed - IPA\ conc.in\ the\ product \quad (7.2)$$

$$Propylene\ response\ factor = \frac{Propylene\ conc.in\ the\ gas\ (mol\ ml^{-1})}{MS\ response\ area\ at\ 41\ m/z\ (a.u.)} \quad (7.3)$$

It is important to note that there was an observable response of 41 m/z signal with the IPA (44 z/m signal) even when propylene was not present in the feed. This could be realized by their perfectly linear relation shown in **Figure 7.3**. Accordingly, any measured response of 41 signal was corrected by subtracting 10.98% of the 44 signal (slope in **Figure 7.3**) as in equation (7.4).

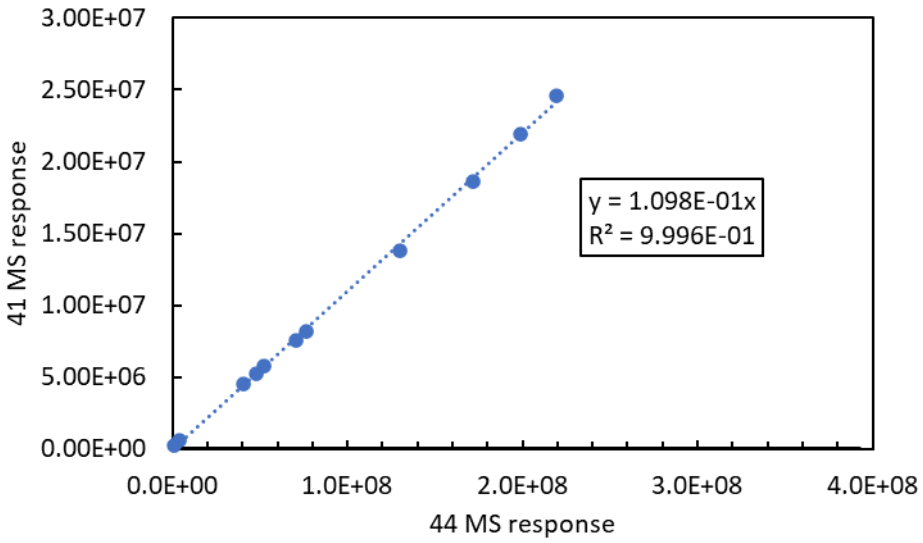

Figure 7.3: Relationship between 41 and 44 m/z signals with different concentrations of isopropylamine.

$$Corrected\ 41\ m/s\ response = measured\ 41\ m/z - 0.1098\ (measured\ 44\ m/z) \quad (7.4)$$

7.1.2.2 Experimental procedure

Using the same reaction setup described in Chapter 2, the reactor was loaded with 20 mg of catalyst (60 – 80 US mesh size) and the catalyst was heated to 40 ^{o}C under 20 ml min^{-1} He gas purge. At the same time, isopropylamine (> 99.5%, Sigma Aldrich) feed was stabilized by pumping at 1 µl min^{-1} rate (using 1 ml syringe) into a vaporizing zone heated at 40 ^{o}C and swept by a 50 ml min^{-1} flow of He to generate a stream of roughly 2.75 kPa isopropylamine in He. A GC-MS with an HP-5 ms UI column (30 m, 0.25 mm, 0.25 µm) was used to monitor the composition of the feed gas. After stabilizing both the reactor temperature and the feed composition, the purging He flow into the reactor was stopped and the feed gas was diverted to the reactor by a three-way value. Isoporpylamine was allowed to saturate the catalyst sample for 1 hour then the liquid feed was stopped to purge the catalyst sample with the 50 ml min^{-1} He flow for 1 hour. After purging the catalyst with He, the reactor temperature was gradually raised from 40 to 640 ^{o}C (4 ^{o}C min^{-1} rate) while simultaneously starting the GC-MS sampling. The GC method was also set to maintain a constant oven temperature of 120 ^{o}C and to take a sample injection every 2 minutes. The concentrations of the products were monitored by MS signals 44 m/z for isopropylamine and 41 m/z for propylene.

7.1.2.3 Peak deconvolution calculations

The propylene TPD curve resulting from the decomposition of isopropylamine on Brønsted or Zn^{2+} Lewis acid sites was deconvoluted into three main peaks using Gaussian-type fit shown in equation (7.5).

$$G_x = h_x \exp\left[-0.5\left(\frac{(T - c_x)}{w_x}\right)^2\right] \tag{7.5}$$

Where *G* represents the gaussian fit, *x* is the peak number, *h* is the peak height parameter, *T* is the TPD desorption temperature, *c* is the center temperature of the peak, and *w* is the peak's width parameter. The three Gaussian curves representing the experimental TPD curve of each catalyst were obtained by fixing the center temperatures (c_x) and estimating h_x and w_x parameters of each peak curve through Matlab software that uses fminsearch function. The estimation was performed to minimize the sum of error squares resulting from the subtraction of the experimental curve points from the theoretical Gaussian curve resulting from the summation of the individual peak Gaussians as in equation (7.6).

$$G_{Theoritical} = \sum_{x=1}^{3} G_x \tag{7.6}$$

7.1.3 Overlayed isopropylamine TPD deconvolution peaks

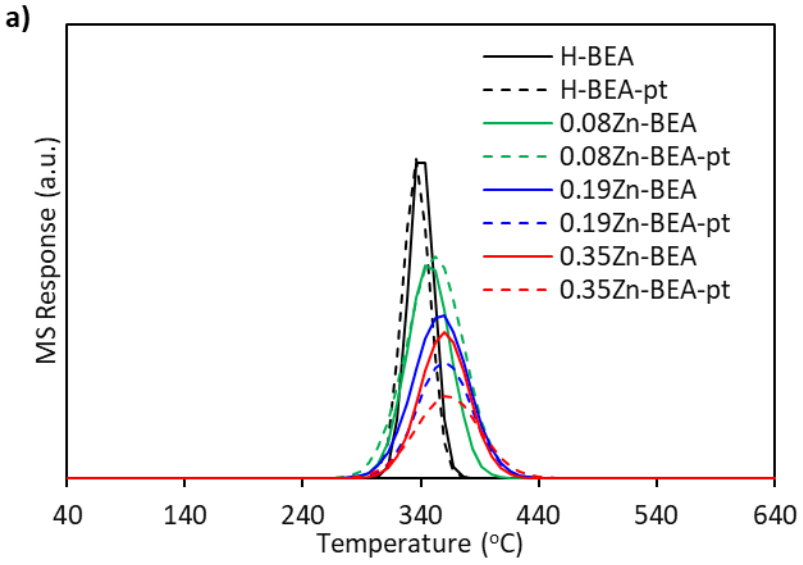

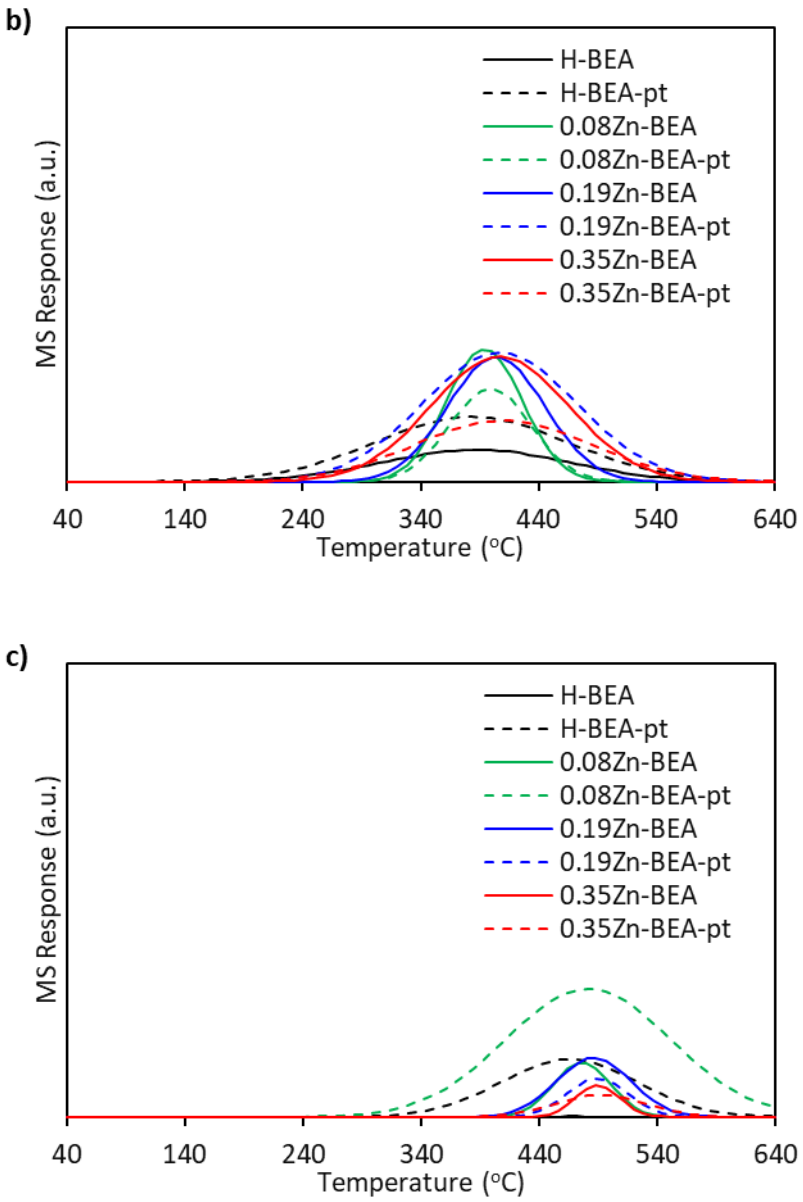

Figure 7.4: Overlayed isopropylamine TPD peaks resulting from the deconvolution of the experimental propylene desorption curves of each catalyst into three peaks with a) 336 – 363 °C peak centers, b) 383 – 410 °C peak centers, and c) 465 – 492 °C peak centers.

7.1.4 Isopropylamine desorption profiles from all tested catalysts

Comparable desorption amounts of isopropylamine from all catalysts were observed but their exact amounts gave limited intuition about the weak acidity of the zeolites and their physical adsorption behavior. Therefore, and for graphical comparison, the desorption curves of isopropylamine and their three-peak Gaussian fits are shown in **Figure 7.5**. The general observation was that higher Zn loading resulted in higher desorption temperatures of physically adsorbed isopropylamine.

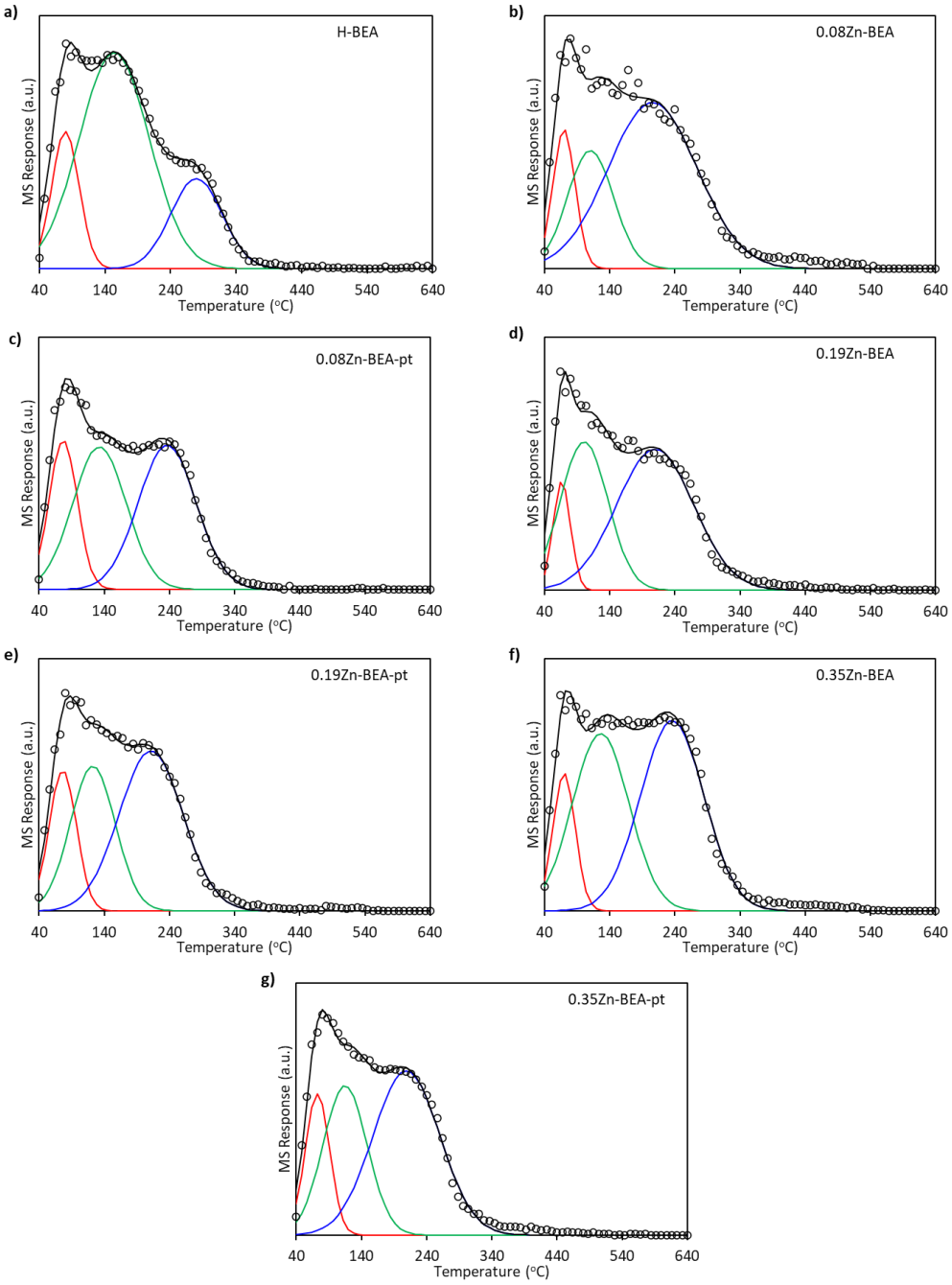

Figure 7.5: Visualization of isopropylamine desorption profiles and their three-peak Gaussians from all tested catalysts.

7.2 Supplementary information relating to Chapter 4

7.2.1 Modeling data tables

Table 7-1: modeling data for butanal reaction on H-BEA at 200 °C

TOS (min)	Cat. Weight	Butanal (feed)	He (feed)	Butanal (product)	2EH (product)	C8 ester (product)	C12 aromatics (product)	Butenes (product)
[min]	[g]				[μmol s^{-1}]			
33	0.01	1.85E-01	3.47E+01	1.77E-01	1.99E-03	1.67E-04	4.80E-04	4.07E-04
33	0.01	3.70E-01	3.14E+01	3.54E-01	3.92E-03	2.55E-04	6.32E-04	5.13E-04
33	0.01	5.55E-01	2.81E+01	5.33E-01	4.66E-03	2.97E-04	2.10E-03	5.25E-04
33	0.01	7.40E-01	2.47E+01	7.13E-01	5.95E-03	3.00E-04	3.17E-03	4.06E-04
33	0.07	1.85E-01	3.47E+01	1.45E-01	5.19E-03	7.44E-04	7.51E-03	2.99E-03
33	0.05	1.85E-01	3.47E+01	1.58E-01	3.89E-03	5.10E-04	4.70E-03	1.98E-03
33	0.03	1.85E-01	3.47E+01	1.64E-01	3.65E-03	4.45E-04	3.19E-03	1.25E-03
33	0.02	1.85E-01	3.47E+01	1.72E-01	2.66E-03	1.84E-04	1.40E-03	6.90E-04
33	0.01	1.85E-01	3.47E+01	1.77E-01	1.99E-03	1.67E-04	4.80E-04	4.07E-04
63	0.01	1.85E-01	3.47E+01	1.78E-01	1.52E-03	1.29E-04	4.03E-04	2.99E-04
93	0.01	1.85E-01	3.47E+01	1.79E-01	1.40E-03	1.00E-04	2.71E-04	2.61E-04
123	0.01	1.85E-01	3.47E+01	1.79E-01	1.28E-03	1.01E-04	2.43E-04	2.13E-04
153	0.01	1.85E-01	3.47E+01	1.79E-01	1.23E-03	9.56E-05	2.20E-04	2.00E-04
183	0.01	1.85E-01	3.47E+01	1.79E-01	1.16E-03	8.74E-05	1.85E-04	1.77E-04
213	0.01	1.85E-01	3.47E+01	1.79E-01	1.11E-03	7.59E-05	1.91E-04	1.64E-04
243	0.01	1.85E-01	3.47E+01	1.79E-01	1.11E-03	7.65E-05	1.78E-04	1.45E-04
63	0.10	1.85E-01	3.47E+01	1.47E-01	4.77E-03	6.72E-04	7.38E-03	2.52E-03
93	0.10	1.85E-01	3.47E+01	1.55E-01	4.44E-03	6.37E-04	5.07E-03	2.09E-03
123	0.10	1.85E-01	3.47E+01	1.61E-01	4.16E-03	5.59E-04	3.37E-03	1.70E-03
153	0.10	1.85E-01	3.47E+01	1.63E-01	4.09E-03	5.32E-04	2.71E-03	1.57E-03
183	0.10	1.85E-01	3.47E+01	1.66E-01	3.88E-03	4.86E-04	2.06E-03	1.34E-03
213	0.10	1.85E-01	3.47E+01	1.66E-01	3.76E-03	4.54E-04	2.07E-03	1.23E-03
243	0.10	1.85E-01	3.47E+01	1.68E-01	3.69E-03	4.28E-04	1.70E-03	1.13E-03

Table 7-2: Modeling data for butanal reaction H-BEA zeolites ion exchanged with Na^+ at 200 ^oC

TOS (min)	Cat. Weight	Butanal (feed)	He (feed)	Butanal (product)	2EH (product)	C8 ester (product)	C12 aromatics (product)	butenes (product)
[min]	[g]				[µmol s^{-1}]			
				0.02Na-BEA				
63	0.1	1.85E-01	3.47E+01	1.48E-01	3.90E-03	5.08E-04	8.22E-03	1.19E-03
93	0.1	1.85E-01	3.47E+01	1.59E-01	3.68E-03	4.79E-04	4.82E-03	9.49E-04
123	0.1	1.85E-01	3.47E+01	1.62E-01	3.38E-03	4.19E-04	3.74E-03	7.49E-04
153	0.1	1.85E-01	3.47E+01	1.64E-01	3.33E-03	4.11E-04	3.01E-03	6.76E-04
183	0.1	1.85E-01	3.47E+01	1.65E-01	3.26E-03	3.56E-04	2.78E-03	6.45E-04
213	0.1	1.85E-01	3.47E+01	1.66E-01	3.12E-03	3.58E-04	2.36E-03	6.20E-04
243	0.1	1.85E-01	3.47E+01	1.67E-01	3.05E-03	3.22E-04	2.19E-03	5.11E-04
				0.10Na-BEA				
63	0.1	1.85E-01	3.47E+01	1.57E-01	4.13E-03	4.84E-04	5.68E-03	7.90E-04
93	0.1	1.85E-01	3.47E+01	1.58E-01	3.46E-03	4.25E-04	5.35E-03	5.52E-04
123	0.1	1.85E-01	3.47E+01	1.61E-01	3.07E-03	3.51E-04	4.25E-03	4.48E-04
153	0.1	1.85E-01	3.47E+01	1.64E-01	2.94E-03	3.26E-04	3.33E-03	3.95E-04
183	0.1	1.85E-01	3.47E+01	1.64E-01	2.91E-03	3.39E-04	3.24E-03	3.88E-04
213	0.1	1.85E-01	3.47E+01	1.66E-01	2.64E-03	3.01E-04	2.62E-03	2.99E-04
243	0.1	1.85E-01	3.47E+01	1.67E-01	2.64E-03	2.97E-04	2.15E-03	2.81E-04
				0.50Na-BEA				
63	0.1	1.85E-01	3.47E+01	1.54E-01	4.85E-03	6.06E-04	6.00E-03	8.85E-04
93	0.1	1.85E-01	3.47E+01	1.58E-01	3.95E-03	5.14E-04	5.57E-03	6.32E-04
123	0.1	1.85E-01	3.47E+01	1.64E-01	3.22E-03	4.21E-04	4.00E-03	4.64E-04
153	0.1	1.85E-01	3.47E+01	1.66E-01	3.06E-03	3.61E-04	3.70E-03	4.26E-04
183	0.1	1.85E-01	3.47E+01	1.68E-01	2.77E-03	3.18E-04	3.04E-03	3.44E-04
213	0.1	1.85E-01	3.47E+01	1.70E-01	2.58E-03	2.97E-04	2.36E-03	3.18E-04
243	0.1	1.85E-01	3.47E+01	1.71E-01	2.41E-03	2.81E-04	1.91E-03	3.00E-04

Table 7-3: Modeling data for butanal reaction on H-BEA ion exchanged with Zn^{2+} at 200 °C

TOS (min)	Cat. Weight	Butanal (feed)	He (feed)	Butanal (product)	2EH (product)	C8 ester (product)	C12 aromatics (product)	butenes (product)
[min]	[g]				[µmol s^{-1}]			
				0.08Zn-BEA				
63	0.1	1.85E-01	3.47E+01	1.44E-01	5.79E-03	5.87E-04	7.87E-03	1.93E-03
93	0.1	1.85E-01	3.47E+01	1.51E-01	5.00E-03	5.12E-04	6.28E-03	1.52E-03
123	0.1	1.85E-01	3.47E+01	1.58E-01	4.88E-03	4.78E-04	4.31E-03	1.27E-03
153	0.1	1.85E-01	3.47E+01	1.59E-01	4.61E-03	4.47E-04	4.09E-03	1.15E-03
183	0.1	1.85E-01	3.47E+01	1.64E-01	4.30E-03	4.17E-04	2.90E-03	1.01E-03
213	0.1	1.85E-01	3.47E+01	1.65E-01	4.35E-03	4.00E-04	2.64E-03	9.14E-04
243	0.1	1.85E-01	3.47E+01	1.65E-01	4.32E-03	3.94E-04	2.47E-03	8.59E-04
				0.19Zn-BEA				
63	0.1	1.85E-01	3.47E+01	1.47E-01	5.64E-03	4.36E-04	7.63E-03	1.63E-03
93	0.1	1.85E-01	3.47E+01	1.56E-01	4.98E-03	3.97E-04	5.26E-03	1.35E-03
123	0.1	1.85E-01	3.47E+01	1.59E-01	4.66E-03	3.58E-04	4.54E-03	1.15E-03
153	0.1	1.85E-01	3.47E+01	1.62E-01	4.33E-03	3.39E-04	3.58E-03	1.07E-03
183	0.1	1.85E-01	3.47E+01	1.63E-01	4.38E-03	2.90E-04	3.37E-03	1.07E-03
213	0.1	1.85E-01	3.47E+01	1.66E-01	4.04E-03	2.69E-04	2.56E-03	9.13E-04
243	0.1	1.85E-01	3.47E+01	1.69E-01	3.74E-03	2.55E-04	2.07E-03	8.19E-04
				0.35Zn-BEA				
63	0.1	1.85E-01	3.47E+01	1.47E-01	5.88E-03	4.36E-04	7.37E-03	1.56E-03
93	0.1	1.85E-01	3.47E+01	1.55E-01	5.35E-03	3.96E-04	5.49E-03	1.23E-03
123	0.1	1.85E-01	3.47E+01	1.56E-01	4.90E-03	3.58E-04	5.29E-03	1.04E-03
153	0.1	1.85E-01	3.47E+01	1.60E-01	4.75E-03	3.08E-04	4.14E-03	9.78E-04
183	0.1	1.85E-01	3.47E+01	1.64E-01	4.42E-03	2.86E-04	3.28E-03	8.40E-04
213	0.1	1.85E-01	3.47E+01	1.65E-01	4.23E-03	2.77E-04	2.83E-03	8.24E-04
243	0.1	1.85E-01	3.47E+01	1.68E-01	3.94E-03	2.63E-04	2.20E-03	6.53E-04

Table 7-4: Modeling data for butanal conversion on H-BEA ion exchanged with Zn^{2+} and thermally pretreated (450 ^{o}C) at 200 ^{o}C

TOS (min)	Cat. Weight	Butanal (feed)	He (feed)	Butanal (product)	2EH (product)	C8 ester (product)	C12 aromatics (product)	butenes (product)
[min]	[g]				[µmol s^{-1}]			
				0.08Zn-BEA-pt				
63	0.1	1.85E-01	3.47E+01	1.50E-01	5.59E-03	6.10E-04	6.29E-03	1.32E-03
93	0.1	1.85E-01	3.47E+01	1.55E-01	5.23E-03	5.69E-04	5.04E-03	9.57E-04
123	0.1	1.85E-01	3.47E+01	1.58E-01	5.06E-03	5.62E-04	4.16E-03	8.41E-04
153	0.1	1.85E-01	3.47E+01	1.61E-01	4.71E-03	5.24E-04	3.60E-03	7.08E-04
183	0.1	1.85E-01	3.47E+01	1.62E-01	4.66E-03	5.24E-04	3.20E-03	6.58E-04
213	0.1	1.85E-01	3.47E+01	1.63E-01	4.39E-03	5.09E-04	2.93E-03	5.95E-04
243	0.1	1.85E-01	3.47E+01	1.66E-01	4.19E-03	4.69E-04	2.27E-03	5.27E-04
				0.19Zn-BEA-pt				
63	0.1	1.85E-01	3.47E+01	1.51E-01	6.09E-03	5.85E-04	5.81E-03	1.26E-03
93	0.1	1.85E-01	3.47E+01	1.53E-01	5.35E-03	5.54E-04	5.65E-03	9.78E-04
123	0.1	1.85E-01	3.47E+01	1.56E-01	4.97E-03	5.33E-04	4.80E-03	8.83E-04
153	0.1	1.85E-01	3.47E+01	1.62E-01	4.39E-03	4.82E-04	3.50E-03	7.09E-04
183	0.1	1.85E-01	3.47E+01	1.62E-01	4.41E-03	4.79E-04	3.36E-03	6.38E-04
213	0.1	1.85E-01	3.47E+01	1.64E-01	4.24E-03	4.70E-04	2.84E-03	5.75E-04
243	0.1	1.85E-01	3.47E+01	1.65E-01	4.32E-03	4.62E-04	2.61E-03	5.70E-04
				0.35Zn-BEA-pt				
63	0.1	1.85E-01	3.47E+01	1.50E-01	6.75E-03	5.52E-04	5.69E-03	1.12E-03
93	0.1	1.85E-01	3.47E+01	1.57E-01	5.56E-03	4.88E-04	4.48E-03	8.07E-04
123	0.1	1.85E-01	3.47E+01	1.60E-01	5.02E-03	4.59E-04	3.87E-03	6.95E-04
153	0.1	1.85E-01	3.47E+01	1.62E-01	4.66E-03	4.32E-04	3.43E-03	6.04E-04
183	0.1	1.85E-01	3.47E+01	1.63E-01	4.62E-03	4.35E-04	3.10E-03	5.53E-04
213	0.1	1.85E-01	3.47E+01	1.65E-01	4.41E-03	3.85E-04	2.71E-03	5.32E-04
243	0.1	1.85E-01	3.47E+01	1.66E-01	4.24E-03	3.77E-04	2.31E-03	4.69E-04

Table 7-5: Summary of the kinetic model results of butanal conversion on Na/H-BEA and Zn/H-BEA catalysts

	Catalyst									
	H-BEA	**0.02Na-BEA**	**0.10Na-BEA**	**0.50Na-BEA**	**0.08Zn-BEA**	**0.08Zn-BEA-pt**	**0.19Zn-BEA**	**0.19Zn-BEA-pt**	**0.35Zn-BEA**	**0.35Zn-BEA-pt**
Binding energy (kJ mol^{-1})										
Butanal	-66.16	-65.82	-65.88	-65.36	-65.83	-66.11	-65.99	-66.14	-66.18	-66.25
2-ethyl-hexenal	-93.18	-93.01	-92.45	-91.26	-93.05	-92.95	-93.12	-92.83	-93.69	-93.09
Activation energy (kJ mol^{-1})										
E_1	0.00	0.00	0.00	0.00	0.00	0.00	0.00	0.00	0.00	0.00
E_2	0.00	0.00	0.00	0.00	0.00	0.00	0.00	0.00	0.00	0.00
E_3	0.00	0.00	0.00	0.00	0.00	0.00	0.00	0.00	0.00	0.00
E_4	79.09	78.52	78.80	77.71	78.60	78.72	79.20	79.17	79.59	79.96
E_5	0.00	0.00	0.00	0.00	0.00	0.00	0.00	0.00	0.00	0.00
E_6	89.90	90.21	90.54	89.19	90.27	89.60	92.00	90.59	92.69	91.66
E_7	0.00	0.00	0.00	0.00	0.00	0.00	0.00	0.00	0.00	0.00
E_8	81.54	80.02	79.50	78.15	81.82	81.93	82.28	82.17	83.26	83.56
E_9	0.00	0.00	0.00	0.00	0.00	0.00	0.00	0.00	0.00	0.00
Constants										
Local entropy fraction F_{loc}	0.92	0.92	0.92	0.92	0.92	0.92	0.92	0.92	0.92	0.92
Sticking probability Θ	1.00	1.00	1.00	1.00	1.00	1.00	1.00	1.00	1.00	1.00
Hydrogen constant α	0.40	0.16	0.12	0.12	0.28	0.20	0.26	0.20	0.22	0.19
Deactivation constant k_d (s Pa^{-1})	1.39E-07	1.40E-07	1.41E-07	1.01E-07	1.38E-07	1.42E-07	1.41E-07	1.39E-07	1.36E-07	1.45E-07

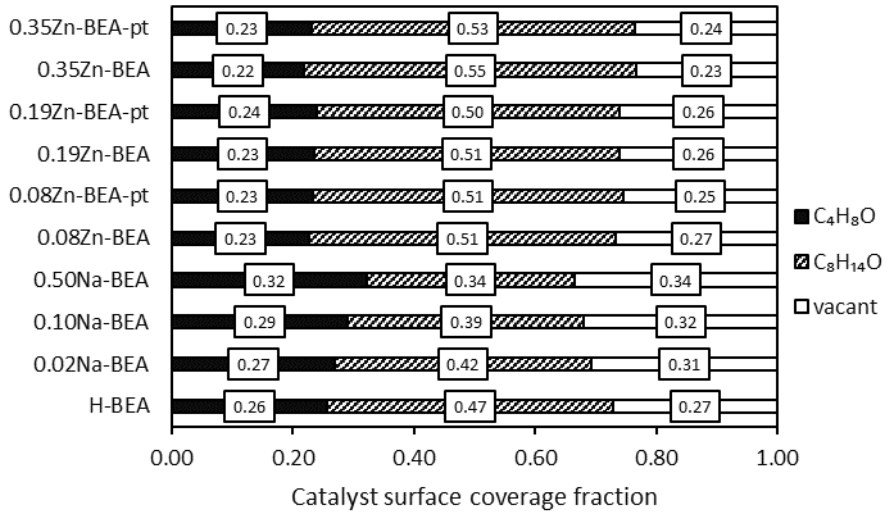

Figure 7.6: Initial surface species fractional coverages on all tested catalysts.

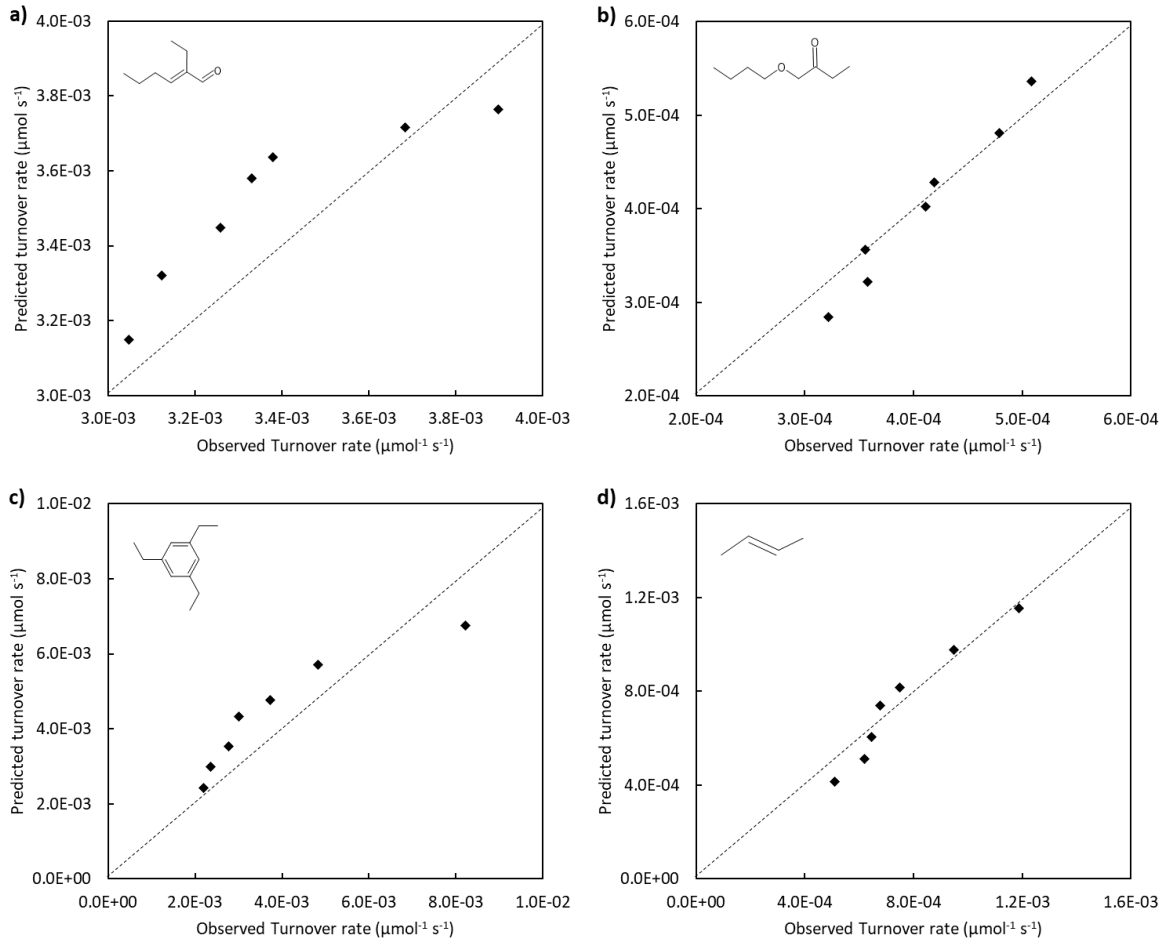

Figure 7.7: Parity charts comparing observed and predicted turnover rates of a) 2-ethyl-2-hexenal product lump, b) butyl butyrate product lump, c) C_{10}+ aromatics lump, and d) butenes on 0.02Na-BEA catalyst. Butanal conversion rates were measured at 200 ^{o}C, 0.54 kPa butanal partial pressure in He, and 100 mg catalyst weight. The displayed structure on the figures indicates the most abundant species in the product lump.

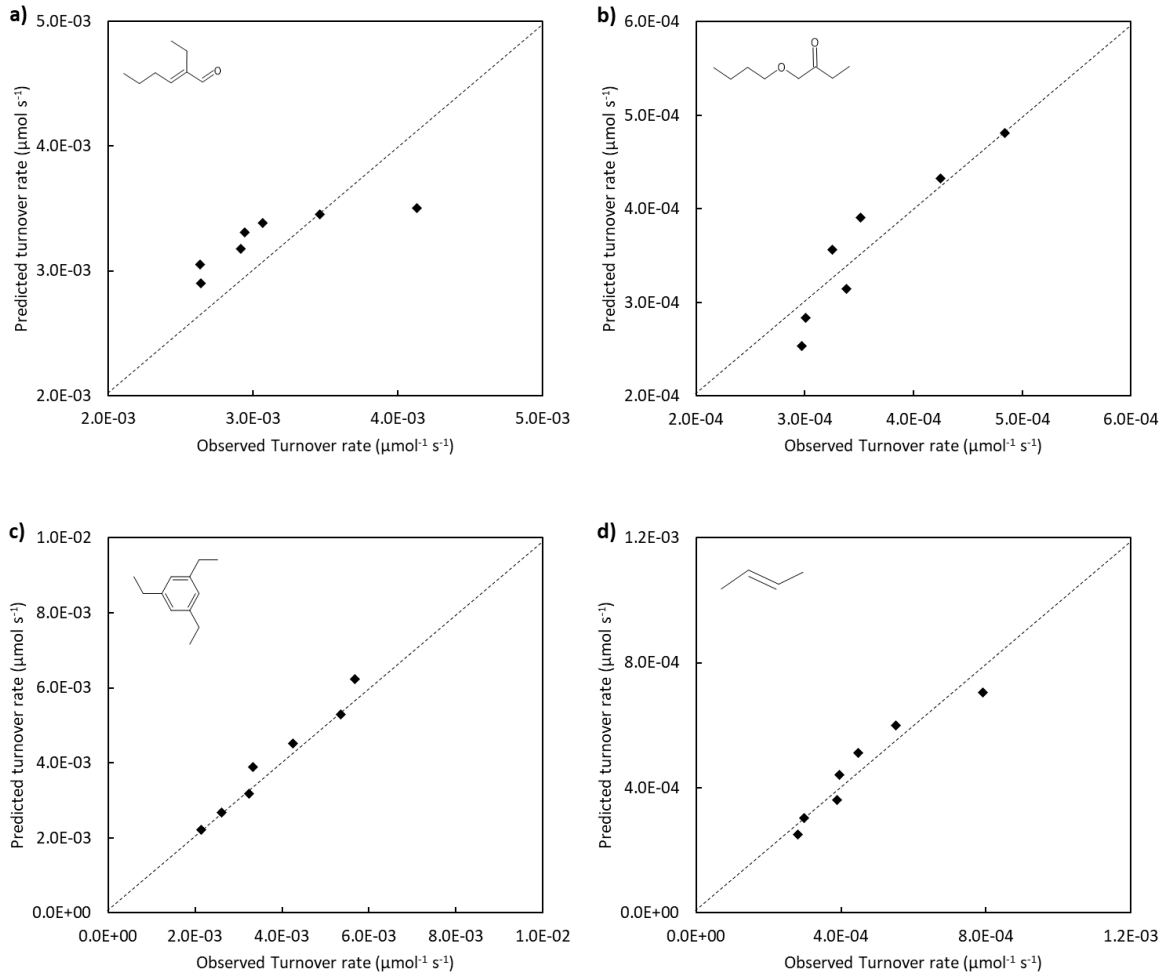

Figure 7.8: Parity charts comparing observed and predicted turnover rates of a) 2-ethyl-2-hexenal product lump, b) butyl butyrate product lump, c) C_{10}+ aromatics lump, and d) butenes on 0.10Na-BEA catalyst. Butanal conversion rates were measured at 200 ^{o}C, 0.54 kPa butanal partial pressure in He, and 100 mg catalyst weight. The displayed structure on the figures indicates the most abundant species in the product lump.

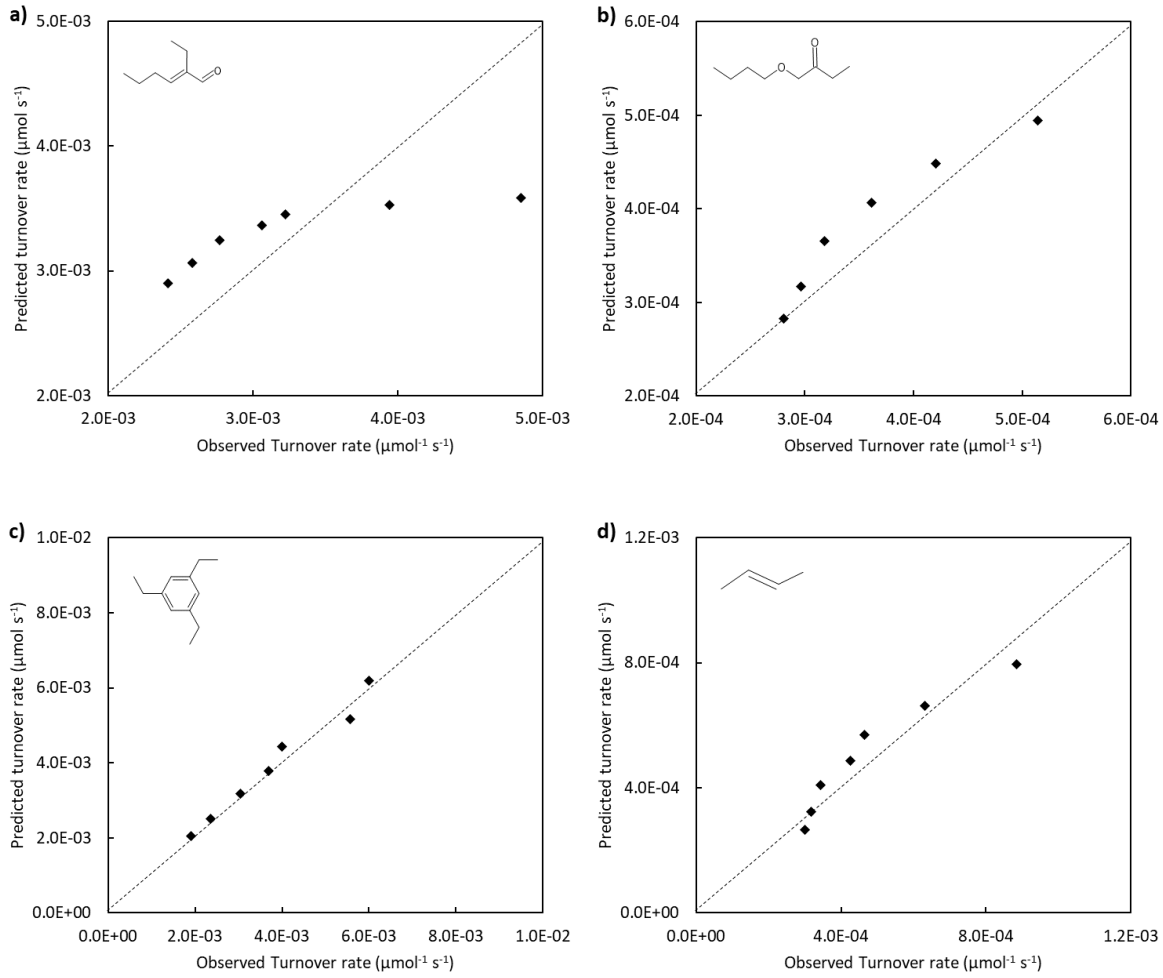

Figure 7.9: Parity charts comparing observed and predicted turnover rates of a) 2-ethyl-2-hexenal product lump, b) butyl butyrate product lump, c) C_{10}+ aromatics lump, and d) butenes on 0.50Na-BEA catalyst. Butanal conversion rates were measured at 200 ^{o}C, 0.54 kPa butanal partial pressure in He, and 100 mg catalyst weight. The displayed structure on the figures indicates the most abundant species in the product lump.

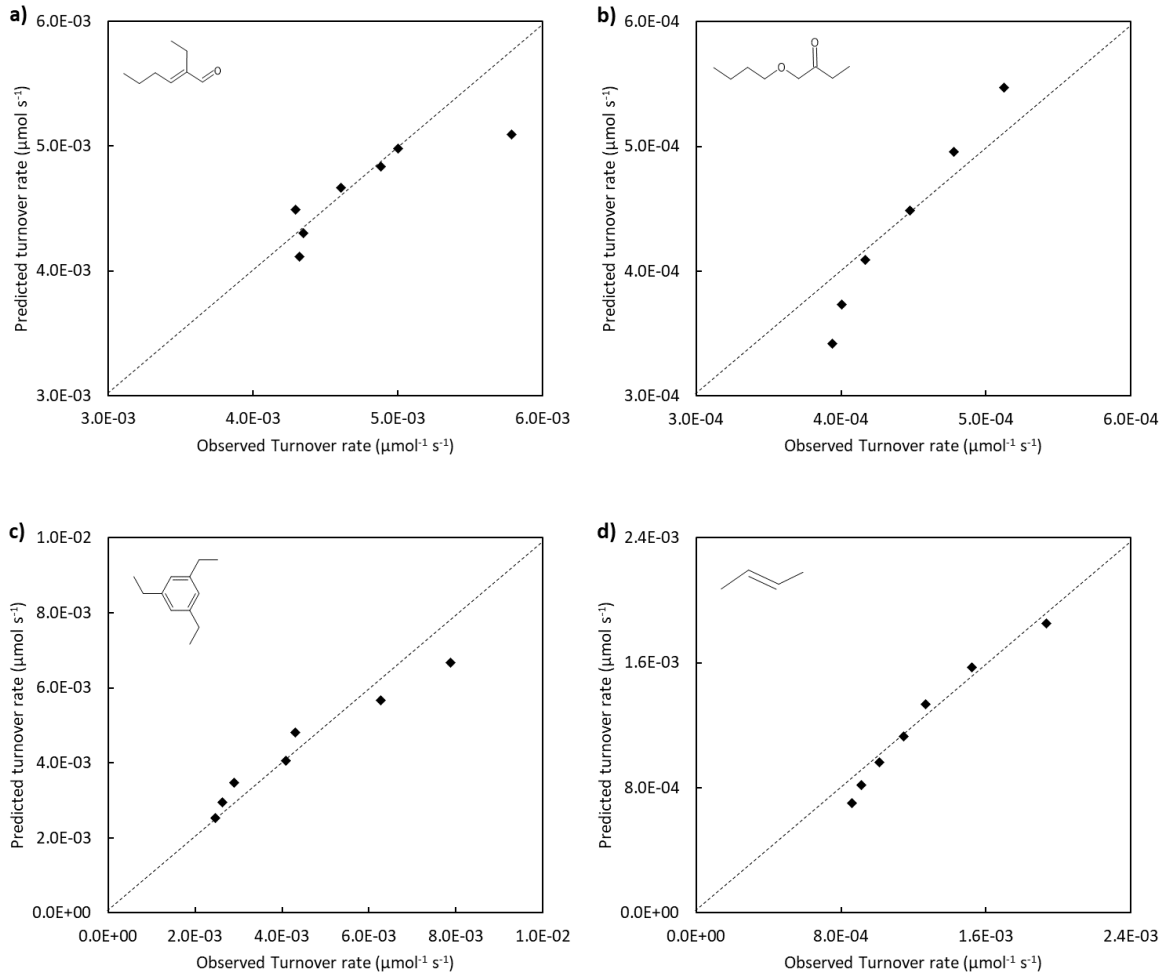

Figure 7.10: Parity charts comparing observed and predicted turnover rates of a) 2-ethyl-2-hexenal product lump, b) butyl butyrate product lump, c) C_{10}+ aromatics lump, and d) butenes on 0.08Zn-BEA catalyst. Butanal conversion rates were measured at 200 ^{o}C, 0.54 kPa butanal partial pressure in He, and 100 mg catalyst weight. The displayed structure on the figures indicates the most abundant species in the product lump.

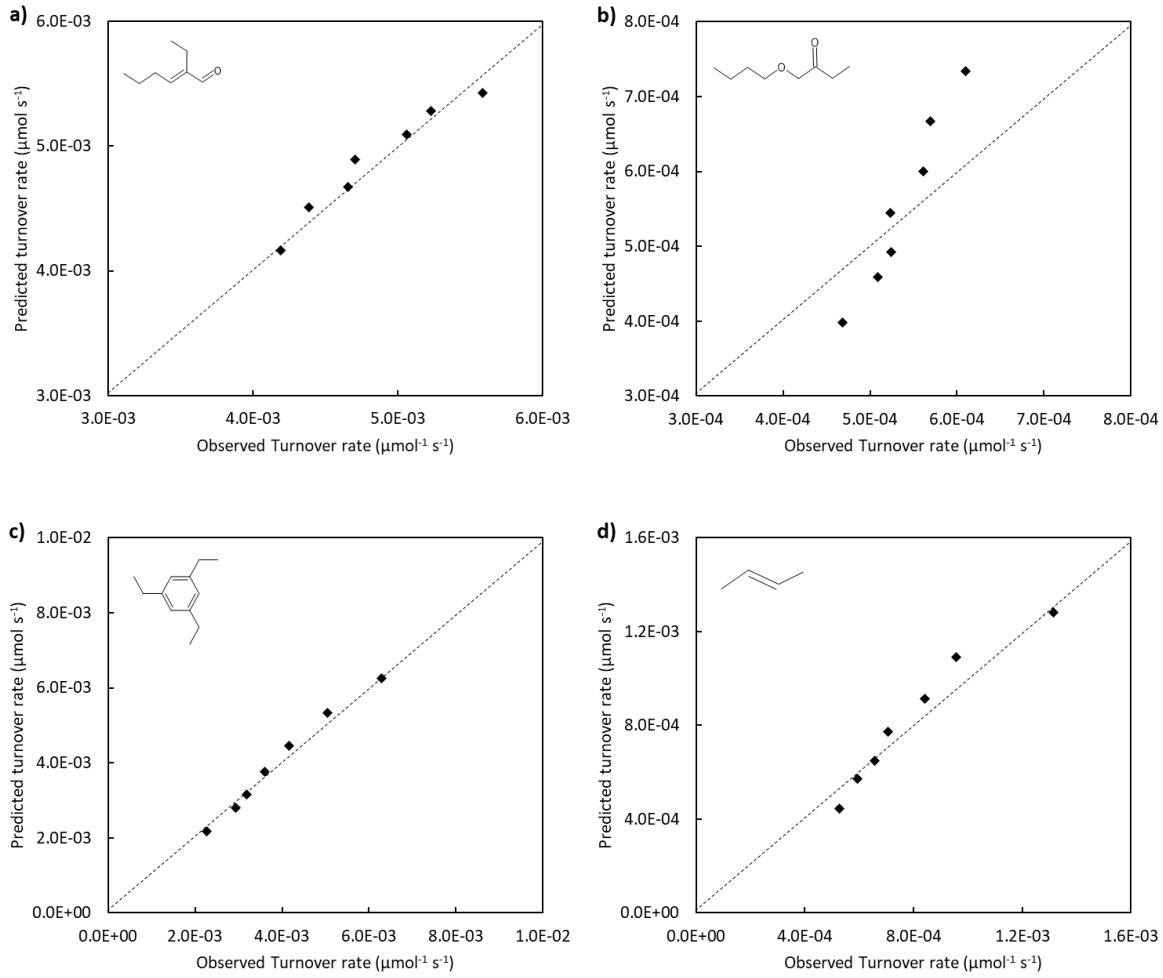

Figure 7.11: Parity charts comparing observed and predicted turnover rates of a) 2-ethyl-2-hexenal product lump, b) butyl butyrate product lump, c) C_{10}+ aromatics lump, and d) butenes on 0.08Zn-BEA-pt catalyst. Butanal conversion rates were measured at 200 ^{o}C, 0.54 kPa butanal partial pressure in He, and 100 mg catalyst weight. The displayed structure on the figures indicates the most abundant species in the product lump.

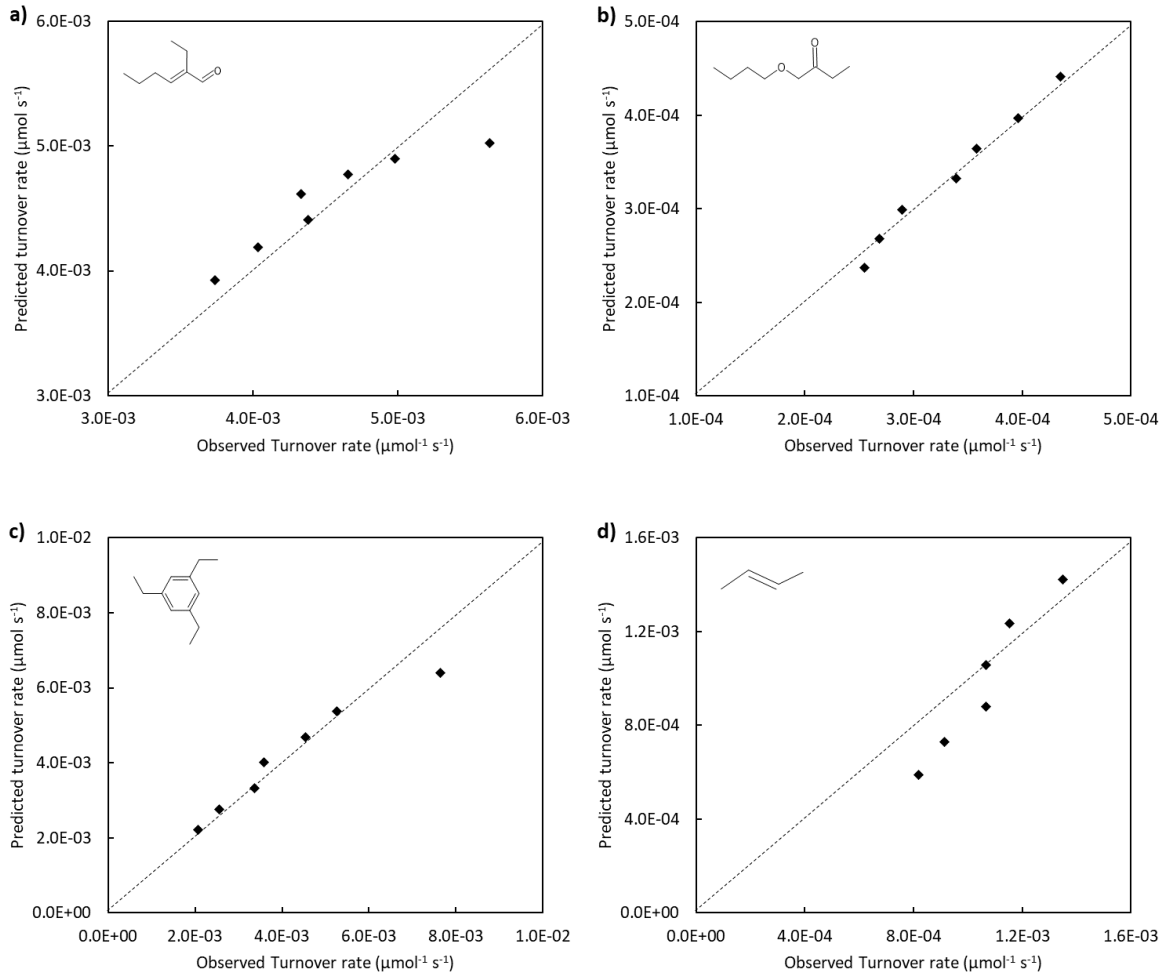

Figure 7.12: Parity charts comparing observed and predicted turnover rates of a) 2-ethyl-2-hexenal product lump, b) butyl butyrate product lump, c) C_{10}+ aromatics lump, and d) butenes on 0.19Zn-BEA catalyst. Butanal conversion rates were measured at 200 ^{o}C, 0.54 kPa butanal partial pressure in He, and 100 mg catalyst weight. The displayed structure on the figures indicates the most abundant species in the product lump.

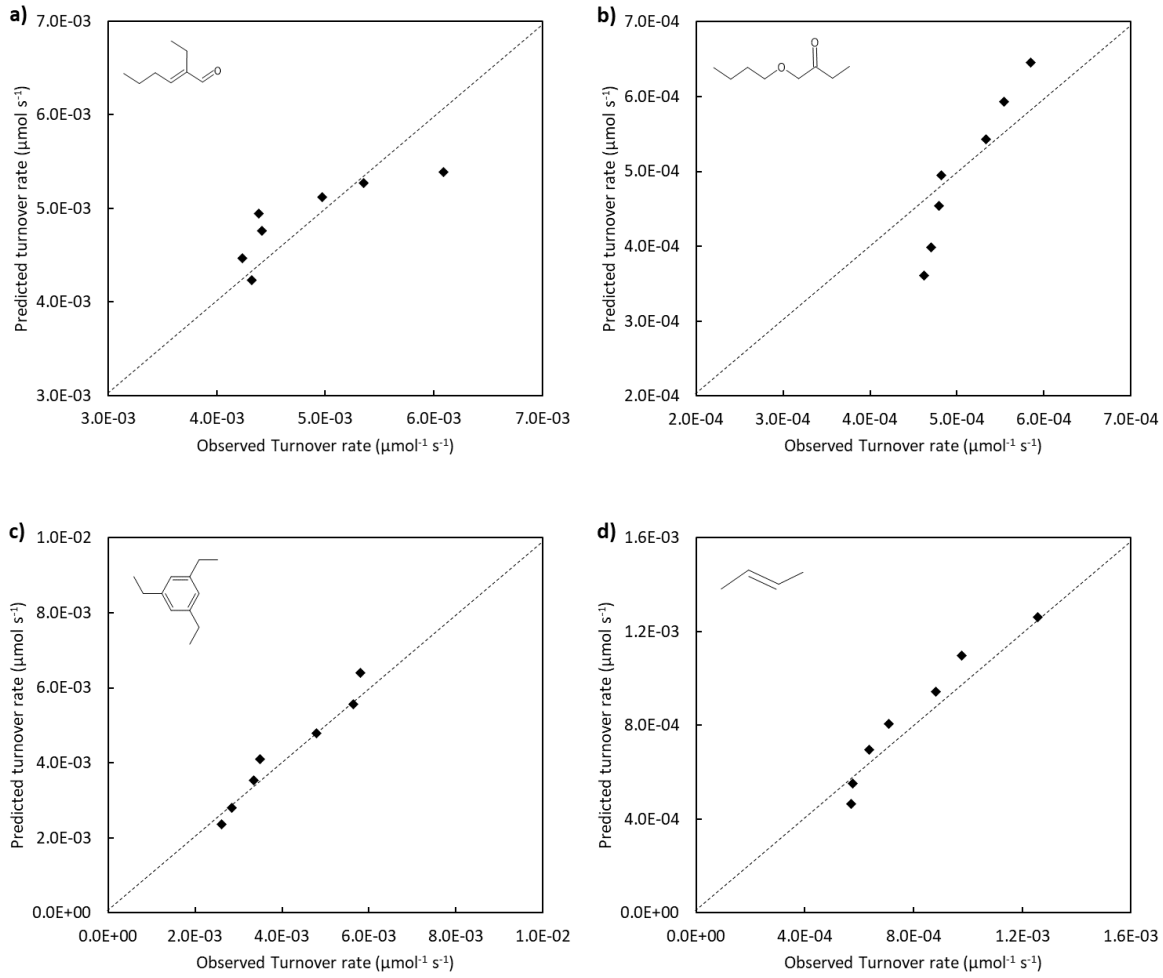

Figure 7.13: Parity charts comparing observed and predicted turnover rates of a) 2-ethyl-2-hexenal product lump, b) butyl butyrate product lump, c) C_{10}+ aromatics lump, and d) butenes on 0.19Zn-BEA-pt catalyst. Butanal conversion rates were measured at 200 ^{o}C, 0.54 kPa butanal partial pressure in He, and 100 mg catalyst weight. The displayed structure on the figures indicates the most abundant species in the product lump.

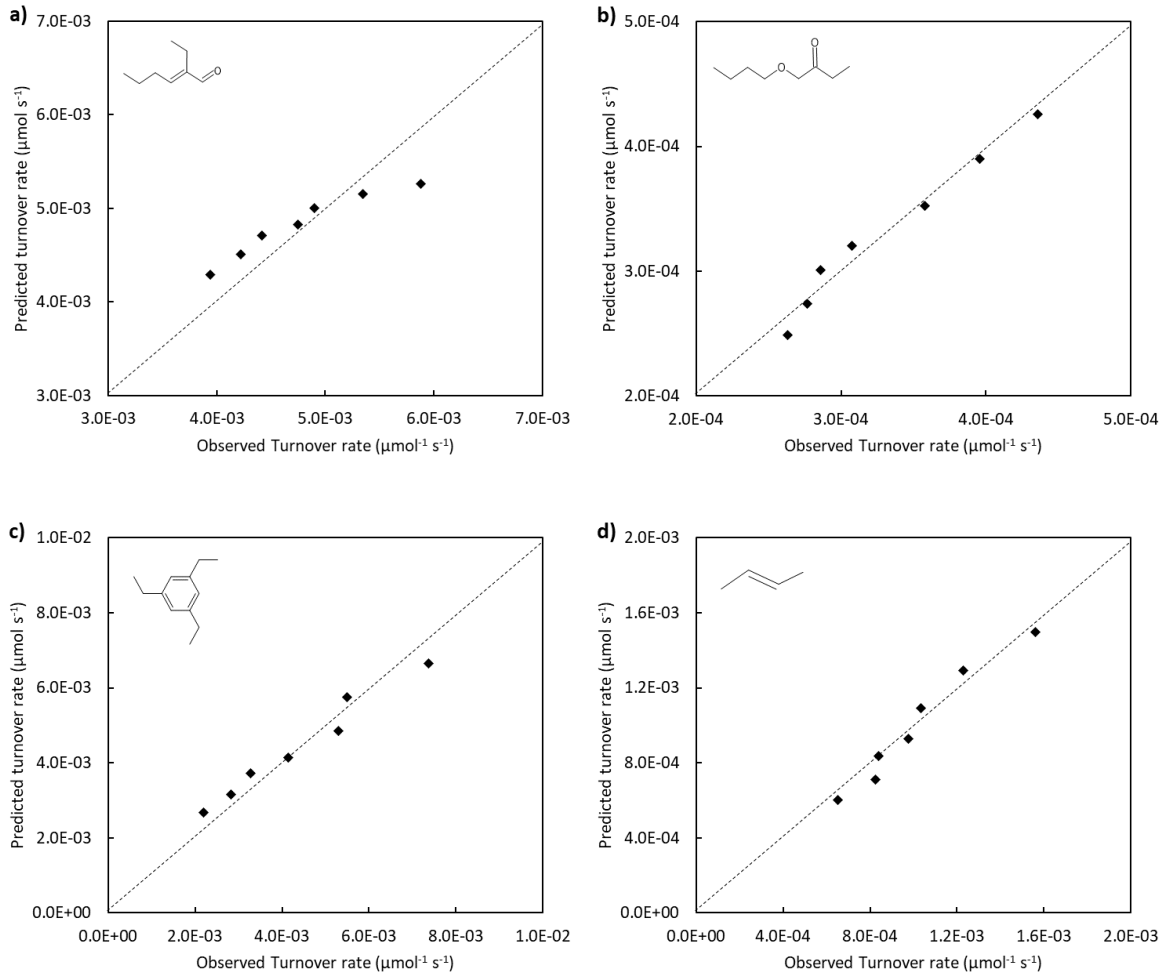

Figure 7.14: Parity charts comparing observed and predicted turnover rates of a) 2-ethyl-2-hexenal product lump, b) butyl butyrate product lump, c) C_{10}+ aromatics lump, and d) butenes on 0.35Zn-BEA catalyst. Butanal conversion rates were measured at 200 ^{o}C, 0.54 kPa butanal partial pressure in He, and 100 mg catalyst weight. The displayed structure on the figures indicates the most abundant species in the product lump.

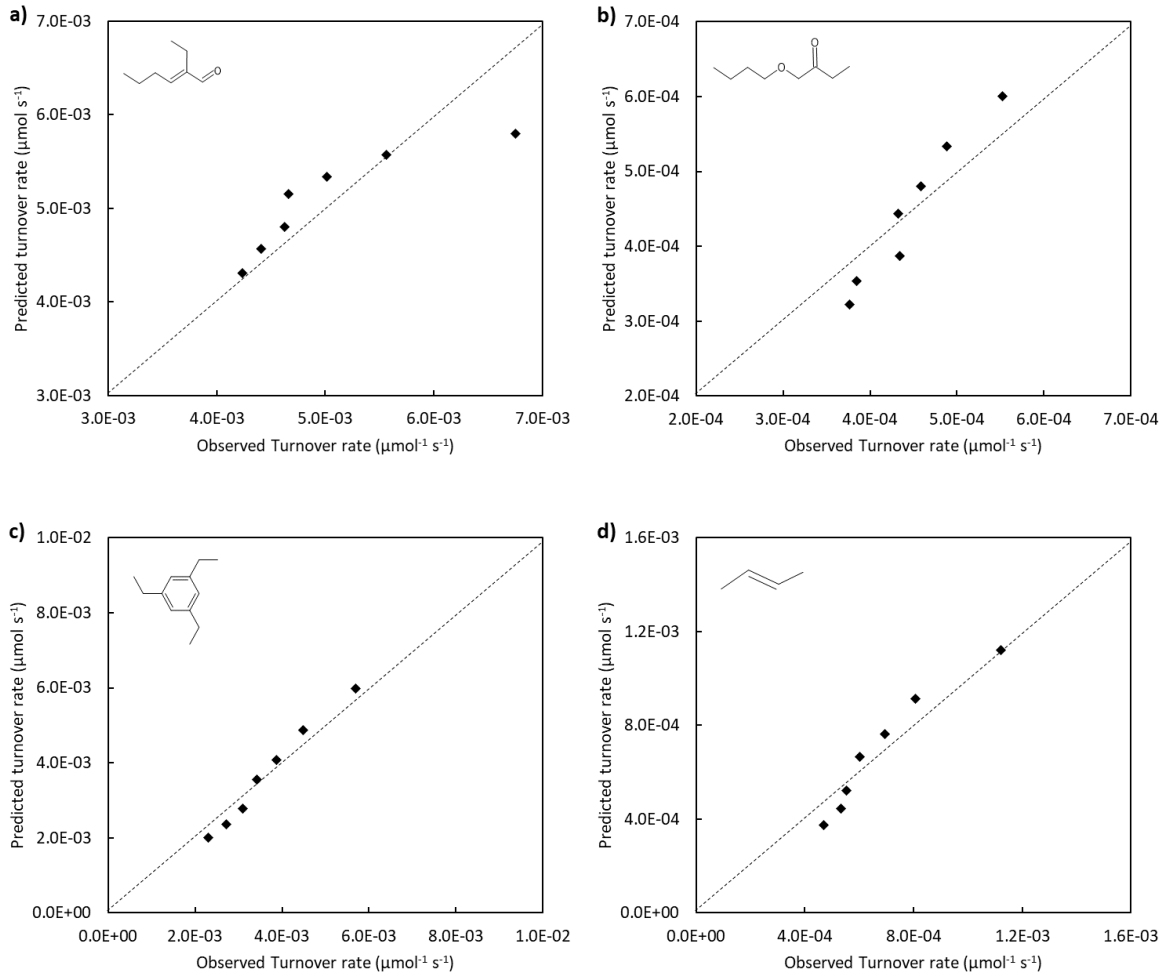

Figure 7.15: Parity charts comparing observed and predicted turnover rates of a) 2-ethyl-2-hexenal product lump, b) butyl butyrate product lump, c) C_{10}+ aromatics lump, and d) butenes on 0.35Zn-BEA-pt catalyst. Butanal conversion rates were measured at 200 ^{o}C, 0.54 kPa butanal partial pressure in He, and 100 mg catalyst weight. The displayed structure on the figures indicates the most abundant species in the product lump.

7.3 Supplementary information relating to Chapter 5

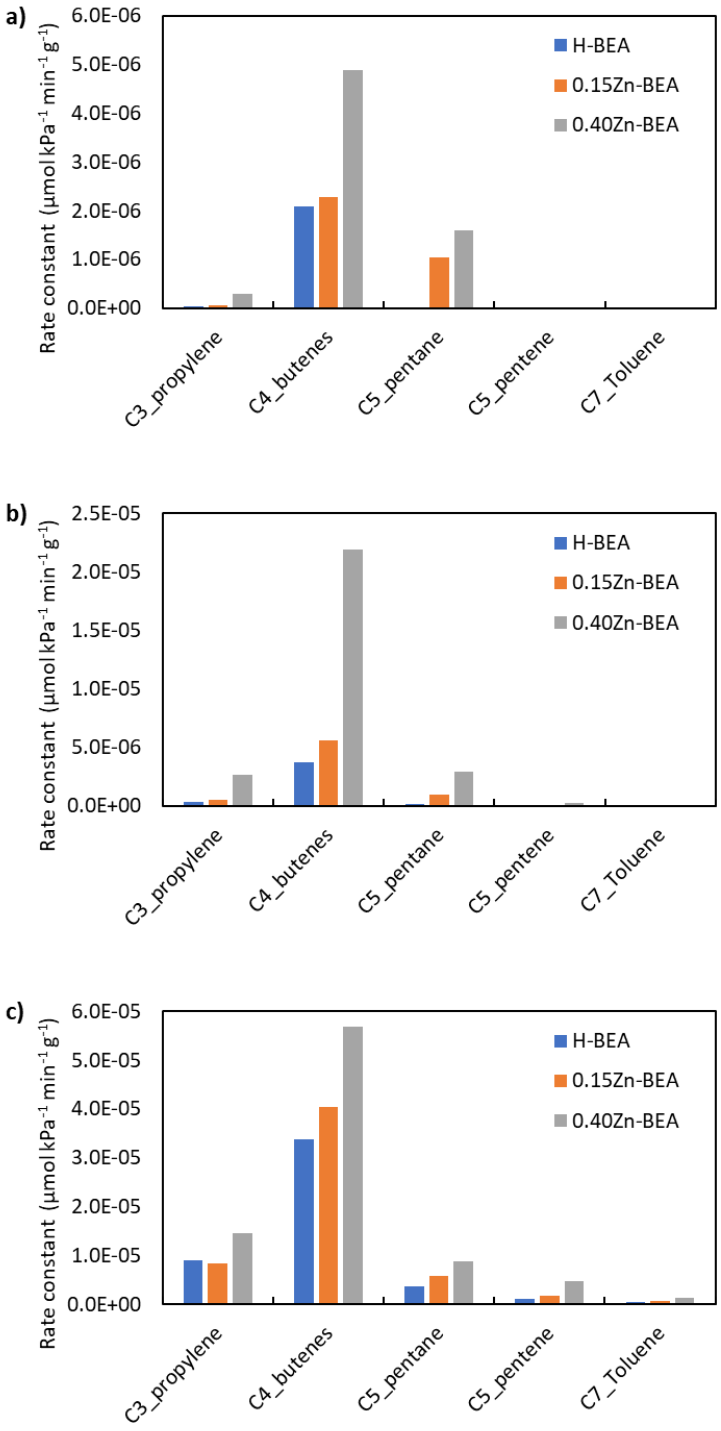

Figure 7.16: Reaction rate constants for the generation of C_3 – C_7 products from the conversion of butanal on different Zn/H-BEA catalysts at a) 300 ºC, b) 350 ºC, and c) 400 ºC.

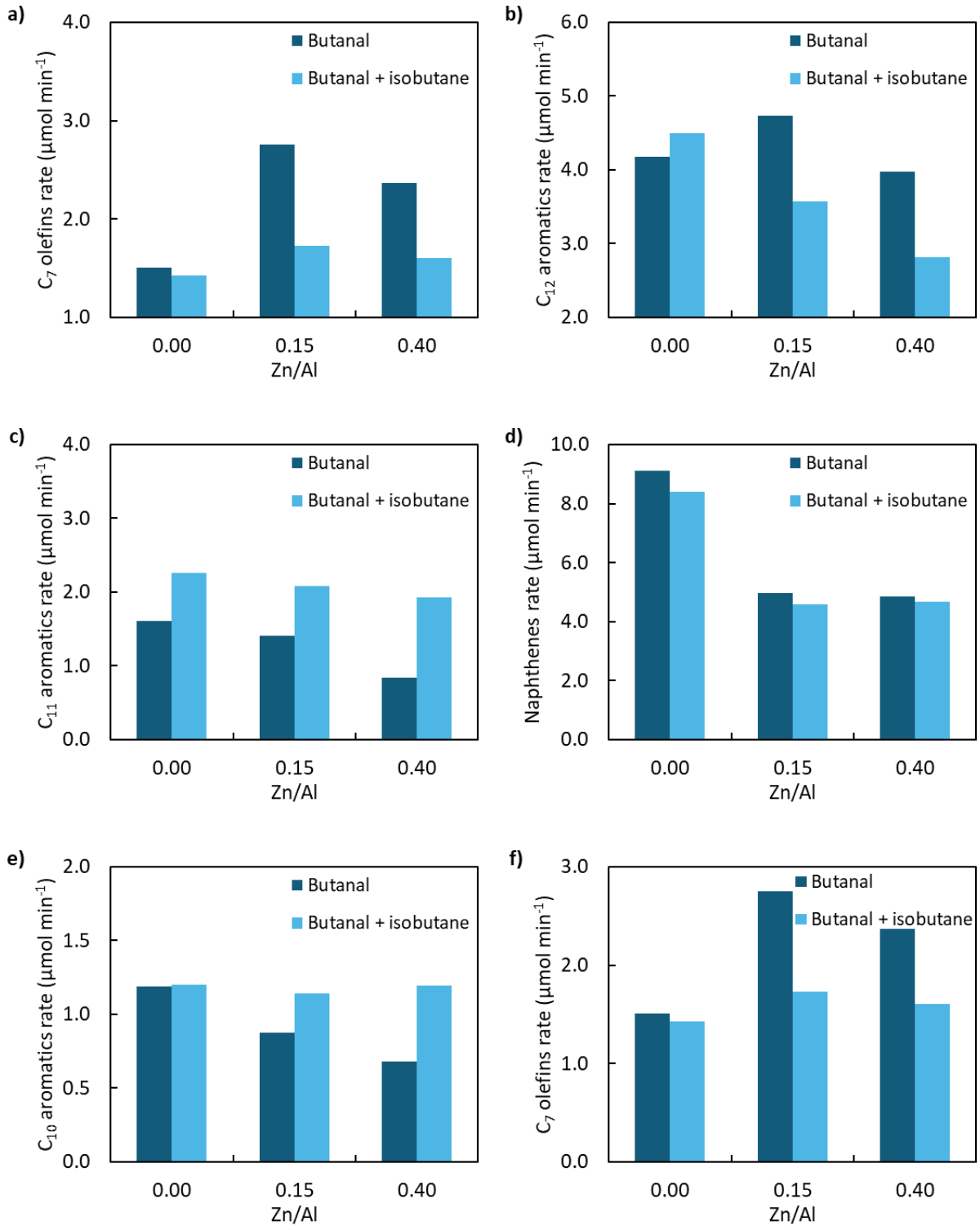

Figure 7.17: Turnover rates of different products from the conversion of butanal or butanal and isobutane on Zn/H-BEA catalysts with varying Zn/Al ratios at 300 ºC and 20 min TOS.

References

[1] C. Walling, J. Am. Chem. Soc. 72 (1950) 1164–1168.

[2] E.G. Derouane, J.C. Védrine, R. Ramos Pinto, P.M. Borges, L. Costa, M.A.N.D.A. Lemos, F. Lemos, F. Ramôa Ribeiro, Catal. Rev. - Sci. Eng. 55 (2013) 454–515.

[3] I. Fechete, Y. Wang, J.C. Védrine, Catal. Today 189 (2012) 2–27.

[4] J. Weitkamp, 131 (2000) 175–188.

[5] S.T. Homeyer, Z. Karpiński, W.M.H. Sachtler, J. Catal. 123 (1990) 60–73.

[6] M. Niwa, S. Sota, N. Katada, Catal. Today 185 (2012) 17–24.

[7] A. Corma, (1997) 63–75.

[8] J.B. Uytterhoeven, L.G. Christner, W.K. Hall, 69 (1965) 2117–2126.

[9] V.L. Zholobenko, L.M. Kustov, V.B. Kazansky, 10 (1990) 5–7.

[10] J.D. Lewis, S. Van De Vyver, Y. Román-Leshkov, Angew. Chemie - Int. Ed. 54 (2015) 9835–9838.

[11] S. Li, A. Zheng, Y. Su, H. Zhang, L. Chen, J. Yang, C. Ye, F. Deng, J. Am. Chem. Soc. 129 (2007) 11161–11171.

[12] K. Kobl, S. Thomas, Y. Zimmermann, K. Parkhomenko, A.C. Roger, Catal. Today 270 (2016) 31–42.

[13] M. Verónica, B. Graciela, A. Norma, L. Miguel, Chem. Eng. J. 138 (2008) 602–607.

[14] M. Usman, D. Cresswell, A. Garforth, Ind. Eng. Chem. Res. 51 (2012) 158–170.

[15] T. Caputo, L. Lisi, R. Pirone, G. Russo, Ind. Eng. Chem. Res. 46 (2007) 6793–6800.

[16] R.D. Cortright, J.A. Dumesic, (2001).

[17] A.H. Motagamwala, J.A. Dumesic, Chem. Rev. (2020).

[18] R.J. Madon, D. Braden, S. Kandoi, P. Nagel, M. Mavrikakis, J.A. Dumesic, J. Catal. 281 (2011) 1–11.

[19] M.A. Christiansen, G. Mpourmpakis, D.G. Vlachos, J. Catal. 323 (2015) 121–131.

[20] J. Park, J. Cho, Y. Lee, M.J. Park, W.B. Lee, Ind. Eng. Chem. Res. 58 (2019) 8663–8673.

[21] R.J. Madon, D. Braden, S. Kandoi, P. Nagel, M. Mavrikakis, J.A. Dumesic, J. Catal. 281 (2011) 1–11.

[22] S. Kandoi, J. Greeley, M.A. Sanchez-castillo, S.T. Evans, A.A. Gokhale, J.A. Dumesic, M. Mavrikakis, 37 (2006).

[23] P. Stoltze, Prog. Surf. Sci. 65 (2000).

[24] X. Sun, S. Mueller, Y. Liu, H. Shi, G.L. Haller, M. Sanchez-Sanchez, A.C. Van Veen, J.A. Lercher, J. Catal. 317 (2014) 185–197.

[25] A.A. Gabrienko, S.S. Arzumanov, D. Freude, A.G. Stepanov, (2010) 12681–12688.

[26] C.D. Chavez Diaz, S. Locatelli, E.E. Gonzo, Zeolites 12 (1992) 851–857.

[27] M.J. Truitt, S.S. Toporek, R. Rovira-Truitt, J.L. White, J. Am. Chem. Soc. 128 (2006) 1847–1852.

[28] D.A. Simonetti, J.H. Ahn, E. Iglesia, J. Catal. 277 (2011) 173–195.

[29] J. Greeley, M. Mavrikakis, J. Am. Chem. Soc. 126 (2004) 3910–3919.

[30] J. Greeley, M. Mavrikakis, J. Am. Chem. Soc. 124 (2002) 7193–7201.

[31] A.A. Gokhale, J.A. Dumesic, M. Mavrikakis, (2008) 1402–1414.

[32] D.A. Ruddy, J.E. Hensley, C.P. Nash, E.C.D. Tan, E. Christensen, C.A. Farberow, F.G. Baddour, K.M. Van Allsburg, J.A. Schaidle, Nat. Catal. 2 (2019) 632–640.

[33] J.A. Schaidle, D.A. Ruddy, S.E. Habas, M. Pan, G. Zhang, J.T. Miller, J.E. Hensley, ACS Catal. 5 (2015) 1794–1803.

[34] C.A. Farberow, S. Cheah, S. Kim, J.T. Miller, J.R. Gallagher, J.E. Hensley, J.A. Schaidle, D.A. Ruddy, ACS Catal. 7 (2017) 3662–3667.

[35] X. Sun, S. Mueller, H. Shi, G.L. Haller, M. Sanchez-Sanchez, A.C. Van Veen, J.A. Lercher, J. Catal. 314 (2014) 21–31.

[36] A.T. Aguayo, P. Castaño, D. Mier, A.G. Gayubo, M. Olazar, J. Bilbao, Ind. Eng. Chem. Res. 50 (2011) 9980–9988.

[37] W. Xu, S.J. Miller, P.K. Agrawal, C.W. Jones, (2014) 434–438.

[38] J.E. Bercaw, P.L. Diaconescu, R.H. Grubbs, R.D. Kay, S. Kitching, J.A. Labinger, X. Li, P. Mehrkhodavandi, G.E. Morris, G.J. Sunley, P. Vagner, (2006) 8907–8917.

[39] S. Dahl, J. Sehested, C.J.H. Jacobsen, E. Törnqvist, I. Chorkendorff, J. Catal. 192 (2000) 391–399.

[40] S. Kandoi, A.A. Gokhale, L.C. Grabow, J.A. Dumesic, M. Mavrikakis, Catal. Letters 93 (2004) 93–100.

[41] C. Stegelmann, N.C. Schiødt, C.T. Campbell, P. Stoltze, 221 (2004) 630–649.

[42] W.E. Stewart, M. Caracotsios, J.P. Sørensen, AIChE J. 38 (1992) 641–650.

[43] L.M. Aparicio, J.A. Dumesic, Top. Catal. 1 (1994) 233–252.

[44] K. Alexopoulos, M. John, K. Van Der Borght, V. Galvita, M.F. Reyniers, G.B. Marin, J. Catal. 339 (2016) 173–185.

[45] S. Czernik, A. V. Bridgwater, Energy and Fuels 18 (2004) 590–598.

[46] A.G. Gayubo, A.T. Aguayo, A. Atutxa, B. Valle, J. Bilbao, J. Chem. Technol. Biotechnol.

80 (2005) 1244–1251.

[47] F. Lin, Y.C. Chin, J. Catal. 341 (2016) 136–148.

[48] T.Q. Hoang, X. Zhu, T. Sooknoi, D.E. Resasco, R.G. Mallinson, J. Catal. 271 (2010) 201–208.

[49] I. Isakov, (1972) 1175–1177.

[50] D. Mier, A.G. Gayubo, A.T. Aguayo, M. Olazar, J. Bilbao, AICHE J. 61 (2015) 857–866.

[51] F. Lin, Y.H. Chin, J. Catal. 311 (2014) 244–256.

[52] H. Luo, T. Prasomsri, Y. Roma, Top Catal. (2015) 529–536.

[53] X. Solans-monfort, J. Bertran, M. Sodupe, (2002) 10220–10226.

[54] M. Xu, W. Wang, M. Hunger, Chem. Commun. 3 (2003) 722–723.

[55] E. Dumitriu, V. Hulea, I. Fechete, A. Auroux, 43 (2001).

[56] J.H. Ahn, B. Temel, E. Iglesia, Angew. Chemie - Int. Ed. 48 (2009) 3814–3816.

[57] D.A. Simonetti, R.T. Carr, E. Iglesia, J. Catal. 285 (2012) 19–30.

[58] D.A. Simonetti, J.H. Ahn, E. Iglesia, ChemCatChem 3 (2011) 704–718.

[59] E.R. Silva, J.M. Silva, P. Massiani, F.R. Ribeiro, M.F. Ribeiro, 108 (2005) 792–799.

[60] M.R. Guisnet, Acc. Chem. Res. 23 (1990) 392–398.

[61] A. Corma, V. Fornés, L. Forni, F. Márquez, J. Martínez-Triguero, D. Moscotti, J. Catal. 179 (1998) 451–458.

[62] C.D. Baertsch, K.T. Komala, Y.H. Chua, E. Iglesia, J. Catal. 205 (2002) 44–57.

[63] R.J. Gorte, Catal. Today 28 (1996) 405–414.

[64] A. Ausavasukhi, T. Sooknoi, D.E. Resasco, J. Catal. 268 (2009) 68–78.

[65] J. Yu, J. Luo, Y. Zhang, J. Cao, C.C. Chang, R.J. Gorte, W. Fan, Microporous Mesoporous Mater. 225 (2016) 472–481.

[66] C.P. Nash, D.P. Dupuis, A. Kumar, C.A. Farberow, A.T. To, C. Yang, E.C. Wegener, J.T. Miller, K.A. Unocic, E. Christensen, J.E. Hensley, J.A. Schaidle, S.E. Habas, D.A. Ruddy, Appl. Catal. B Environ. 301 (2022) 120801.

[67] J. Penzien, A. Abraham, J.A. Van Bokhoven, A. Jentys, T.E. Mu, C. Sievers, J.A. Lercher, J. Phys. Chem. B 108 (2004) 4116–4126.

[68] S. Tamiyakul, T. Sooknoi, L.L. Lobban, S. Jongpatiwut, Appl. Catal. A Gen. 525 (2016) 190–196.

[69] H. Yieru, O. Qingyu, Y. Weile, Anal. Chem. 62 (1990) 2063–2064.

[70] M.B. R. J. Madon, Ind. Eng. Chem. Fundam. 21 (1982) 438–447.

[71] G.W. Huber, S. Iborra, A. Corma, Chem. Rev. 106 (2006) 4044–4098.

[72] Q. Lu, W.Z. Li, X.F. Zhu, Energy Convers. Manag. 50 (2009) 1376–1383.

[73] F. Dalena, A. Senatore, A. Marino, A. Gordano, M. Basile, A. Basile, Methanol Production and Applications: An Overview, Elsevier B.V., 2018.

[74] S.I. Mussatto, G. Dragone, P.M.R. Guimarães, J.P.A. Silva, L.M. Carneiro, I.C. Roberto, A. Vicente, L. Domingues, J.A. Teixeira, Biotechnol. Adv. 28 (2010) 817–830.

[75] S.M. Scully, J. Orlygsson, Biological Production of Alcohols, Elsevier Inc., 2019.

[76] I. Yarulina, A.D. Chowdhury, F. Meirer, B.M. Weckhuysen, J. Gascon, Nat. Catal. 1 (2018) 398–411.

[77] M. Stöcker, Microporous Mesoporous Mater. 29 (1999) 3–48.

[78] M. Xu, J.H. Lunsford, D.W. Goodman, A. Bhattacharyya, Appl. Catal. A Gen. 149 (1997) 289–301.

[79] V. Chandra, S. Palla, D. Shee, S.K. Maity, "Applied Catal. A, Gen. 526 (2016) 28–36.

[80] M. Inaba, K. Murata, I. Takahara, K.I. Inoue, Adv. Mater. Sci. Eng. 2012 (2012).

[81] A.M. Varvarin, K.M. Khomenko, V. V Brei, 106 (2013) 617–620.

[82] D. Zhang, R. Al-Hajri, S.A.I. Barri, D. Chadwick, Chem. Commun. 46 (2010) 4088–4090.

[83] D. Gunst, K. Alexopoulos, K. Van Der Borght, M. John, V. Galvita, M.F. Reyniers, A. Verberckmoes, Appl. Catal. A Gen. 539 (2017) 1–12.

[84] X. Zhu, L.L. Lobban, R.G. Mallinson, D.E. Resasco, J. Catal. 271 (2010) 88–98.

[85] P.A. Kots, A. V Zabilska, I.I. Ivanova, ChemCatChem (2020) 248–258.

[86] T.Q. Hoang, X. Zhu, L.L. Lobban, D.E. Resasco, R.G. Mallinson, Catal. Commun. 11 (2010) 977–981.

[87] C.D. Chang, A.J. Silvestri, J. Catal. 47 (1977) 249–259.

[88] S. Ilias, A. Bhan, ACS Catal. 3 (2013) 18–31.

[89] S.R. Blaszkowski, R.A. Van Santen, J. Am. Chem. Soc. 118 (1996) 5152–5153.

[90] P. Huber, F. Studt, P.N. Plessow, J. Phys. Chem. C 126 (2022) 5896–5905.

[91] J.N. Kondo, K. Ito, E. Yoda, F. Wakabayashi, K. Domen, J. Phys. Chem. B 109 (2005) 10969–10972.

[92] D. Gabriëls, W.Y. Hernández, B.F. Sels, P. Van Der Voort, A. Verberckmoes, Catal. Sci. Technol. 5 (2015) 3876–3902.

[93] M. Bjørgen, K.P. Lillerud, U. Olsbye, S. Bordiga, A. Zecchina, J. Phys. Chem. B 108 (2004) 7862–7870.

[94] L. Yu, S. Huang, S. Zhang, Z. Liu, W. Xin, S. Xie, L. Xu, ACS Catal. 2 (2012) 1203–

1210.

[95] Y. Yang, F. Lin, H. Tran, Y.C. Chin, ChemCatChem (2017) 287–299.

[96] C. Liu, T.J. Evans, L. Cheng, M.R. Nimlos, C. Mukarakate, D.J. Robichaud, R.S. Assary, L.A. Curtiss, J. Phys. Chem. C 119 (2015) 24025–24035.

[97] J.A. Biscardi, E. Iglesia, Catal. Today 31 (1996) 207–231.

[98] A.G. Stepanov, S.S. Arzumanov, A.A. Gabrienko, V.N. Parmon, I.I. Ivanova, D. Freude, ChemPhysChem 9 (2008) 2559–2563.

[99] Y. Ono, Catal. Rev. 34 (1992) 179–226.

[100] S.S. Arzumanov, A.A. Gabrienko, A. V. Toktarev, Z.N. Lashchinskaya, D. Freude, J. Haase, A.G. Stepanov, J. Phys. Chem. C (2019).

[101] S.Y. Yu, W. Li, E. Iglesia, Abstr. Pap. Am. Chem. Soc. 219 (2000) U249–U249.

[102] S.Y. Yu, T. Waku, E. Iglesia, Appl. Catal. A Gen. 242 (2003) 111–121.

[103] J.A. Biscardi, G.D. Meitzner, E. Iglesia, J. Catal. 179 (1998) 192–202.

[104] V.B. Kazansky, A.I. Serykh, Phys. Chem. Chem. Phys. 6 (2004) 3760–3764.

[105] G.M. Zhidomirov, A. V. Larin, D.N. Trubnikov, D.P. Vercauteren, J. Phys. Chem. C 113 (2009) 8258–8265.

[106] A.L. Yakovlev, A.A. Shubin, G.M. Zhidomirov, R.A. Van Santen, Catal. Letters 70 (2000) 175–181.

[107] A. Bhan, W.N. Delgass, Catal. Rev. - Sci. Eng. 50 (2008) 19–151.

[108] P. Unruean, T. Plianwong, S. Pruksawan, B. Kitiyanan, R.M. Ziff, Catalysts 9 (2019).

[109] A.A. Gabrienko, S.S. Arzumanov, M. V. Luzgin, A.G. Stepanov, V.N. Parmon, J. Phys. Chem. C 119 (2015) 24910–24918.

[110] A.A. Gabrienko, S.S. Arzumanov, A. V. Toktarev, I.G. Danilova, I.P. Prosvirin, V. V. Kriventsov, V.I. Zaikovskii, D. Freude, A.G. Stepanov, ACS Catal. 7 (2017) 1818–1830.

[111] S.M.T. Almutairi, B. Mezari, P.C.M.M. Magusin, E.A. Pidko, E.J.M. Hensen, ACS Catal. 2 (2012) 71–83.

[112] C.A. Gaertner, J.C. Serrano-Ruiz, D.J. Braden, J.A. Dumesic, Ind. Eng. Chem. Res. 49 (2010) 6027–6033.

[113] G.M. Zhidomirov, A.A. Shubin, V.B. Kazansky, R.A. Van Santen, Theor. Chem. Acc. 114 (2005) 90–96.

[114] S.S. Arzumanov, A.A. Gabrienko, A. V. Toktarev, D. Freude, J. Haase, A.G. Stepanov, J. Phys. Chem. C 124 (2020) 20270–20279.

[115] M.J. Climent, A. Corma, V. Fornés, R. Guil-Lopez, S. Iborra, Adv. Synth. Catal. 344 (2002) 1090–1096.

[116] A.M. Hernández-Giménez, J. Ruiz-Martínez, B. Puértolas, J. Pérez-Ramírez, P.C.A. Bruijnincx, B.M. Weckhuysen, Top. Catal. 60 (2017) 1522–1536.

[117] W. Shen, G.A. Tompsett, R. Xing, W.C. Conner, G.W. Huber, J. Catal. 286 (2012) 248–259.

[118] R.T. Carr, M. Neurock, E. Iglesia, J. Catal. 278 (2011) 78–93.

[119] E.T. Thostenson, Z. Ren, T.-W. Chou, Compos. Sci. Technol. 61 (2001) 1899–1912.

[120] R.J. Gorte, Catal. Letters 62 (1999) 1–13.

[121] J.W. Ward, J. Catal. 11 (1968) 238–250.

[122] M. Lefrancois, G. Malbois, J. Catal. 20 (1971) 350–358.

[123] A.M.. van der E. and D.C.K. J.A. van Bokhoven, Stud. Surf. Sci. Catal. 142 (2002).

[124] T. Seki, H. Kabashima, K. Akutsu, H. Tachikawa, H. Hattori, 401 (2001) 393–401.

[125] A.G. Panov, J.J. Fripiat, Catal. Letters 57 (1999) 25–32.

[126] J. Penzien, C. Haeßner, A. Jentys, K. Köhler, T.E. Müller, J.A. Lercher, J. Catal. 221 (2004) 302–312.

[127] H. Tsuji, F. Yagi, H. Hattori, K. Hideaki, J. Catal. (1994) 759–770.

[128] S.J. Khang, O. Levenspiel, 12 (1973) 185–190.

[129] A. Monzón, E. Romeo, A. Borgna, Chem. Eng. J. 94 (2003) 19–28.

[130] S. Xiu, A. Shahbazi, Renew. Sustain. Energy Rev. 16 (2012) 4406–4414.

[131] A. Oasmaa, S. Czernik, Energy and Fuels 13 (1999) 914–921.

[132] J.S. Martinez-Espin, M. Mortén, T.V.W. Janssens, S. Svelle, P. Beato, U. Olsbye, Catal. Sci. Technol. 7 (2017) 2700–2716.

[133] R. Khare, A. Bhan, J. Catal. 329 (2015) 218–228.

[134] S. Lippert, W. Baumann, K. Thomke, J. Mol. Catal. 69 (1991) 199–214.

[135] M. Subaramanian, P.M. Ramar, J. Rana, V.K. Gupta, E. Balaraman, Chem. Commun. 56 (2020) 8143–8146.

[136] M. Bertero, G. De La Puente, U. Sedran, Fuel 95 (2012) 263–271.

[137] A.M. Hernández, G. Javier, R. Martínez, B. Puértolas, Top. Catal. 60 (2017) 1522–1536.

[138] R.N. Hayes, R.P. Grese, M.L. Gross, J. Chem. Soc. Perkin Trans. 2 (1990) 267–271.

[139] S. Kotrel, M.P. Rosynek, J.H. Lunsford, J. Catal. 191 (2000) 55–61.

[140] C.L. Yaws, ed., in: First edit, McGraw-Hill Education, New York, 1999.

[141] L.C. Grabow, M. Mavrikakis, ACS Catal. 1 (2011) 365–384.

[142] J. A. Dumesic, D.F. Rudd, L.M. Aparicio, J.E. Rekoske, and A.A. Treviño, (1993).

[143] A. Ungureanu, S. Royer, T. V. Hoang, D. Trong On, E. Dumitriu, S. Kaliaguine, Microporous Mesoporous Mater. 84 (2005) 283–296.

[144] M. Caracotsios, (n.d.).

[145] R.M. West, D.J. Braden, J.A. Dumesic, J. Catal. 262 (2009) 134–143.

[146] H. Kawakami, (1986) 1385–1397.

[147] T. Tago, H. Konno, S. Ikeda, S. Yamazaki, W. Ninomiya, Y. Nakasaka, T. Masuda, Catal. Today 164 (2011) 158–162.

[148] C.T. Campbell, Top. Catal. 1 (1994) 353–366.

[149] C.T. Campbell, ACS Catal. 7 (2017) 2770–2779.

[150] R.A.F. Tomás, J.C.M. Bordado, J.F.P. Gomes, Chem. Rev. 113 (2013) 7421–7469.

[151] J.C. Gentry, Asia-Pacific J. Chem. Eng. 2 (2007) 272–277.

[152] M.R. Rahimpour, M. Jafari, D. Iranshahi, Appl. Energy 109 (2013) 79–93.

[153] V.M. Benitez, C.L. Pieck, Catal. Letters 136 (2010) 45–51.

[154] S.A. D'Ippolito, C.R. Vera, F. Epron, P. Samoila, C. Especel, P. Marécot, L.B. Gutierrez, C.L. Pieck, Appl. Catal. A Gen. 370 (2009) 34–41.

[155] M. V. Luzgin, V.A. Rogov, S.S. Arzumanov, A. V. Toktarev, A.G. Stepanov, V.N. Parmon, Angew. Chemie 120 (2008) 4635–4638.

[156] M. V. Luzgin, V.A. Rogov, S.S. Arzumanov, A. V. Toktarev, A.G. Stepanov, V.N. Parmon, Catal. Today 144 (2009) 265–272.

[157] S. Tamiyakul, T. Sooknoi, L.L. Lobban, S. Jongpatiwut, Appl. Catal. A Gen. 525 (2016) 190–196.

[158] D. Zeng, G. Zhu, C. Xia, Fuel Process. Technol. 226 (2022) 107087.

[159] A.A. Gabrienko, Z.N. Lashchinskaya, S.S. Arzumanov, A. V. Toktarev, D. Freude, J. Haase, A.G. Stepanov, ChemPhysChem 23 (2022).

[160] X. Niu, J. Gao, Q. Miao, M. Dong, G. Wang, W. Fan, Z. Qin, J. Wang, Microporous Mesoporous Mater. 197 (2014) 252–261.

[161] J. Liu, N. He, W. Zhou, L. Lin, G. Liu, C. Liu, J. Wang, Q. Xin, G. Xiong, H. Guo, Catal. Sci. Technol. 8 (2018) 4018–4029.

[162] Y. Sun, T.C. Brown, Int. J. Chem. Kinet. 34 (2002) 467–480.

[163] A.G. Stepanov, S.S. Arzumanov, A.A. Gabrienko, A. V Toktarev, V.N. Parmon, D. Freude, J. Catal. 253 (2008) 11–21.

[164] C. Song, K. Liu, D. Zhang, S. Liu, X. Li, S. Xie, L. Xu, Appl. Catal. A Gen. 470 (2014) 15–23.

[165] S.S. Arzumanov, A.A. Gabrienko, A. V. Toktarev, D. Freude, J. Haase, A.G. Stepanov, J. Catal. 378 (2019) 341–352.

[166] A.A. Gabrienko, Z.N. Lashchinskaya, S.S. Arzumanov, A. V. Toktarev, D. Freude, J. Haase, A.G. Stepanov, J. Phys. Chem. C 125 (2021) 21471–21480.

[167] D. Mier, A.T. Aguayo, M. Gamero, A.G. Gayubo, J. Bilbao, Ind. Eng. Chem. Res. 49 (2010) 8415–8423.

[168] I. Milas, M.A.C. Nascimento, Chem. Phys. Lett. 373 (2003) 379–384.

[169] A. Hagen, F. Roessner, Catal. Rev. - Sci. Eng. 42 (2000) 403–437.

[170] J. Abbot, B.W. Wojciechowski, J. Catal. 108 (1987) 346–355.